POLITECNICO DI MILANO

Tesi di laurea Specialistica in Ingenieria della prevenzione e Sicurezza dell'industria di processo


# CFD validation of 2-phase ammonia release in atmospheric boundary layer

# (Desert Tortoise experiment)

RELATORE: Prof. Valentina Busini

STUDENTE: Michele Zanetti (Matricola 765496)

# Contents

# Summary

*Introduction*

The ammonia is one of the most important product of the chemical industry, in the past the ammonia production was the reference to understand the industrial evolution of a country, in fact the world production of ammonia in 2004 was about 109.000.000 tons. The driving force that promoted the ammonia production was the necessity to produce fertilizers for corps. Due to this bear the necessary to store ammonia in an efficient way. Three methods exist for storing liquid ammonia (Hale, Nitrogen, 1979) (Hale, Nitrogen, 1980):

- Pressure storage at ambient temperature in spherical or cylindrical pressure vessels having capacities up to about t
- Atmospheric storage at in insulated cylindrical tanks for amounts to about per vessel
- Reduced pressure storage at about 0°C in insulated, usually spherical pressure vessels for quantities up to about 2500 t per sphere.

The first two methods are preferred and is opinion that reduced pressure storage is less attractive.

An area which deserves special attention with respect to safety is the storage of liquid ammonia. In contrast to some other liquefied gases (e.g., LPG, LNG), ammonia is toxic and even a short exposure to concentration of may be fatal. The explosion hazard from air/ammonia mixtures is rather low, as the flammability limits of 15-27% are rather narrow. The ignition temperature is . Ammonia vapor at the boiling point of has vapor density of ca. of that of ambient air. The important reason why ammonia must be analyzed is its peculiar behavior: the molecular weight of ammonia is 17 g/mol , that is lighter than air 28.9 g/mol. The comparison of the molecular weights yield to anticipate a “light gas” behavior; this is not true due to the temperature field caused by the two-phase release.

*Theoretical background*

Analyzing the behavior of ammonia subject to a release from a pressurized vessel we have to take into account many aspects. The major factors which influence the amount of material which becomes airbone during an accidental release are the storage pressure and volatility of the material as reflected in its normal boiling point or vapor pressure curve. Releases of pressurized gases usually dissipate rapidly by the energetic mixing associated with high-momentum jet. Releases of pressurized liquids often pose a greater threat because they can form an immediate large air-borne mass of aerosol droplets. The aerosol increases the cloud density both directly and by depressing the cloud temperature by evaporation (as ammonia). Heavier than air clouds tend to disperse less than neutrally buoyant clouds both because they typically flow in the lower wind speeds near the ground, and also because dispersion is suppressed inside a heavy gas cloud.

Liquids stored below their normal boiling point, or as supercooled liquids normally present a lower risk because the discharged liquids form little or no airbone aerosol. Rather they rainout immediately and form a pool of relatively low volatility. However, even high boiling-point materials can form aerosols if discharged from an elevated point, or if they

are stored under pressure with a padding gas. Aerosol formation occurs by mechanical shearing, termed aerodynamic breakup, the foregoing flow behavior shows that the flashing region is a complex problem and the transition between initial super-heated liquid state and the following two-phase jet is not well understood (R.K. Calay, 2007).

The liquid in aerosol form initially has a vapor pressure of one atmosphere, and continues to evaporate as it follows a trajectory along the plume. Typically the droplets cool thereby increasing the temperature driving force. This continues until the temperature driving force reaches an equilibrium so that heat loss by evaporation balances heat gain by conduction and radiation from the surroundings. The vapor pressure of the droplets decreases upon cooling, which reduces the evaporation rate of the aerosol and also that of the pool which forms from rainout or drops reaching the ground.

Rainout from aerosol clouds can form a wetted surface and/or a spreading pool. Rainout lowers the concentration in the cloud, but also tends to prolong the hazardous event by subsequent evaporation. A short discard event is transformed into a long lasting event by rainout and evaporation (Americal institute of chemical engineers , 1999).

*Governing equations*

The conservation equations for mass, momentum, energy (temperature) and concentration have been used to simulate the process of interest.

$$\frac{\mathrm{D}\rho}{\mathrm{D}t} = -\rho(\nabla \cdot \mathrm{v})$$

$$\frac{\partial \rho \mathrm{v}}{\partial t} + \left(\nabla \cdot \rho(\mathrm{v} \cdot \mathrm{v})\right) + (\nabla \cdot \mathrm{P}) - \sum_{\mathrm{s}} \rho_{\mathrm{s}} \mathrm{F}_{\mathrm{s}} = 0$$

$$\begin{aligned}
&\frac{\partial}{\partial t}\left[\rho\left(e + \frac{1}{2}V^2\right)\right] + \frac{\partial}{\partial x}\left[\rho u\left(e + \frac{1}{2}V^2\right)\right] \\
&\quad + \frac{\partial}{\partial y}\left[\rho v\left(e + \frac{1}{2}V^2\right)\right] \\
&\quad + \frac{\partial}{\partial z}\left[\rho w\left(e + \frac{1}{2}V^2\right)\right] \\
&\quad = -\frac{\partial q_x}{\partial x} - \frac{\partial q_y}{\partial y} - \frac{\partial q_z}{\partial z} \\
&\quad + \frac{\partial}{\partial x}\left(u\sigma_{xx} + v\sigma_{xy} + w\sigma_{xz}\right) \\
&\quad + \frac{\partial}{\partial y}\left(u\sigma_{yx} + v\sigma_{yy} + w\sigma_{yz}\right) \\
&\quad + \frac{\partial}{\partial z}\left(u\sigma_{zx} + v\sigma_{zy} + w\sigma_{zz}\right) + \rho u g_x + \rho v g_y + \rho w g_z
\end{aligned}$$

With the help of the $\kappa - \varepsilon$ model, which is almost universally adopted in the study of dispersion despite its known limitations. The turbulent viscosity was calculated using the Prandtl-Kolmogorov equation. As a function of turbulent kinetic energy, κ, and its dissipation rate, ε, by the closure model defined as follows:

$$\begin{aligned}
&\frac{\partial}{\partial t}(\rho k) + \frac{\partial}{\partial x_j}\left[u_j(\rho k)\right] \\
&\quad = \frac{\partial}{\partial x_j}\left[\left(\mu + \frac{\mu_t}{\sigma_\kappa}\right)\frac{\partial k}{\partial x_j}\right] + G_k \\
&\quad - \rho\varepsilon
\end{aligned}$$

$$\begin{aligned}
&\frac{\partial}{\partial t}(\rho\varepsilon) + \frac{\partial}{\partial x_j}\left[u_j(\rho\varepsilon)\right] \\
&\quad = \frac{\partial}{\partial x_j}\left[\left(\mu + \frac{\mu_t}{\sigma_\varepsilon}\right)\frac{\partial \varepsilon}{\partial x_j}\right] \\
&\quad + C_{1_\varepsilon}\frac{\varepsilon}{k}G_k - C_{2_\varepsilon}\rho\frac{\varepsilon^2}{k}
\end{aligned}$$

The liquid phase consisting of particle droplets was modeled by a Lagrangian approach. The discrete phase particle trajectories can be computed by integrating the force balance equation. The fluid phase influences the particle via drag, turbulence and momentum transfer. The particle influence the fluid phase through source terms. Mass, momentum as well as energy transfer between the phases were included. For the discrete phase (small droplets of liquid ammonia).

*DPM temperature laws*

The inert heating or cooling laws (equations and) are applied when the particle temperature is less than the vaporization temperature that have been defined, $T_{vap}$, and after the volatile fraction, $f_{v,0}$, of a particle has been consumed.

$$T_P < T_{vap}$$

$$m_p \leq (1 - f_{v,0}) m_{p,0}$$

The equation above. is applied until the temperature of the droplet reaches the vaporization temperature.

When using $\mathrm{T_P} < \mathrm{T_{vap}}$, DPM uses a simple heat balance to relate the particle temperature, $T_p(t)$, to the convective heat transfer and the absorption/emission of radiation at the particle surface:

$$m_p c_p \frac{dT_p}{dt} = hA_p\left(T_\infty - T_p\right) + \varepsilon_p A_p \sigma(\theta_R^4 - T_p^4)$$

The equation is applied to predict the convective boiling of a discrete phase droplet until the temperature of the droplet has reached the boiling temperature, $T_{bp}$, and while the mass of the droplet exceeds the nonvolatile fraction, $(1 - f_{v,0})$:

$$T_p \geq T_{bp}$$

$$m_p > (1 - f_{v,0}) m_{p,0}$$

When the droplet temperature reaches the boiling point, a boiling rate equation is applied:

$$\frac{d(d_p)}{dt} = \frac{4k_\infty}{\rho_p c_{p,\infty} d_p}\left(1 + 0.23\sqrt{Re_d}\right) ln\left[1 + \frac{c_{p,\infty}(T_\infty - T_p)}{h_{fg}}\right]$$

*Field study setup*

The Desert Tortoise field study, was a series of four pressurized liquid ammonia releases made with varying release times and release rates, that was conducted in August and September of 1983 by Lawerence Livermore National Laboratory (LLNL). The test location chosen for the experiments was the Frenchman's Flat, Nevada, that provided flat terrain with relatively steady and predictable winds.

A pair of tanker trucks were placed on site and the lines leading from each tanker were routed to a common 6-inch diameter spill line. The spill line was extended a sufficient distance cross-wind, such that the tankers and other site equipment would not represent upwind obstacles to the release. The spill line was terminated at an exit plate which reduced the exit diameter to either 3.19 or 3.72 inches. The setup was configured so that the released ammonia would be in the liquid phase when it reached the exit plate.

The field experiment recorded data on flow and temperature from the release, along with meteorological data and video recordings of the release. Concentrations were monitored at distances of 100 and 800 meters from the source.

Once released to the atmosphere, the liquid flashed into a two-phase jet of gaseous ammonia and liquid ammonia drops. Two cross-jet lines of monitors were positioned at 100 meters and 800 meters. Additional monitors were positioned at much greater distances, but failed to collect significant data. Monitors at the 100 meter distance were placed with a horizontal spacing of 15.24 meters. At the 800 meter distance the horizontal spacing was 100 meters. (Christopher G. DesAutels, 2010) (Goldwire, 1985).

*2D Test case: mesh description*

In order to better understand the behavior of the DPM under specific conditions, a 2D mesh has been designed. The mesh is a 3 meters high and a 5 meters long rectangle, with an injection at 1.5 m from the ground. The cells are about 660,000, and are thicken near the droplet release, allowing every simulation to compute 200 droplets from a 1 cm release (Figure 0-1).

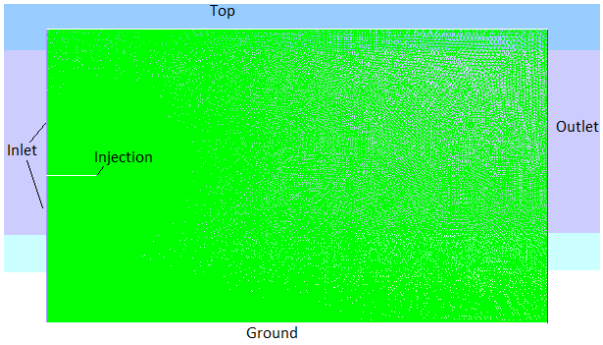


*Figure 0-1: 2D mesh*

The boundary conditions used for this case are: velocity inlet for the inflow, pressure outlet for the outflow, wall for the ground and top, and velocity inlet for the droplets release.

*2D mesh validation*

When a simulation has to be performed the first step is to check the independence of the results from the mesh size: the cell number can not influence the results. In order to choose the best grid, 3 grids have been designed: 130000 cells grid, 660000 cells grid and a 2700000 cells grid.

The first grid was designed applying a structure function starting from the nozzle (which cell number had been set to 100) and defining the maximum cell size. With this method has been designed the 130000 cells mesh. The 660000 and 2700000 cells mesh were obtained thanks to the "Adapt" option (Fluent user manual) which sets a node in the middle of the cells, resulting with the quadruplication of the number of cell per every adaption. Figure 0-2and Figure 0-3 show the comparison of the ammonia mole fraction in two directions.

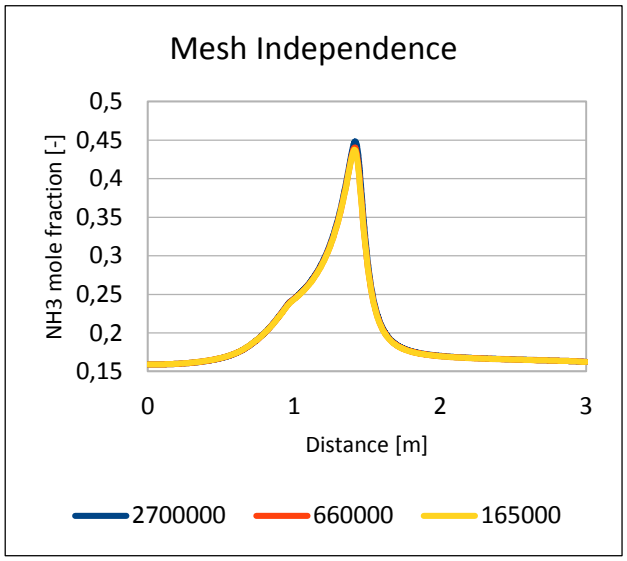


*Figure 0-2: Ammonia mole fraction along y axis*

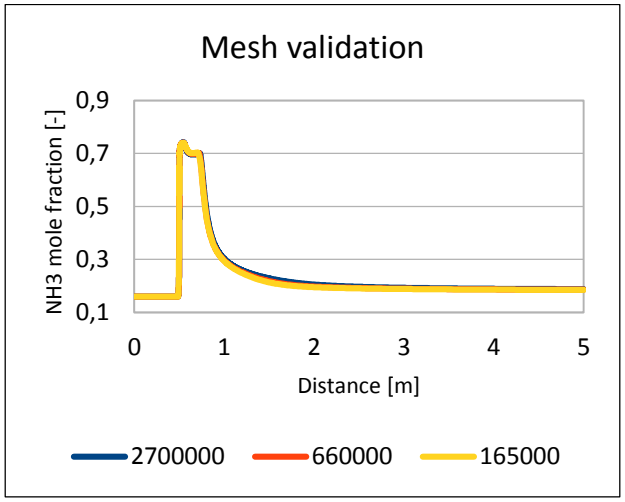


*Figure 0-3: Ammonia mole fraction along x axis*

*Test case: settings description*

With the objective to understand the behavior of the Discrete Phase Model, many simulations were performed emphasizing the sensitivity of the model to the boundary conditions, because was noticed the non physical droplet temperature was reached under some conditions. Tab. 1 shows the

properties used to describe the mixture template. Tab. 2 shows the properties defined for the fluids description. The properties followed by * are the standard functions in Fluent. The only customizable property is the piecewise-polynomial describing the ammonia , due to the improper range of temperature described by the standard function.

| | Case description |
|---|---|
| Type | Pressure based |
| Velocity formulation | Absolute |
| Energy | On |
| Viscous | Standard $\kappa - \varepsilon$<br>Standard wall function<br>Full buoyancy effects |
| Species transport | Diffusion energy source |

*Tab. 1: Mixture properties description*

| | Air | Ammonia |
|---|---|---|
| Viscosity | Constant* | Constant* |
| $C_p$ | Piecewise-polynomial* | Piecewise-polynomial |
| Thermal coeff. | Constant* | Constant* |

*Tab. 2: Fluid property description*

| | |
|---|---|
| Density ( Kg/m3 ) | 683 |
| Cp ( J/Kg K ) | -5311.9 + 121.71 $T$ – 0.5051 $T^2$+ 0.0007 $T^3$ |
| Thermal conducivity (W/m K) | 0.665 |
| Latent Heat ( J/Kg ) | 1368293 |
| Vaporization temperature ( K ) | 100 |

*Tab. 3: Drolet functions*

The description of the droplets (see Tab. 3) was performed following the DIPPR (Design institute of physical property data) database, with constant parameters, except the saturation vapor pressure which was described with a piecewise linear function.

Many aspects were analyzed: Tab. 4 summarizes all the cases and their differences.

| | Droplet. Temp. | Release NH3 conc. | Inflow NH3 conc. | DPM bound. Cond. | Inflow mixt. temp |
|---|---|---|---|---|---|
| Case1 | 238 | 0.16 | 0.16 | Escape | 300 |
| Case 2 | 240 | 0.16 | 0.16 | Escape | 300 |
| Case 3 | 238 | 0.16 | 0.16 | Trap | 300 |
| Case 4 | 240 | 0.16 | 0.16 | Trap | 300 |
| Case 5 | 238 | 0.53 | 0.53 | Escape | 300 |
| Case 6 | 238 | 0.53 | 0.53 | Escape | 300 |
| Case 7 | 238 | 0.16 | 0.16 | Wall-film | 300 |

*Tab. 4: Cases settings*

### *2D Test case: results and discussion*

Many issues regarding the minimum temperature reached by the systems were encountered during the simulations. In order to understand the behavior of the DPM was performed a sensitivity analysis.

The comparison of the results between Case 1 and Case 2 led to deeply different results in terms of droplet temperature, despite the only difference refers to the droplet injection temperature: the minimal droplet temperature reached in case 1 is below the boiling temperature and is 212,14 K, on the other hand the minimal temperature reached in Case 2 is 239.85 (which is the boiling temperature set for the ammonia). The reason of this lays in the different laws taken into account in the calculations; the equations used do not allow to the droplet to reach a lower temperature then the boiling point.

The same conclusion can be reached analyzing the results gained with Case 3 and Case 4, the only difference, compared to the previous, is

the adoption of the Trap boundary condition. In these simulations another aspect must be taken into account: the Trap conditions forces the instantaneous evaporation of the liquid phase as the droplet reaches the boundary.

This behave led to inconsistent air temperature (1 K in both cases) and also affected the droplet temperature only in Case 3 (due to the equation applied).

| | Droplet minimum temperature | Air minimum temperature |
|---|---|---|
| Case 3 | 183 K | 1 K |
| Case 4 | 239.85 K | 1 K |

*Tab. 5:minimum temperatures*

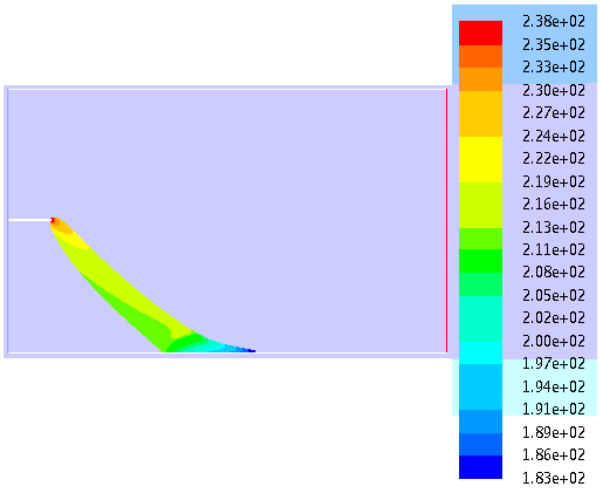


*Figure 0-4 Droplet temperature Case 3*

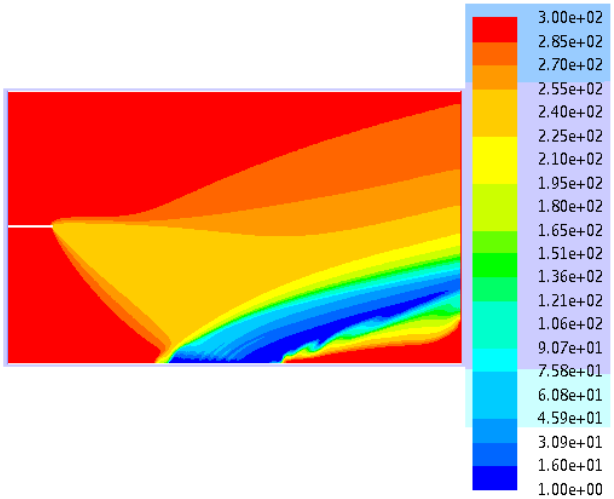


*Figure 0-5: Air temperature case 3*

The only way to quench this shortcoming is to impose the lower limit temperature of the system.

Case 5 and Case 6 were performed in order to check the correspondence of the lower temperature reached with the vaporization pressure:

| | Droplet release temperature | $NH_3$ minimum concentration allowed | Droplet minimum temperature |
|---|---|---|---|
| Case 1 | 238 | 0.16 | 212 |
| Case 5 | 238 | 0.53 | 226 |
| Case 6 | 238 | 0.9 | 236 |

*Tab. 6*

The same results can not be reached with the Trap boundary condition due to the effect of the cooling air. Comparing the results obtained with cases 1, 5 and 6 was proved the respect of the Raoult law in order to describe the equilibrium temperature between the liquid and vapor ammonia phase, moreover, this consistent behavior underlines that the temperature issues analyzed with the previous cases are caused by bug of the Ansys fluent.

In Case 7 the wall-film boundary condition was tested. This type of boundary condition requires the switch to a unsteady simulation. In this situation the DPM shows its stochastic behavior.

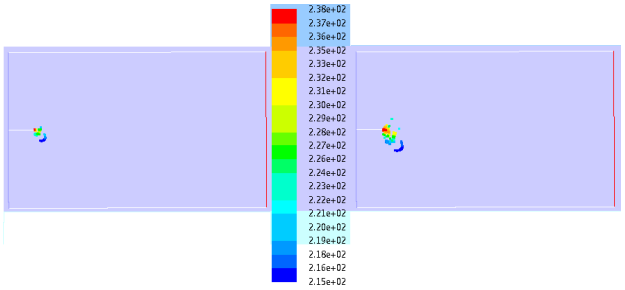

*Figure 0-6: Droplet Temp at time 0.1 and 0.2 sec*

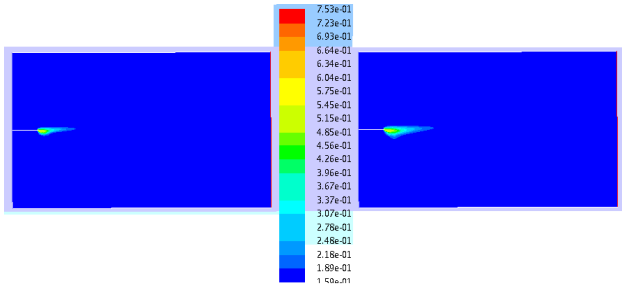

*Figure 0-7:Ammonia mole fraction at time 0.1 and 0.2*

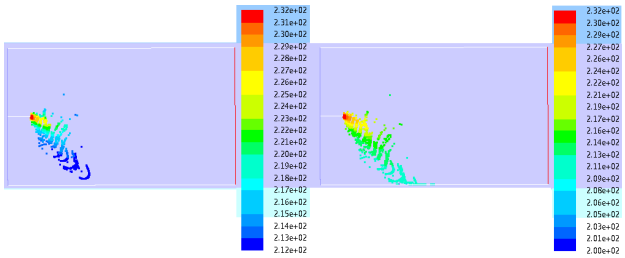

*Figure 0-8: Droplet Temp at time 0.8 and 0.9 sec*

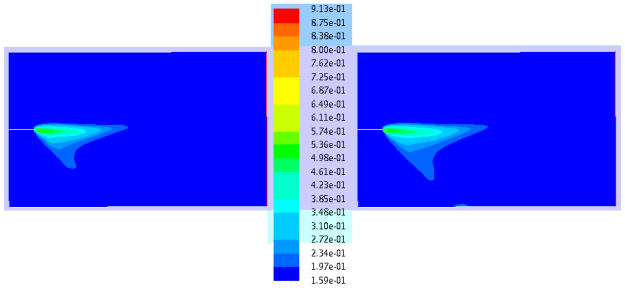

*Figure 0-9: Amonia mole fraction at 0.8 and 0.9 sec*

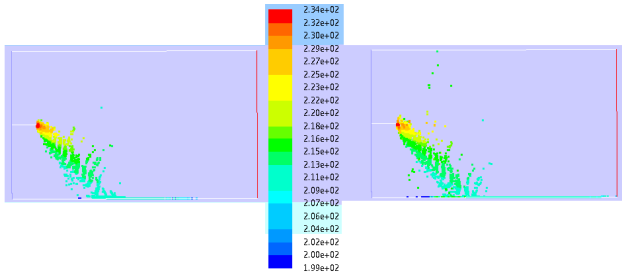

*Figure 0-10: Droplet Temp at time 1 and 1.2 sec*

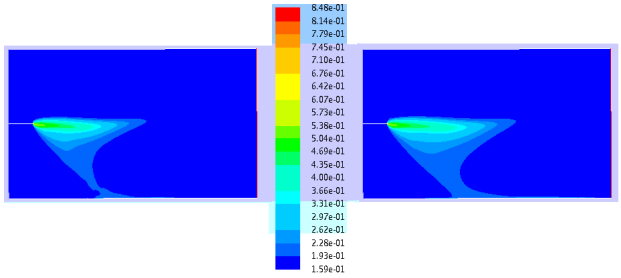

*Figure 0-11: Ammonia mole fraction at time 1 and 1.2 sec*

As long as the droplet follows its trajectory, the temperature drops according to the heat balance due to evaporation. From Figure 0-8 to Figure 0-11 is shown the formation of the pool: the droplets still cool down due to evaporation. The simulation stops when the pool widen and starts to escape from the outflow boundary. The minimum temperatures reached by the system at every time step are listed below:

From Figure 0-7 to Figure 0-11 the ammonia mole fraction at every time step is shown, as long as the droplet are injected the plume widen. Particular attention must be paid at time 0.9 sec: can be noticed the increase of the ammonia near the ground, this is due to the formation of the pool, which can be seen in Figure 0-8.

### *3D case settings*

Four cases were described in order to reproduce the Desert Tortoise experiment, Case 1 and Case 2 are made with the same general settings of the 2D cases, Case 3 and Case 4 are made with the settings shown in Table 7 and 8:

| Air + NH3 mixture | |
|---|---|
| Density | Ideal gas |
| Cp | Mixing-Law |
| Thermal conducivity | Mass-weighted mixing law |
| Viscosity | Mass-weighted mixing law |
| Mass diffusivity | Kinetic – theory |
| Thermal diff. coefficients | Kinetic – theory |

*Tab. 7:mixture definition*

| | |
|---|---|
| NH3 (l) | Property temperature dependence |
| Density ( Kg/m3 ) | 683 |
| Cp ( J/Kg K ) | -5311.9 + 121.71 $T$ – 0.5051 $T^2$+ 0.0007 $T^3$ |
| Thermal conducivity (W/m K) | 0.665 |
| Latent Heat ( J/Kg ) | 1368293 |
| Vaporization temperature ( K ) | 100 |
| Boiling Point ( K ) | 239.85 |
| Volatile component fraction ( % ) | 100 |
| Binary diffusion coefficient ( m2/s ) | 3.05e-05 |
| Saturation vapor pressure (Pa) | -1E+07 - 196704 $T$ – 909.48 $T^2$ + 1.4137 $T^3$ |

*Tab. 8:Droplet functions*

### *3D case mesh validation*

The domain is 900x200x200 m3 (respectively: lenght, width, height).Only half domain of the Desert Tortoise was modeled in order to save computational effort. So that, the release surface is a half circle with a diameter of 0.53 m at 0.79 m height; it is also used as the injection for the NH3 droplets with the DPM. A 1 meter long solid part is shaped at the release in order to soften the turbulence that would be created just placing a surface, the rest of the domain is empty. The inlet is modeled as a velocity inlet with a user defined function for the description of the velocity field, the outlet is a pressure outlet, the top and the sides are symmetry planes, the ground is a wall with a roughness of 0.03 m. The resolution of the mesh is about 1250000 cells. Figure 0-12 shows the 3D mesh. Figure 0-13 shows a particular of the injection surface.

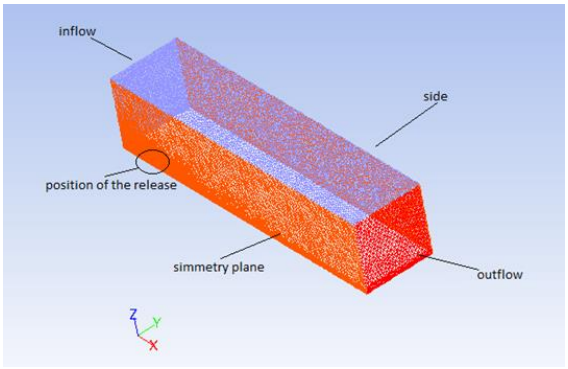


*Figure 0-12: 3D case*

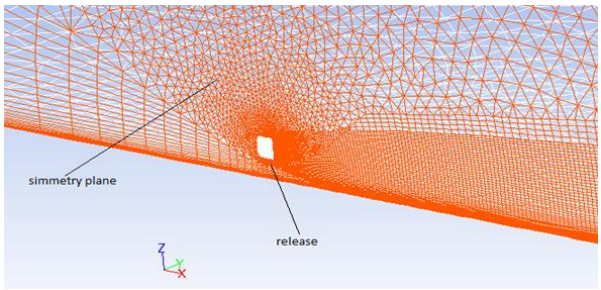


*Figure 0-13: 3D case injection particular*

It can be seen in the particular that the mesh was built with a particular structure: the first 15 meters (from the bottom) has been designed with parallelepiped cells, because the flow was anticipated to be smooth and regular in front of the release. The rest of the domain is made with exagonal cells in order to reduce the number of cells within the domain.

In order to validate the results gained with the mesh described a new mesh was obtained thanks to the “adapt” option provided by Fluent ( see a fluent user manual). The result is a mesh with about 10,000,000 cells. The comparison between the two meshes is shown in Figure 0-14: the plot regards the ammonia molar fraction along the x axis. By the comparison of the graphs is possible to assume the independence of the results from the mesh.

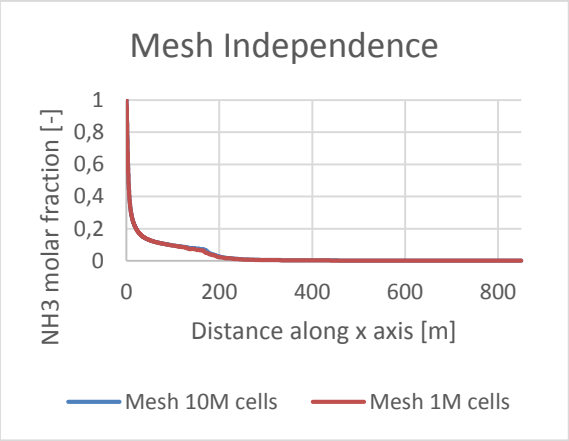


*Figure 0-14: ammonia molar fraction along x axis*

*Case 1 and Case 2*

For these cases the same settings of the 2D test cases have been used. The simulations regard the comparison between a case set up considering the Escape (case 1) boundary condition and the Trap (case 2) boundary condition. The problems regarding the temperature persist, indeed, the temperatures are:

| | Droplet temp. [K] | Air temp. [K] | Rain-out |
|---|---|---|---|
| Case 1 | 159 | 201 | 68 % |
| Case 2 | 1 | 1 | 75 % |

*Tab. 9: minimum temperatures reached by cases*

The results gained thanks to these two cases led to not accurate results: both the width and the altitude of the plume are not correctly predicted, the plumes generated are too light and too narrow compared with the experimental data. This results force the definition of a new series of cases.

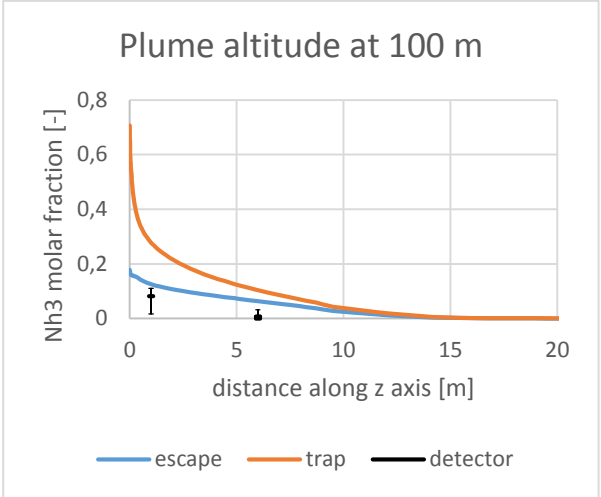


*Figure 0-15: Case 1 and2, molar conc ammonia at 100 m along the z xis*

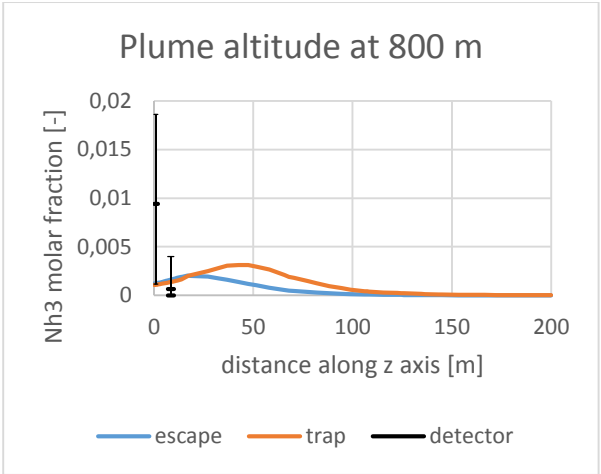


*Figure 0-16: Case 1 and 2, molar concentration of ammonia at 800 m along the z xis*

*Case 3 and Case 4*

The new settings deeply influenced the results gained: now the plumes are lower and wider, this means that the temperature field is influencing the species field through the density. The most important aspect that changes with the different description of the release is the rain out: see table 10.

| | Droplet temp release [K] | Calculated Rain-out | Experim. Rain-out |
|---|---|---|---|
| Case 3 | 240 | 80 % | 40% |
| Case 4 | 238 | 30 % | 40% |

*Tab. 10: Calculated and expected rainout*

The comparison between the two cases led to appreciable results: as long as we consider section more and more distance from the release the effect of the different description of the source is less and less important; at 100 m the plume in Case 4 is wider and lower then Case 3. See Figure 0-17 and 0-18.

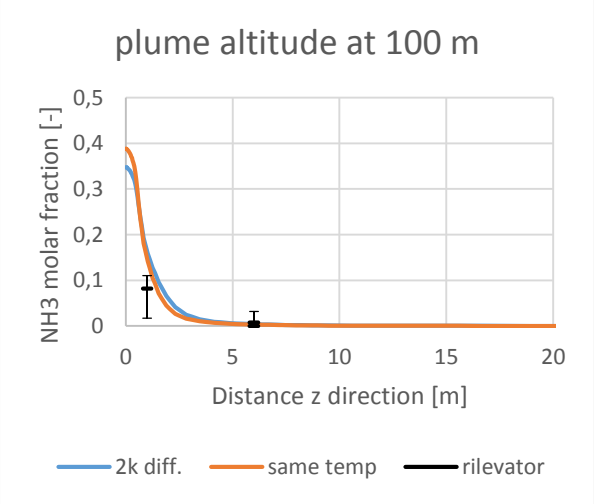


*Figure 0-17: Case3 and 4, molar concentration of ammonia at 100m along the z xis*

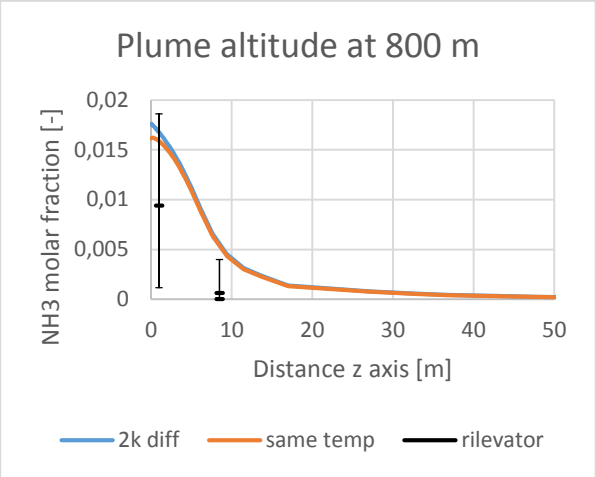


*Figure 0-18: Case 3 and 4, molar concentration of ammonia at 800 m along the z xis*

The reason that led to an improve of the results must be found in the definition of the properties temperature dependent.

The results gained were checked with the method of the Parabola plot (Hanna & Chang, 1993). The method lays on the calculation of two parameters gained by the ratio between the experimental data and the results gained, these parameters are the geometric mean bias (MG) and the geometric variance (VG)

Geometric mean bias (MG) values of 0.5- 2.0 can be thought of as a "factor of two" over predictions and under predictions in the mean respectively. A geometric variance (VG) value of about 1.5 indicates a typical of two scatter between the individual pairs of predicted and observed data. If there is only a mean bias in the predictions and no random scatter is present, then the relation $(lnVG) = (lnMG)^2$, is valid, defining the minimum possible value of VG for a given MG.

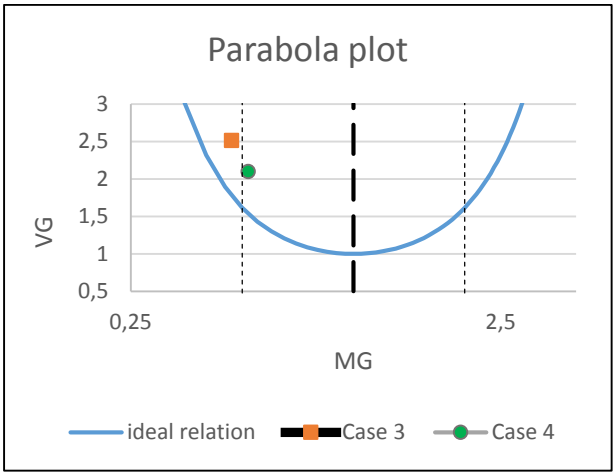


*Figure 0-19: case 3 and case 4 parabola plot*

The parabola plot confirms the supposition mad analyzing the plots: the Cases tend to overestimate the results, Case 4 has a geometric mean higher then 0.5, case 3 has a MG lower then 0.5 this means that case 3 over estimates the results more then 2 times. Case 1 and case 2 led to results so non predictive that result with values of MG bigger then 500.

*Conclusions*

The purpose of this work is to set up a case able to reproduce the experimental data of the Desert Tortoise experiment. The goal has been reached after the study of the Discrete Phase Model, which is a stochastic model that works in a Lagrangian frame. The results from the 2D test case led to understand the main problem of the model: the laws that describe the physic of the problem are depending of the release temperature.

When droplets, below the boiling point, are injected into the domain their temperature drop can not be limited by the proper description of the condensation and solidification (temperatures reach 1 K), the method to avoid this inconsistence is either to limit the lower temperature of the system or to describe the condensation process throw a user defined function.

When the droplets above the boiling point are injected into the domain their temperature is no more related, by a heat balance, to the continuous phase but only the mass loss is calculated (that's why the minimum temperature reached by the droplet is equal to the boiling temperature). Other authors chose this description of the release in order to avoid temperature problems.

An other important aspect that has been taken into analysis is the boundary condition that refers to the DPM the boundary condition analyzed are: Trap, Escape, Wall-film. The Trap boundary condition forces the evaporation of the droplet when it reaches the ground, leading to a temperature drop of the surrounding air (1 K) when a huge rain out is carried out, which is inconsistent. Again, limiting the temperature of the system is the only way to quench this issue.

The Escape boundary condition didn't led to temperature problems, but the mass loss related to the assumption of this condition do not fit the purpose of this work and have been rejected in the description of the 3D case representative of the Desert Tortoise experiment.

The Wall-film boundary condition is the only one that works only in a time dependent simulation. The advantage of this condition is that takes into account all the aspect of the physic of the droplet when reaching the ground: break, pool formation, evaporation, etc… the eventually condensation over the surface of the droplet is still not taken into account.

In order to represent the Desert Tortoise two set of cases have been described: the first set is described with the help of the standard functions set up by Fluent, the second set has been built with the help of the DIIPR data regarding the air and the ammonia, and, where possible, temperature dependent laws have been preferred.

The Cases set up with the less accurate set of settings led to results far from the experimental data in our possess, failing in the prediction of the altitude and the width of the plume. The Introduction of a more accurate set of settings led to a more real-like simulation, which has been analyzed with the Parabola plot method, confirming a overestimation of the results.

In order to achieve a more realistic description a sentivity analysis should be carried on, leading to the choice of those factors and laws more representative of the case analyzed.

# 1 Introduction

The ammonia is one of the most important product of the chemical industry, in the past the ammonia production was the reference to understand the industrial evolution of a country, in fact the world production of ammonia in 2004 was around 109,000,000 tons. The leading force that promoted the ammonia production was to produce fertilizers for corps. Due to this bear the necessary to store ammonia in an efficient way. Three methods exist for storing liquid ammonia:

1) Pressure storage at ambient temperature in spherical or cylindrical pressure vessels having capacities up to about 1500 t
2) Atmospheric storage at 240 K in insulated cylindrical tanks for amounts to about 50000 t per vessel
3) Reduced pressure storage at about 273 K in insulated, usually spherical pressure vessels for quantities up to about 2500 t per sphere.

The first two methods are preferred and is opinion that reduced pressure storage is less attractive.

Analyzing the behavior of ammonia subject to a release from a pressurized vessel we have to take into account many aspect. First we have to consider that the phase released is liquid at the vessel conditions (if we suppose no change phase in the release section set between the stagnation condition and the exit orifice) but at the normal conditions ( T= 1atm, P=101325 Pa) the stable phase is gas. The phase exchange, assisted with the rapid expansion due to the pressurized storage, determine a drop of the temperature which prevents the total evaporation of the liquid phase. Is coarsely possible to divide the zone immediately after the release into two zone to gain a better understanding of the problem. In the first zone the behavior of the compound is mainly determinate by the pressure gradient that sets the momentum at the release and the rapid expansion and evaporation driving the component to the atmospheric pressure and to its minimum temperature, in the second zone the effect of temperature grows leading to evaporation of the liquid phase until reaches the atmospheric temperature. This clarification is important because helps to identify a pseudo-source in which the ammonia is expanded; this theoretical surface will be the source in the CFD calculations. This method is helpful to avoid the description of the distribution of the droplets size that is generated by mechanical friction during the release at the nozzle, so is coarsely possible to define an average droplets size instead of defining the all distribution it is important to underline that the droplet size may have a strong effect on the downstream temperature of the plume.

The other important reason why ammonia must be analyzed is its peculiar behavior: the molecular

weight of ammonia is 17 Kg/mol, that is lighter than air (28,9 Kg/mol). The comparison of the molecular weights yield to anticipate a “light gas” behavior; this is not true due to the two-phase release: the evaporation of the liquid ammonia cools down the temperature of the stream leading to the condensation of the water vapor determining, taking into account the liquid ammonia itself, an increase of the average density. This leads to a plume that doesn’t lift, typical of the “heavy gas”, and, if the liquid mass flow rate is enough, to the formation of a pool. As long we move downstream the entrainment of air, due to the turbulence, becomes predominant, the average density drops, and the plume becomes comparable first to a “neutral gas” (where the vertical dispersion is determined by the vertical gradient of temperature of the air) then to a light gas (where the vertical dispersion is increased by the density gradient between the ammonia and the air).

An area which deserves special attention with respect to safety is the storage of liquid ammonia. In contrast to some other liquefied gases (e.g., LPG, LNG), ammoniais toxic and even a short explosure to concentration of 2500 ppm may be fatal. The explosion hazard from air/ammonia mixtures is rather low, as the flammability limits of 15-27% are rather narrow. The ignition temperature is 924 K. Ammonia vapor at the boiling point of 240 K has vapour density of ca. 70% of that of ambient air. However, ammonia and air, under certains conditions, can form mixtures which are denser then air, because the mixture is at lower temperature due to evaporization of ammonia. On accidental release the resulting cloud can contain a mist of liquid ammonia, and the density of the cloud may be greater than that of air.

In ammonia production, storage, and handling the main potential health hazard is the toxicity of the product itself. The threshold of perception of ammonia varies from person to person and may also be influenced by atmospheric conditions, values as low as 0.4 – 2 mg/m3 (0.5 – 3 ppm) are reported but 50 ppm may easily detected by everybody. Surveys found concentrations from 9-45 ppm in various plant areas.

Exposure to higher ammonia concentration has the following effects: 50 – 72 ppm does not disturb respiration significantly; 100 ppm irritates the nose and the throat; 200 ppm will cause headache and nausea; 2500 to 4500 ppm may be fatal after short exposure; 5000 ppm and higher causes death by respiratory arrest.

The ammonia is a so common use compound that is impossible to gather all the accidents that occured in history. Anyhow, in order to let the reader to better understand the amount of accident in which ammonia was involved is below purposed (Table 1) a summary of ammonia accidents in the United states to which OSHA (Occupational Safety & Health Administration is part of the United States Department of Labor) responded.

| OSHA ENFORCEMENT FINDINGS- ACCIDENTS INVOLVING THE RELEASE AMMONIA | | |
|---|---|---|
| **CALENDAR YEAR** | **NUMBER OF ACCIDENTS** | **NUMBER OF FATALITIES** |
| 2006 | 6 | 1 |
| 2005 | 3 | 0 |
| 2004 | 6 | 2 |
| 2003 | 6 | 2 |
| 2002 | 5 | 2 |
| 2001 | 9 | 3 |
| 2000 | 8 | 3 |
| 1999 | 8 | 2 |
| 1998 | 8 | 3 |
| 1997 | 10 | 1 |
| 1996 | 7 | 2 |
| 1995 | 10 | 2 |
| 1994 | 13 | 5 |
| 1993 | 15 | 4 |
| 1992 | 12 | 1 |
| 1991 | 14 | 2 |
| 1990 | 20 | 4 |
| 1989 | 8 | 1 |
| 1988 | 6 | 2 |
| 1987 | 9 | 1 |
| 1986 | 12 | 2 |
| 1985 | 17 | 1 |
| 1984 | 12 | 4 |
| **TOTAL** | **224** | **50** |

*Table 1: Incidents and fatalities occurred in the United States between 1984 and 2006*

# 2 State of the art

## 2.1 Two phase releases

In many postulated releases from chemical and process plants, the material contained within the plant is ejected through a break as a two-phase jet or cloud which then disperses into the surrounding atmosphere. Estimation of the behavior of released material is necessary for hazard assessment and, for two-phase releases, is obviously more complicated than in the case of single-phase (gas) clouds. Specifically, the liquid phase may be dispersed as small droplets in the flow field, and these droplets evaporate causing changes in the temperature and composition of the surrounding gas. If the surrounding atmosphere is humid, then water vapour may condense on the droplets (which have dropped in temperature due to evaporation) and this gives a further complicating factor in the cloud behaviour. Different approaches, of varying complexity, have previously been taken to predict the behaviour following such releases. The approaches can be divided into three main categories. The first, and simplest, is the `box' model, in which a buoyancy-driven flow in a wind field is regarded as being transported in a cylindrical shape whilst retaining a self-similar internal concentration field, i.e. the concentration distribution always has the same shape when scaled with the cloud radius and height. The cloud can increase in volume by entrainment of air through its boundaries, and can slump under the action of gravity, spreading outward in a manner analogous to that in the classic dam break problem. This allows solution of a system of `lumped' ordinary differential equations for species mass, momentum and energy together with an equation of state. Another category of models is known as `similarity' or `slab' models, such as that due to Colenbrander, and are really extensions to plumes of the `box' approach, which applies primarily to puff releases. For transient plumes, a set of partial differential equations involving time and one spatial dimension as interdependent variables is solved. The third main type of model uses a computational fluid dynamics (CFD) approach in which the equations are discretized and solved in all three spatial dimensions.

### *2.1.1 Theorical background*

We focus here on high-momentum atmospheric releases of a liquefied gas or two-phase fluids through a break or a pressure relief system. The release is supposed to originate from a relatively small hole so that continuous, i.e. quasi-steady, conditions at the outlet can be assumed. The cloud is defined as the smallest control volume containing the contaminant. In its first stage, where its initial momentum

dominates, the cloud will also be referred to as jet. In most cases involving two-phase releases, the flow is choked at the exit and an external depressurization zone, where the pressure decreases down to the atmospheric pressure, is formed. When the exiting liquid is sufficiently superheated with respect to ambient conditions, it is atomized by violent vaporization (flashing atomization). Otherwise, the liquid or two-phase mixture is disintegrated due to liquid surface instabilities (aerodynamic atomization). Downstream from this region, air entrainment at the perimeter of the cloud becomes important, which causes it to further widen. At least for some distance, the cloud may be dense, i.e. heavier than air, as a result of high molecular weight ,e.g. chlorine. or low temperature and airborne droplets ,e.g. evaporating ammonia (Britter, 1989).

The dispersion of the contaminant in the atmosphere can be described in terms of cloud trajectory and dilution. From an integral point of view, the trajectory is given by a momentum balance on the cloud; the main effects involved are cross-wind, gravity and friction on the ground after touchdown. The dilution is controlled by the rate of air entrained in the cloud. Near the outlet, this is governed by the turbulence generated by the jet itself; it is then controlled by atmospheric turbulence when the jet velocity has decreased close to that of the ambient wind. Moreover, the interaction with a cross-wind induces an enhancement of the entrainment rate. In the case of dense clouds, gravity may also have an effect on air entrainment, related to gravity-induced turbulence as well as suppression of atmospheric turbulence due to stable stratification. In the following, the region of passive dispersion due to atmospheric turbulence only is referred to as the far-field and the upstream region as the near-field.

The dispersion process may be significantly affected by the presence of an aerosol phase. First, two-phase releases can lead to much higher discharge mass flow rates than single-phase gas releases (Fauske & Epstein) and, thus, increase the hazard zone distance. Moreover, the jet density may be significantly higher. It can firstly be increased by the mere presence of the liquid phase. However, this is only significant very close to the outlet, where the liquid mass fraction averaged over the jet cross-section is not negligibly small. The aerosol effect on jet density is mainly due to phase change phenomena. When the liquid contaminant evaporates, the jet may significantly cool down and, thus, increase in density. A gas which has a smaller molecular weight than air like ammonia can then behave as a heavy gas. The cooling process may also lead to the condensation of the entrained humidity. If the contaminant is hygroscopic, this can lead to its persistence to significantly larger distances from the outlet. The formation of the aqueous aerosol will cause the mixture to warm up more rapidly and have less density (Wheatley, 1986). Furthermore, a part of the liquid may not remain airborne in the jet and fall to the ground where an evaporating pool could build up; such a pool may also be formed from the jet impingement on a surface. This so-called rainout could induce a drastic reduction of the

downstream contaminant concentration but increases the danger close to the source as well as the duration of the dispersion. Besides, it may lead to soil contamination. Finally, the presence of the aerosol also affects the turbulent structure of the jet and, therefore, the air entrainment, the direction of influence (enhancement or suppression). depending on the particle size.

## 2.2 TWO PHASE DISPERSION MODELS

The dispersion models which take into account the presence of an aerosol phase have appeared only recently ( in the last twenty years) in the literature. They are either integral or multidimensional models. Integral models are obtained by integrating the balance equations for mass, momentum, energy and species over the cloud cross-section. The lateral variations of the local variables, such as velocity, concentration and temperature, can be obtained by introducing lateral profiles in the integrated balance equations. If these profiles are flat 'top-hat' profiles., the model reduces to the so-called 'box' model. Non uniform profiles, which are supposed to be geometrically similar after a zone of flow establishment, can also be adopted. In multidimensional models, the local time-averaged equations of mass, momentum, energy and species are locally solved in the whole space. Unlike the integral models where turbulent diffusion is implicitly given through the profile shape function, closure must be provided for turbulent stresses.

Because of the high variety of possible situations to be considered in hazard assessment, but which cannot or have not been covered by experiments, the dispersion models are often extrapolated beyond the range where they have been validated. The need for physically-based models is, therefore, very important to increase the reliability of this extrapolation. Moreover, due to the frequent need to study a large number of scenarios, a compromise between model detail and computing time/cost is often required. These conditions are best fulfilled by one-dimensional _integral or box. models, which can be in most cases helpful. However, in some situations associated with obstructed terrain, multidimensional models could be recommended, as it is shown, e.g., (Wurtz, Bartzis, & Venetsanos). They are however complex, costly to run and often faced with numerical difficulties, and require a high degree of expertise.

In the following description, every necessary jet property at the outlet, such as the mass flow rate, is supposed to be known. However, within a short distance just downstream from the outlet, the flow can experience drastic changes which must be considered for subsequent dispersion calculations. The physical phenomena taking place in this region comprise (i). flashing if the liquid is sufficiently pressurized, (ii). Gas expansion when the flow is choked and (iii). liquid fragmentation. The corresponding quantities to be determined as initial conditions for subsequent dispersion are the flash

fraction, the jet mean temperature, velocity and diameter, and the drop size. Due to its relatively short length, a global and simplified modelling approach is normally adopted in this region, also in the case of multidimensional models. Therefore, these initial conditions are first described, followed by the description of the integral and multidimensional dispersion models.

### *2.2.1 Flashing*

Flashing occurs when the liquid is sufficiently superheated at the outlet (with respect to atmospheric conditions). and corresponds to the violent boiling of the jet. The vapor quality after flashing, or flash fraction, is most often determined in the models by assuming isenthalpic depressurization of the mixture between the outlet and the plane downstream over which thermodynamic equilibrium at ambient pressure is attained, i.e., any transfer with the surroundings as well as the kinetic energy change are neglected; the temperature reached is the saturation temperature at atmospheric conditions. It should be noted that this calculation is applied in the models as soon as the liquid is superheated.
In this approach, the neglect of the kinetic energy change seems to be justified due to the large contribution of the heat of vaporization in the energy equation (Wheatley, 1986). However, a more general expression, where this assumption is relaxed, is recommended by (Britter R. E.). Adiabatic and frictionless conditions as well as the absence of air entrainment are reasonable approximations provided that the distance up to the point where thermodynamic equilibrium at atmospheric pressure is reached, is short enough. Atmospheric pressure is in general attained after a flow length of about two orifice diameters and the flashing phenomenon is observed to occur very fast so that these assumptions should be met in practice. When the liquid is not sufficiently superheated for flashing atomization to occur, the flow path before thermodynamic equilibrium is restored, could be greater. However, the degree of non-equilibrium being low in this case, the above assumptions should still be acceptable.

### *2.2.2 Expansion*

When the flow is choked at the outlet, the gas phase expands to ambient pressure within a downstream distance of about two orifice diameters. This causes a strong acceleration of the two-phase mixture and usually an increase of the jet diameter. In the models, the velocity and diameter of the jet at the end of the expansion zone are given by the momentum and mass balance, respectively, integrated over a control volume extending from the outlet to the plane where atmospheric pressure is first reached. It is assumed that no air is entrained in this region. An alternative model based on isentropic expansion has been proposed by Woodward (Woodward, 1992). This led to substantially different results.

This control volume approach, which cannot provide the variations within the expansion zone, appears to be suitable in view of its short length. The absence of air entrainment is also justified by the strong lateral expansion. Because of the lack of experimental data, the alternative predictions obtained by using the model of Woodward could not yet be validated. Finally, it should be noted that the flow speed can be increased by a factor as high as 10 in this region, which has important consequences on the downstream dispersion (Wheatley, 1986).

### *2.2.3 Expansion zone: source of the CFD domain*

Flashing is violent break-up of the pressurized liquid into small droplets which occurs when a super-heated liquid comes in contact with ambient conditions (atmospheric temperature and pressure) at a point of a leak. The combination of hydrodynamic instabilities and thermal non-equilibrium conditions lead to flashing. The meta-stable liquid can only come to its equilibrium condition by releasing its super-heat through evaporation which consists of boiling and vaporizing of the droplets as they disperse in ambient air and provide an explosive characteristic to the process. Fig. 2-1. shows a schematic representation of a flashing liquid jet issuing from a circular nozzle. The flashing location depends upon the geometry of the leak, initial conditions and the liquid properties. In Fig. 2-1 flashing is shown occurring outside the nozzle but flashing may begin inside the pipe or vessel. It has been observed experimentally that the 'expansion' region is made up of large droplets and liquid ligaments moving with increasing velocity. The velocity starts to decrease in the entrainment region due to mixing with ambient air as jet propagates. The axial temperature keeps decreasing well below the boiling temperature at ambient pressure further downstream and reaches its minimum as droplets evaporate. Beyond this point the temperature rises to ambient value. The droplet sizes and velocity mean values also decrease due to evaporation in the entrainment region. The radial variation of droplet size, temperature and velocity at different locations along the axis of the jet shows approximately Gaussian distribution. The foregoing flow behavior shows that the flashing region is a complex problem and the transition between initial superheated liquid state and the following two-phase jet is not well understood. However, varying combinations of boiling and evaporation processes are present alongside severe mechanical break-up of droplets and turbulent mixing between the jet constituents and between these and the ambient air.

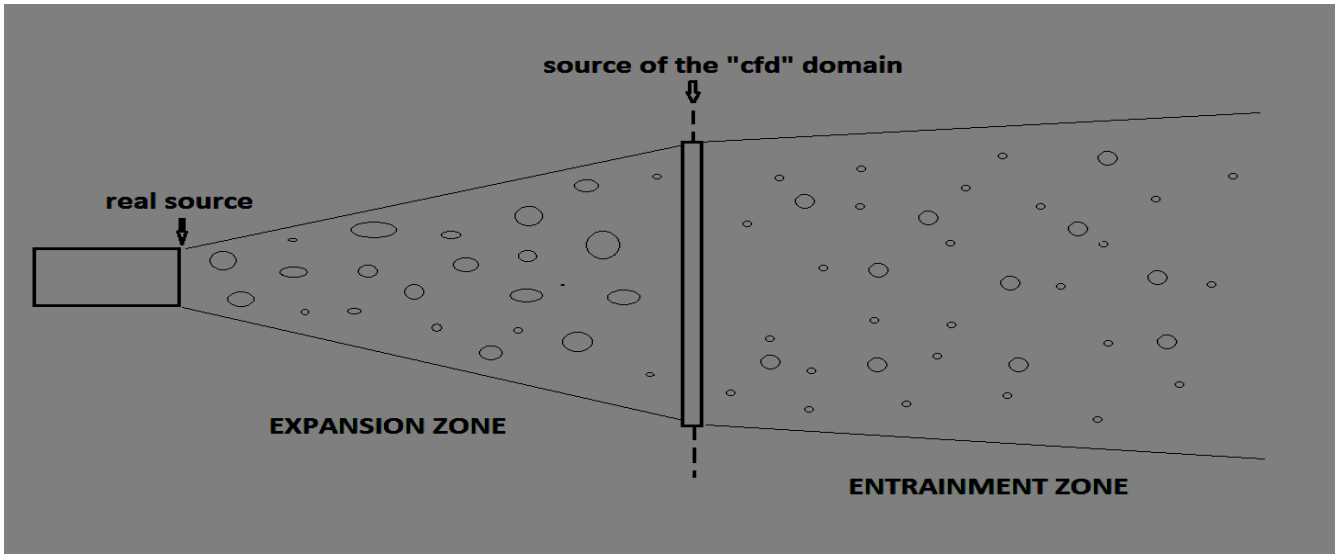


*Fig. 2-1: Schematic rapresentation of the expansion zone*

When the flow is choked at the outlet, the gas phase expands to ambient pressure within a downstream distance of about two orifice diameters. This causes a strong acceleration of the two-phase mixture and usually an increase of the jet diameter. In the models, the velocity and diameter of the jet at the end of the expansion zone are given by the momentum and mass balance, respectively, integrated over a control volume extending from the outlet to the plane where atmospheric pressure is first reached. It is assumed that no air is entrained in this region. An alternative model based on isentropic expansion has been proposed by (Woodward., 1992). This lead to substantially different results. This control volume approach, which cannot provide the variations within the expansion zone, appears to be suitable in view of its short length. The absence of air entrainment is also justified by the strong lateral expansion. Because of the lack of experimental data, the alternative predictions obtained by using the model of Woodward could not yet be validated. Finally, it should be noted that the flow speed can be increased by a factor as high as 10 in this region, which has important consequences on the downstream dispersion (Wheatley, 1986)

### *2.2.4 Drop Size*

The models incorporating fluid dynamic and thermodynamic non-equilibrium phenomena, like rainout or droplet evaporation, require sub models for the determination of the initial drop size. There are basically two main mechanisms for atomization: flashing and aerodynamic atomization. With flashing atomization, the fragmentation results from the violent boiling and bursting of bubbles in the superheated liquid, whereas aerodynamic atomization is the result of instabilities at the liquid surface. Most authors do not use any specific criterion to determine which mechanism dominates and

deliberately select one of them. Nevertheless, (Ianello, Rothe, & Wallis, 1989) use a mechanistic criterion based on a critical superheat corresponding to the activation of a nucleation site. It requires, however, the specification of a characteristic nucleation site radius for which reliable predictive relations are not available consider that the actual regime is the one which predicts the smallest stable drop size. A comparison of these criteria with available empirical relations relying on experiments with low velocity jets (Brown, 1962) could be fruitful. In any case, more studies on this transition region where both fragmentation regimes may play a role are clearly needed. In the case of aerodynamic fragmentation, the maximum stable drop size is usually given by a critical Weber number, which represents the ratio of inertia over surface tension forces:

$$We_{max} = \Delta U^2 \rho_g d_{max}/\sigma \qquad (2.1)$$

where $\sigma$ is the (static) surface tension of the liquid, $\rho_g$ the gas density,$d_{max}$ the maximum stable droplet diameter and $\Delta U$ the mean relative velocity between both phases. In the models, $\Delta U$ is calculated as the jet mean absolute velocity at the end of the expansion zone in the case of choked flow conditions and the subcritical outlet velocity otherwise. This implies that interfacial stress occurs at contact with the surrounding still air, which is justified in the case of a single-phase liquid jet. However, if a two-phase choked flow were to occur at the outlet, the fragmentation will be induced by the shear stress between the liquid and the accelerating released gas and, thus, a more appropriate relative velocity should be based on the difference between the jet velocity at the end of the expansion zone _representative of the gas velocity. and the exit velocity (representative of the liquid velocity). Moreover, the number $We_{max}$ default values ranging are between 17 and 44, with a possible dependence on stagnation pressure (or exit velocity), have been tested by (Muralidhard, 1995); their best prediction for the liquid capture on the ground was obtained with the value of $We_{max}$ depending on pressure. The experimental observations provide maximum Weber values between 5 and 20 for low-viscosity liquids, with the most commonly used value being 12. The value of 20 can be deduced from a balance on the drop between drag and surface tension forces with a drag coefficient of 0.4, which is an acceptable approximation for a rigid sphere in the turbulent regime ($We_{max} = \Delta U \quad d_{max}/\mu_g$between 500 and $2E5$) as long as the relative velocity is small enough compared to the speed of sound. This is an upper limit for the maximum stable droplet diameter $d_{max}$ since in reality the particle is deformed and experiences a higher drag during the fragmentation process.

For the flashing atomization, (Ianello, Rothe, & Wallis, 1989) propose a mechanistic model based on a Weber number where the characteristic relative velocity $\Delta U$ is composed of two components, in the axial and radial direction, respectively. The axial component is due to the vapour acceleration in the expansion zone; the relative velocity is taken as the difference between the jet velocities at the end

and at the beginning of this zone. The radial component comes from the momentum transfer caused by the rapidly growing bubbles; it is given by the maximum bubble expansion velocity. On the other hand, (Woodward, 1992) have established a correlation for the maximum stable diameter to match rainout experimental data. As indicated by the authors, this relation may not necessarily agree with values measured independently because of incompleteness in some other parts of the dispersion model. Among the relations they considered, the one depending on a so-called 'partial expansion energy', which is a measure of the superheat, gave the best results. Moreover, some authors adopt constant default values for the drop size based on experimental results. They usually range between 10 and 100 μm (Pattison & Martini). Moreover, it should be noted that if flashing occurs upstream from the orifice (e.g. in a long pipe), the different flow regimes at the exit could lead to specific fragmentation processes, as shown by the drop size data obtained for the aerodynamic fragmentation of a dispersed-annular flow regime.

Regarding the assumed drop size distribution, every model considers a unique equivalent size except (Ianello, Rothe, & Wallis, 1989) who adopt a log-normal distribution and (Pereira & Chen) who use two size classes. The assumption of one-size droplets is obviously contrary to observations but simplifies the matter. A sensitivity analysis regarding this assumption should, however, be performed. Finally, other authors have shown (Kukkoken, 1993), due to compensating effects, the droplet evaporation rate does not strongly depend on the initial drop size below 100 mm. On the other hand, the results of other authors show (Muralidhard, 1995) that the rainout fraction is very sensitive to the initial drop size.

### *2.2.5 Integral model*

Integral models can either deal with both the near-field and far-field or consider the near-field only. In the latter case, they are regarded as source term for a far-field dispersion model. However, they are similar in principle Some of these models can handle ground-level clouds, i.e., clouds in contact with the ground.

The models are all based on the balance equations for mass, momentum, energy and species, integrated over the jet cross-section; they mainly differ by the adopted closure relations. A common frame based on the mixture balance equations is first proposed to enable a comparison between the models. Then, the closure relations, or sub models, are described.

### *2.2.6 Cloud thermodynamics*

The enthalpy of the jet (mean or centreline value). is given by the two-phase mixture enthalpy balance equation. However, additional relationships are necessary to determine how the overall enthalpy change affects the jet composition and temperature. The jet is a mixture of the released material (liquid and/or vapour)., dry air and, for all considered models but the one of Woodward et al., ambient humidity (liquid and or vapour). Most often, the overall mixture enthalpy is expressed as a function of the enthalpies of the jet components by assuming that the mixture is in thermodynamic equilibrium. Gas and vapour are supposed to behave as an ideal gas. The partial pressures of the released material and the water are usually supposed to be given by their respective vapour pressure at the jet temperature (ideal mixture). The mass and enthalpy equation are separately written for the liquid and gas phases. When ambient humidity condensation is considered, the liquid water is either included in the liquid phase leading to binary droplets or added in the gas phase to form a fog. Heat and mass transfer coefficients are introduced for transfers at the drop surface so that drops and gas or fog can adopt different temperatures.

Kukkonen et al. checked the homogeneous equilibrium model predictions with those of a non-equilibrium approach (different velocities and temperatures for the droplets and the surrounding gas) in the case of two-phase ammonia cloud dispersion in dry and moist air. They concluded that the homogeneous equilibrium approximation seems to be adequate for droplet sizes lower than 100 μm. However, it is noted that this conclusion is only valid as far as the vaporization rate is concerned and may not apply to rainout. It may also not be valid for cases where entrainment is fast, as in the high momentum region of a jet. Moreover, Kukkonen et al. tested the effect of an introduction of ammonia/water interaction in the phase equilibrium. The assumption of non-ideal behaviour of the mixture lowered the volatility of the liquid phase, but exhibited no significant influence on the average temperature. It had, however, the effect of maintaining a low contaminant concentration much further downstream from the source. These authors also performed calculations with the assumption of zero and 100% ambient relative humidity. The difference in temperature could in some part of the dispersion reach 20 K. Similar calculations with Wheatley's model in the case of ammonia with zero and 100% ambient relative humidity have been also performe. The difference in the jet density and concentration for these extremes was less than 10%. However, the results were restricted to the near-field where gravity effects were not considered significant.

### *2.2.7 Rainout*

As explained by (Wheatley, 1986), provided that the drops are large enough, they are affected by gravity to a greater extent than the surrounding gas. The drops do not remain the same size during

their motion but steadily evaporate as the surrounding vapour is diluted by air. From the spectrum of drop sizes formed initially, some drops may be large enough that they fall out of the jet rapidly with no appreciable vaporization, while others may be small enough that they evaporate before reaching the ground. The quantity of rainout is a very important item for dispersion calculations. The description of this complex phenomenon is, however, circumvented by most modelers by assuming that the drops are sufficiently small to remain airborne until complete evaporation. Wheatley has devised a simple criterion for the absence of rainout, leaving aside the problem of what to do otherwise. From the maximum stable drop size in the initial section, the maximum gravitational settling velocity can be found from a force balance. By taking the drop axial velocity equal to the mean initial jet velocity (after the expansion zone), a bound for the initial drop trajectories can be defined. If it subtends a sufficiently small angle with the jet axis (taking it to be horizontal), this implies that rainout can be ignored. Other authors (Ianello, Rothe, & Wallis, 1989) extended this approach by applying the above criterion to the whole spectrum of drop sizes. This enables the fraction of liquid which rains out to be calculated. A more sophisticated approach has been proposed by (Woodward, 1992). The aerosol consists of single-sized spherical droplets. The local droplet diameter and trajectory is obtained by solving the balance equations on the drop for mass, energy and momentum in the vertical direction, simultaneously with the gas jet mean quantities. The horizontal drop velocity is set equal to the horizontal component of the local velocity in the jet, although in a previous version slip velocity was allowed for in the horizontal direction. Rainout occurs when the drop hits the ground. An other author (Muralidhard, 1995) proposed another simple criterion. The liquid phase is supposed to be well mixed within the jet. Rainout is considered to occur when the jet centreline hits the ground (the liquid phase due to ambient humidity condensation is however supposed to remain airborne in the jet). In accordance with the no-slip assumption made in the models, the drop inertia in the axial direction is not taken into account. Consequently, a relatively large drop which is not predicted to rainout according to Wheatley's approach, or which will fall out at a certain distance as predicted by Woodward's model, may eventually rainout further downstream.

- Transition criteria

Generally, for some specific conditions, the model application range is exceeded or some model relationships must be modified. These conditions correspond to physical transitions for which criteria must be provided. First, a transition between elevated and ground-level clouds must be specified. This simply occurs when the lower boundary of the jet reaches the ground. Moreover, for models which apply only in the region dominated by the initial jet momentum where gravity as well as atmospheric turbulence have no significant effect, transitions towards these regimes must be given. Must be

adopted the following criteria to determine when the dispersion is not dominated by the initial momentum any more:

$u_m/u_a \leq 0.8$ Pasive dispersion important

$Ri = |\rho_m - \rho_a| gD/\rho_m u_m^2 \geq 0.1$ Buoyancy effects important

where *D* is the jet cross-section diameter and Ri the Richardson number of the jet which represents the ratio of jet buoyancy over jet inertia. Equivalent criteria are mentioned by the other authors when needed.

### *2.2.8 Multidimensional models*

The two-phase multidimensional dispersion models that we consider subsequently are the one of Wu¨rtz et al., Garcia and Crespo, Vandroux-Koenig and Berthoud, Pereira and Chen.

- *Wurtz et al.'s model*

This three-dimensional model includes the mixture mass, momentum and energy balance equations as well as the mass balance equation for the contaminant component. The mixture is composed of the contaminant (liquid and/or) gas. and the ambient gas (no humidity condensation is considered). Thermodynamical equilibrium is assumed, i.e. all the components share locally the same temperature and pressure. The two-phase mixture is supposed to behave ideally, i.e. Raoult's law is used for the calculation of the partial pressures. A single-phase turbulence model, based on the eddy diffusivity concept, is adopted and modified to take into account anisotropy effects. A vertical slip velocity is allowed for between the liquid and gas phase. Special attention was paid on the model's ability to handle complex terrain. In particular, liquid deposition on solid surfaces is taken into account. Remarks already made regarding the assumption of thermodynamic equilibrium in the integral models also apply here. The first validation tests performed by the authors have shown the better performance of this model against a 1-D model when obstacles are present.

- *Garcia and Crespo's model*

This three-dimensional model contains the mixture mass and momentum balance equations as well as the mass balance equation for the contaminant component w48x. The total enthalpy is taken proportional to the contaminant mass fraction. The treatment of the thermodynamics as well as the composition of the mixture are similar to Wurtz et al.'s model. The relative mean velocity between the phases is neglected. The classical

*k*ye model is used with an additional dissipation term due to the droplets.

- *Vandroux-Koenig and Berthoud's model*

This model is devoted to the prediction of the near-field dispersion of liquefied propane (Vandroux-Koening, 1997). It is a Eulerian–Eulerian two-fluid model which considers three components: propane (liquid and vapour), dry air and water (liquid and vapour). The condensed water is included in the gas phase to form a homogeneous fog mixture. Balance equations are written for the mass of each constituent, for the momentum of the gas mixture and of the propane droplets, and for the gas mixture energy. The temperature of the propane droplets is supposed to be uniform, equal to the saturation temperature at atmospheric pressure, so that no energy balance equation is needed for the liquid phase. To close the system of equations, a single-phase turbulence model based on the Prandtl's mixing length theory is introduced for the gas phase. For interfacial transfers, a constant droplet diameter is assumed throughout the calculation. The momentum and heat interfacial transfer terms are calculated from a drag and a heat transfer coefficient, respectively, for rigid spheres. The mass transfer is modelled by assuming that the heat transferred from the gas phase to the droplets completely contributes to vapour production.

According to the authors, the propane droplets are predicted to persist much further downstream than experimentally observed. Several possible causes were investigated for this underestimation of droplet evaporation. Neither the assumption of a constant diameter nor the fact that no initial radial velocity was taken into account could explain this underevaluation. On the other hand, the assumption of a uniform temperature in the droplet or the inadequacy of the turbulence model (the droplets may in reality disperse more than the gas phase) have been proposed as possible explanations. One important assumption which could strongly hamper evaporation and which was not yet discussed, is to take the droplet temperature equal to the saturation temperature at ambient pressure instead of the one corresponding to the vapour partial pressure at the surface (lower due to the dilution of the contaminant vapour). This assumption contradicts the experimental observation that liquid temperature can decrease below the normal boiling point. More parametric studies as well as the comparison of the prediction with the results of controlled laboratory experiments adapted to the validation of the uncertain aspects of the model are required to solve these inconsistencies.

- *Pereira and Chen's model*

This Eulerian–Lagrangian model is also devoted to the near-field dispersion of liquefied propane; the single-phase version developed for the far-field dispersion is not considered here. It is constituted of a Eulerian description of the mixture phase composed of air and propane vapour (no humidity is taken into account). having the same velocity and temperature but different volume fractions, and a

Lagrangian modelling of the droplet phase which is composed of various droplet-size groups having their own initial characteristics (velocity, temperature, diameter). In the gas phase, the $\kappa - \varepsilon$ model is adopted. The effect of the dispersed phase on the gas phase is limited to the mass, momentum and enthalpy transport due to the phase–change process. For each of the two size classes of droplets, the equation of motion is written. The interfacial force is determined by using a drag coefficient valid for solid spheres and with the relative velocity evaluated from the mean local gas velocity. The heat and mass transfer is calculated with a heat transfer coefficient for a rigid sphere and by assuming that the heat transferred from the gas phase to the droplet contributes completely to the evaporation. The surface temperature of the propane droplets is supposed to be equal to the saturation temperature at atmospheric pressure.

The Lagrangian approach has the advantage to account for the instantaneous flow properties encountered by the particles. A second cited advantage of the Eulerian–Lagrangian approach is the possibility to readily handle the evolution of a distribution of particle diameters, which remains difficult to predict in a Eulerian–Eulerian scheme. However, transient situations are more easily solved by a Eulerian–Eulerian approach. This seems to favor the choice of Lagrangian models for the description of the continuous releases considered here. The first advantage is, however, not used by Pereira and Chen since only the mean local gas characteristics are taken into account in the droplet equations.

# 3 MATERIALS AND METHODS

This work will purpose a method to describe the Desert Tortoise experiment with CFD simulation. The program used to achieve this goal is Ansys Fluent (version 12.1). A summary of the leading equations adopted by the program to solve ammonia pressurized dispersions are listed below.

## 3.1 The equations of change

The equation of change are statements of the conservation of mass, momentum and energy.

A general property balance can be made on an elemental volume $V$ moving with the stream velocity $v$. The properties (mass, momentum and energy) per unit volume are denoted by $\psi$, the flux of the property by $\Psi$ (Eckert & Drake, 1972). The net flow across the surface will be given by the closed surface integral of the flux,

$$\oint_s (\psi \cdot dS) \tag{3.1}$$

Notice that the integral flow is negative for the net inflow and positive for the net outflow.

The generation of the property per unit volume and time is denoted by $\dot{\psi}_g$, and the generation within the volume is

$$\int_V \dot{\psi}_g dV \tag{3.2}$$

The time rate of change of the property in the volume is

$$\frac{d}{dt}\left(\int_V \psi_g dV\right) \tag{3.3}$$

Since the time rate of change within the volume must equal the net flow across the surface plus the generation. The balance becomes

$$\int_V \left(\frac{\partial \psi}{\partial t}\right) dV + \oint_S \psi(v \cdot dS) = \int_V \dot{\psi}_g dV - \oint_S (\Psi \cdot dS) \tag{3.4}$$

Applying the Gauss' theorem, we obtain

$$\int_V \left[\frac{\partial \psi}{\partial t} + (\nabla \cdot \psi v) + (\nabla \cdot \Psi) - \dot{\psi}_g\right] dV = 0 \tag{3.5}$$

Since the expression is true for any region in the space,

$$\frac{\partial \psi}{\partial t} + (\nabla \cdot \psi v) + (\nabla \cdot \Psi) - \dot{\psi}_g = 0 \tag{3.6}$$

Which is the general equation for the property $\psi$.

### *3.1.1 The continuity equation*

Consider a control volume, fixed in the space, of arbitrary shape and of finite size: the surface that bounds this control volume is called the control surface. The fluid moves through the fixed control volume, flowing across the control surface.

In this specific situation, the macroscopic property of mass per unit volume is the density $\rho$.

The fact that in this case no mass is created or destroyed can then be expressed in the way that the difference between the mass flow into the control volume and the mass flow out of it must equal the increase in mass during time in the control volume. Denoting the mass decrease by a negative quantity, this statement can be expressed with the following equation:

$$\left[\frac{\partial(\rho v_x)}{\partial x} + \frac{\partial(\rho v_x)}{\partial x} + \frac{\partial(\rho v_x)}{\partial x}\right] dxdydz = -\frac{\partial \rho}{\partial t}(dxdydz) \qquad (3.7)$$

The term in brackets is simply $(\nabla \cdot \rho v)^2$, thus the general balance equation becomes:

$$\frac{\partial \rho}{\partial t} + (\nabla \cdot \rho v) = 0 \qquad (3.8)$$

Here $(\nabla \cdot \rho v)$ is called the "divergence of $\rho v$" ; the vector $\rho v$ is the mass flux, and its divergence equals the net rate mass efflux per unit volume.

Applying a relation between the vectors, we get:

$$\frac{\partial \rho}{\partial t} + \rho(\nabla \cdot v) + (v \cdot (\nabla \rho)) = 0 \qquad (3.9)$$

Thus, in terms of the substantial derivative, the equation becomes:

$$\frac{D\rho}{Dt} = -\rho(\nabla \cdot v) \qquad (3.10)$$

If the materiali s incompressible, then the density is constant and one obtains $(\nabla \cdot v) = 0$

### *3.1.2 The momentum equation*

The law of conservation of momentum is essentially an extension of Newton's law stating that the sum of all forces acting on a mass must be equal to the mass multiplied by its acceleration. The macroscopic property of momentum per unit volume is ; the flux of momentum is the pressure tensor P. However, unlike mass, momentum can be generated by field forces such as gravity. The general equation then becomes:

$$\frac{\partial \rho v}{\partial t} + \left(\nabla \cdot \rho(v \cdot v)\right) + (\nabla \cdot P) - \sum_s \rho_s F_s = 0 \quad (3.11)$$

Where the $F_s's$ are the field forces per unit mass.

The equation of motion can be modified by splitting the pressure tensor into a static pressure term and a viscous tensor term, that can be expressed, by using the Stokes equation, as:

$$\underline{\tau} = -\mu(\nabla v + \nabla v^T) + (\frac{2}{3}\mu - \kappa)(\nabla \cdot v)\delta \quad (3.12)$$

Furthermore, considering only the gravity as field force and the liquid be newtonian, it can be written as:

$$\frac{\partial \rho v}{\partial t} + \left(\nabla \cdot \rho(v \cdot v)\right) = -\nabla \cdot \underline{\rho} - \nabla \cdot \underline{\tau} + \rho g = 0 \quad (3.13)$$

In terms of substantial derivate, this equation becomes:

$$\rho \frac{Dv}{Dt} = -\nabla \rho + \nabla \cdot \underline{\tau} + \rho g \quad (3.14)$$

Following the most common simplifications of the equation of motion will be discussed:

- For constant ρ and μ, using the Newtonian expression of τ into the equation of motion, leads to the famous Navier-Stokes equation:

$$\rho \frac{Dv}{Dt} = -\nabla \rho + \mu \nabla^2 v + \rho g \quad (3.15)$$

- When the acceleration terms in the Navier-Stokes equation are neglected, that is when $\rho \frac{Dv}{Dt} = 0$, we get the Stokes flow equation:

$$0 = -\nabla \rho + \mu \nabla^2 v + \rho g \quad (3.16)$$

- When viscous forces are neglected, that is $\nabla \cdot \underline{\tau} = 0$, the equation of motion becomes

$$\rho \frac{Dv}{Dt} = -\nabla \rho + \rho g \quad (3.17)$$

Which is know as the Euler equation for "inviscid" fluids; although no fluid is truly "inviscid", there are many flows in which the viscous forces are relatively unimportant.

### *3.1.3 The energy equation*

The energy equation is a scalar equation, meaning that it has no particular criterion associated with it. The procedure for deriving the energy equation is similar to those presented for the continuity and momentum equations. In this case, the change in energy of the fluid within the control volume is equal to the net thermal energy transferred into the control volume plus the rate of work done by

external forces. The energy of the fluid is expressed in this case as the sum of the absolute thermodynamic integral energy per unit mass, $e$, and the kinetic energy per unit mass, $^1/_2 V^2$. The change in the total energy per unit volume of the fluid in the control volume is:

$$\frac{\partial y}{\partial x}\left[\rho\left(e+\frac{1}{2}V^2\right)\right] \quad (3.18)$$

As it was found above for the momentum transfer into and out the control volume, the net transfer of energy per unit volume through the control volume is:

$$\frac{\partial}{\partial x}\left[\rho u\left(e+\frac{1}{2}V^2\right)\right]+\frac{\partial}{\partial y}\left[\rho v\left(e+\frac{1}{2}V^2\right)\right]+\frac{\partial}{\partial z}\left[\rho w\left(e+\frac{1}{2}V^2\right)\right] \quad (3.19)$$

This equation is obtanined by replacing the momentum term by the energy term. The net thermal energy transferred into the control volume is determined by the heat flux $q_i$, positive for heat going from within the control volume to the surroundings in the i-th direction (that is the x-, y-, z- direction). The total heat per unit volume transferred to the control volume is:

$$-\frac{\partial q_x}{\partial x}-\frac{\partial q_y}{\partial y}-\frac{\partial q_z}{\partial z} \quad (3.20)$$

The rate of work per unit volume being done by the surface force is found by multiplying the stress, $\sigma_{ij}$, by the velocity in the j-direction for each i-th face. The net rate of work being done from all sides is:

$$\frac{\partial}{\partial x}\left(u\sigma_{xx}+v\sigma_{xy}+w\sigma_{xz}\right)+\frac{\partial}{\partial y}\left(u\sigma_{yx}+v\sigma_{yy}+w\sigma_{yz}\right)+\frac{\partial}{\partial z}\left(u\sigma_{zx}+v\sigma_{zy}+w\sigma_{zz}\right) \quad (3.21)$$

Lastly, the rate of work per unit volume done by the gravity force vector is:

$$\rho u g_x+\rho v g_y+\rho w g_z \quad (3.22)$$

Putting all these terms togheter, we get:

$$\begin{aligned}\frac{\partial}{\partial t}\left[\rho\left(e+\frac{1}{2}V^2\right)\right]+\frac{\partial}{\partial x}\left[\rho u\left(e+\frac{1}{2}V^2\right)\right]+\frac{\partial}{\partial y}\left[\rho v\left(e+\frac{1}{2}V^2\right)\right]+\frac{\partial}{\partial z}\left[\rho w\left(e+\frac{1}{2}V^2\right)\right]=\\ -\frac{\partial q_x}{\partial x}-\frac{\partial q_y}{\partial y}-\frac{\partial q_z}{\partial z}+\frac{\partial}{\partial x}\left(u\sigma_{xx}+v\sigma_{xy}+w\sigma_{xz}\right)+\frac{\partial}{\partial y}\left(u\sigma_{yx}+v\sigma_{yy}+w\sigma_{yz}\right)+\\ \frac{\partial}{\partial z}\left(u\sigma_{zx}+v\sigma_{zy}+w\sigma_{zz}\right)+\rho u g_x+\rho v g_y+\rho w g_z\end{aligned} \quad (3.23)$$

## 3.2 DPM

In this work, the model adopted to describe the motion of the droplets is the Discrete phase model. The DPM simulates a discrete phase in a Lagrangian frame of reference. This second phase consists of spherical particles (which may be taken to represent droplets or bubbles) dispersed in the

continuous phase. Ansys Fluent computes the trajectories of these discrete phase entities, as well as heat and mass transfer to/from them. The coupling between the phases and its impact on both the discrete phase trajectories and the continuous phase flow can be included.

- calculation of the discrete phase trajectory using a Lagrangian formulation that includes the discrete phase inertia, hydrodynamic drag, and the force of gravity, for both steady and unsteady flows
- prediction of the effects of turbulence on the dispersion of particles due to turbulent eddies present in the continuous phase
- heating/cooling of the discrete phase
- vaporization and boiling of liquid droplets
- coupling of the continuous phase flow field prediction to the discrete phase calculations
- droplet breakup and coalescence

### *3.2.1 The EULER- Lagrange Approach*

The Lagrangian discrete phase model follows the Euler-Lagrange approach. The fluid phase is treated as a continuum by solving the time-averaged Navier-Stokes equations, while the dispersed phase is solved by tracking a large number of particles, bubbles, or droplets through the calculated flow field. The dispersed phase can exchange momentum, mass, and energy with the fluid phase.

A fundamental assumption made in this model is that the dispersed second phase occupies a low volume fraction, even though high mass loading ($\dot{m}_{particles} \geq \dot{m}_{fluid}$) is acceptable. The particle or droplet trajectories are computed individually at specified intervals during the fluid phase calculation. This makes the model appropriate for the modeling of spray dryers, coal and liquid fuel combustion, and some particle-laden flows, but inappropriate for the modeling of liquid-liquid mixtures, fluidized beds, or any application where the volume fraction of the second phase is not negligible.

### *3.2.2 Equations of motion of particles*

The DPM predicts the trajectory of a discrete phase particle (or droplet or bubble) by integrating the force balance on the particle, which is written in a Lagrangian reference frame. This force balance

equates the particle inertia with the forces acting on the particle, and can be written (for the $x$ direction in Cartesian coordinates) as

$$\frac{du_p}{dt} = F_D(u - u_P) + \frac{g_x(\rho_p - \rho)}{\rho_p} + F_x \quad (3.24)$$

Where $F_x$ is an additional acceleration (force/unit particle mass) term, $F_D(u - u_P)$ is the drag force per unit particle mass and

$$F_D = \frac{18\mu}{\rho_p d_p^2} \frac{C_D Re}{24} \quad (3.25)$$

Here, $u$ is the fluid phase velocity, $u_P$ is the particle velocity, $\mu$ is the molecular viscosity of the fluid, $\rho$ is the fluid density, $\rho_p$ is the density of the particle, $d_p$ and is the particle diameter. Re is the relative Reynolds number, which is defined as

$$Re \equiv \frac{\rho d_P |u_P - u|}{\mu} \quad (3.26)$$

### *3.2.3 Turbulent dispersion of particles (stochastic tracking)*

The stochastic tracking (random walk) model includes the effect of instantaneous turbulent velocity fluctuations on the particle trajectories through the use of stochastic methods.

When the flow is turbulent, Ansys Fluent will predict the trajectories of particles using the mean fluid phase velocity, $\bar{u}$, in the trajectory $u = \bar{u} + u'$ (3.27). Optionally, you can include the instantaneous value of the fluctuating gas flow velocity,

$$u = \bar{u} + u' \quad (3.27)$$

to predict the dispersion of the particles due to turbulence.

In the stochastic tracking approach, Ansys Fluent predicts the turbulent dispersion of particles by integrating the trajectory equations for individual particles, using the instantaneous fluid velocity, $\bar{u} + u'(t)$, along the particle path during the integration. By computing the trajectory in this manner for a sufficient number of representative particles (termed the "number of tries"), the random effects of turbulence on the particle dispersion may be accounted for.

Ansys Fluent uses a stochastic method (random walk model) to determine the instantaneous gas velocity. In the discrete random walk (DRW) model, the fluctuating velocity components are discrete piecewise constant functions of time. Their random value is kept constant over an interval of time given by the characteristic lifetime of the eddies.

The DRW model may give nonphysical results in strongly nonhomogeneous diffusion-dominated flows, where small particles should become uniformly distributed. Instead, the DRW will show a tendency for such particles to concentrate in low-turbulence regions of the flow.

### *3.2.4 The integral time*

Prediction of particle dispersion makes use of the concept of the integral time scale, $T$, which describes the time spent in turbulent motion along the particle path, $ds$:

$$T = \int_0^\infty \frac{u'_p(t)u'_p(t+s)}{\overline{u'^2_p}} ds \qquad (3.28)$$

The integral time is proportional to the particle dispersion rate, as larger values indicate more turbulent motion in the flow. It can be shown that the particle diffusivity is given by $\overline{u'_\iota u'_\jmath} T$

For small "tracer" particles that move with the fluid (zero drift velocity), the integral time becomes the fluid Lagrangian integral time, $T_L$. This time scale can be approximated as

$$T_L = C_L \frac{k}{\varepsilon} \qquad (3.29)$$

Where $C_L$ is to be determined as it is not well known. By matching the diffusivity of tracer particles, , $\overline{u'_\iota u'_\jmath} T_L$ to the scalar diffusion rate predicted by the turbulence model, $v_t/\sigma$, one can obtain

$$T_L \approx 0.15 \frac{k}{\varepsilon} \qquad (3.30)$$

for the $\kappa - \varepsilon$ model and its variants.

### *3.2.5 Discrete random walk model*

In the discrete random walk (DRW) model, or "eddy lifetime" model, the interaction of a particle with a succession of discrete stylized fluid phase turbulent eddies is simulated. Each eddy is characterized by

- a Gaussian distributed random velocity fluctuation, $u'$, $v'$, and $w'$
- a time scale, $\tau_e$

The values of $u'$, $v'$, and $w'$ that prevail during the lifetime of the turbulent eddy are sampled by assuming that they obey a Gaussian probability distribution, so that

$$u' = \varsigma\sqrt{\overline{u'^2}} \quad (3.31)$$

where $\varsigma$ is a normally distributed random number, and the remainder of the right-hand side is the local RMS value of the velocity fluctuations. Since the kinetic energy of turbulence is known at each point in the flow, these values of the RMS fluctuating components can be defined (assuming isotropy) as

$$\sqrt{\overline{u'^2}} = \sqrt{\overline{v'^2}} = \sqrt{\overline{w'^2}} = \sqrt{2k/3} \quad (3.32)$$

for the $\kappa - \varepsilon$ model. When the RSM is used, nonisotropy of the stresses is included in the derivation of the velocity fluctuations:

$$u' = \varsigma\sqrt{\overline{u'^2}} \quad (3.33)$$

$$v' = \varsigma\sqrt{\overline{v'^2}} \quad (3.34)$$

$$w' = \varsigma\sqrt{\overline{w'^2}} \quad (3.35)$$

when viewed in a reference frame in which the second moment of the turbulence is diagonal.

The characteristic lifetime of the eddy is defined either as a constant:

$$\tau_e = 2T_L \quad (3.36)$$

where $T_L$ is given by Equation $T_L = C_L \frac{k}{\varepsilon}$ ( 3.29 in general, or as a random variation about $T_L$:

$$\tau_e = -T_L log(r) \quad (3.37)$$

where $r$ is a uniform random number between 0 and 1 and $T_L$ is given by Equation $T_L \approx 0.15 \frac{k}{\varepsilon}$ ( 3.30. The option of random calculation of $\tau_e$ yields a more realistic description of the correlation function.

The particle eddy crossing time is defined as

$$t_{cross} = -\tau\, ln\left[1 - \left(\frac{L_e}{\tau|u-u_p|}\right)\right] \quad (3.38)$$

where $\tau$ is the particle relaxation time, $L_e$ is the eddy length scale, $|u - u_p|$ and is the magnitude of the relative velocity.

The particle is assumed to interact with the fluid phase eddy over the smaller of the eddy lifetime and the eddy crossing time. When this time is reached, a new value of the instantaneous velocity is obtained by applying a new value of $\varsigma$ in Equation $u' = \varsigma\sqrt{\overline{u'^2}}$
( 3.31.

In order to obtain a better representation of an injector, the particles can be *staggered* either spatially or temporally. When particles are staggered spatially, the model randomly samples from the region in which the spray is specified (e.g., the sheet thickness in the pressure-swirl atomizer) so that as the calculation progresses, trajectories will originate from the entire region. This allows the entire geometry specified in the atomizer to be sampled while specifying fewer streams in the input panel, thus decreasing computational expense.

When injecting particles in a transient calculation using relatively large time steps in relation to the spray event, the particles can clump together in discrete bunches. The clumps do not look physically realistic, though Ansys Fluent calculates the trajectory for each particle as it passes through a cell and the coupling to the gas phase is properly accounted for. To obtain a statistically smoother representation of the spray, the particles can be staggered in time. During the first time step, the particle is tracked for a random percentage of its initial step. This results in a sample of the initial volume swept out by the particle during the first time step and a smoother, more uniform spatial distribution at longer time intervals.

### *3.2.6 DPM Boundary conditions*

This thesis will focus on the effect of the boundary conditions related to the DPM:

- the "trap" boundary condition reflects the effect of an instantaneous evaporation of the droplet when reaches the boundary surface (see Fig. 3-1).

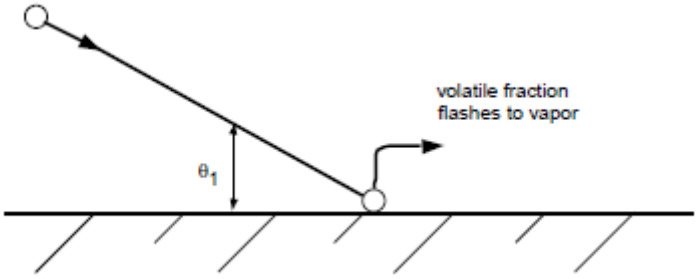


*Fig. 3-1: Trap boundary condition*

- The "escape" describes a droplet that disappears when reaches the boundary surface and the mass that the droplet still carries is no more taken into account (see Fig. 3-2).

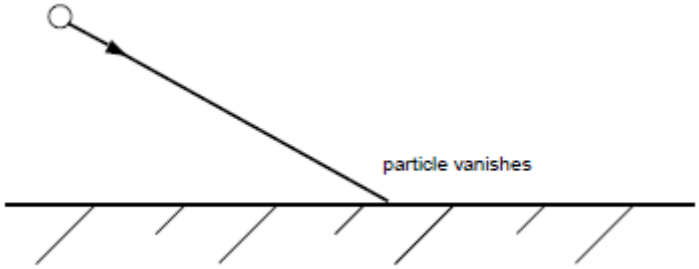


*Fig. 3-2: Escape boundary condtion*

- The "wall-film" describes many regimes of the droplets: stick, rebound, spread and splash, which are based on the impact energy and wall temperature (see Fig. 3-3).

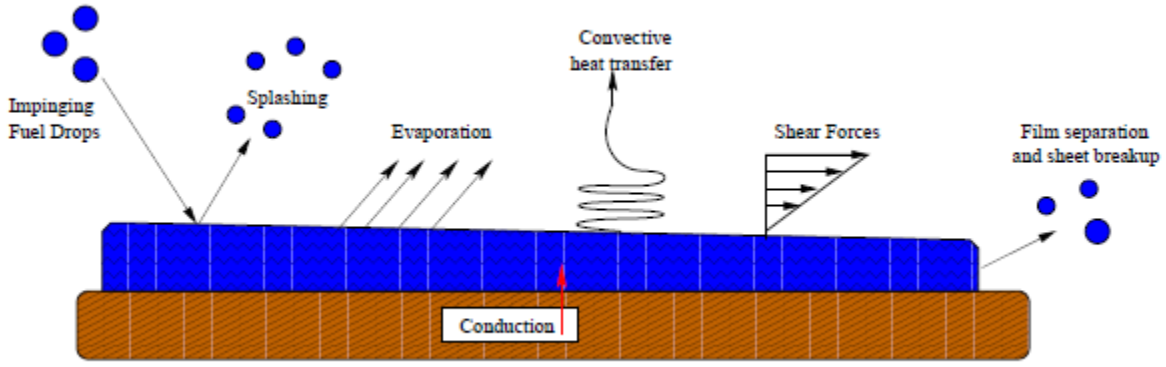


*Fig. 3-3: Wall-film boundary condition*

Compared to the previous boundary conditions (e.g. trap and escape) the "wall film" describes properly the physical behavior of the droplets at the expense of the computational effort.

### *3.2.7 Coupling between the Discrete and Continuous phases*

As the trajectory of a particle is computed, Ansys Fluent keeps track of the heat, mass, and momentum gained or lost by the particle stream that follows that trajectory and these quantities can be incorporated in the subsequent continuous phase calculations. Thus, while the continuous phase always impacts the discrete phase, you can also incorporate the effect of the discrete phase trajectories on the continuum. This two-way coupling is accomplished by alternately solving the discrete and continuous phase equations until the solutions in both phases have stopped changing. This interphase exchange of heat, mass, and momentum from the particle to the continuous phase is depicted qualitatively in Fig. 3-4

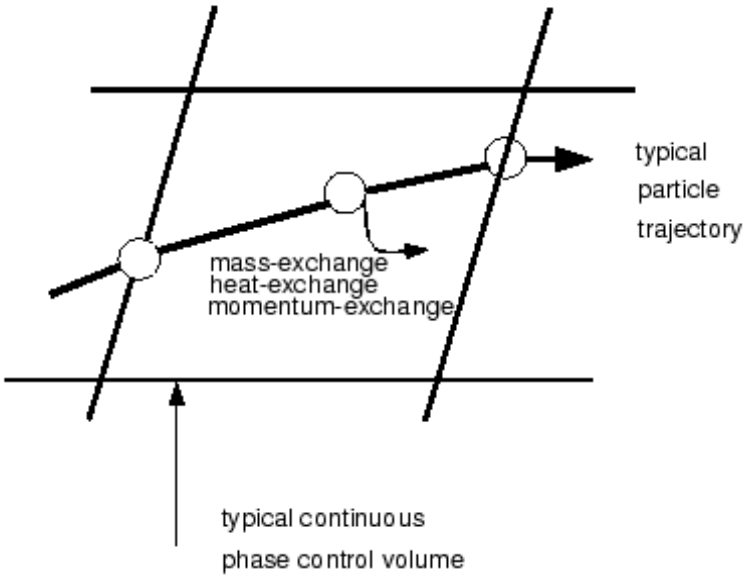


*Fig. 3-4:Heat, Mass and momentum Transfer between the Discrete and the continuous phases*

### *3.2.8 Momentum exchange*

The momentum transfer from the continuous phase to the discrete phase is computed in fluent by examining the change in momentum of a particle as it passes through each control volume in the model. This momentum change is computed as

$$F = \sum \left( \frac{18\mu C_D Re}{\rho_p d_p^2 24} (u_p - u) + F_{other} \right) \dot{m_p} \Delta t \qquad (3.39)$$

Where: $u$ is the viscosity of the fluid, $\rho_p$ is the density of the particles, $d_p$ is the diameter of the particle, Re is the relative Reynolds number, $u_p$is the velocity of the particle, $u$ is the velocity of the fluid, $C_D$ is a drag coefficient, $\dot{m}_p$ the mass flow rate of the particles, $\Delta t$ the time step and $F_{other}$ are other interaction forces.

### 3.2.9 *Heat exchange*

The heat transfer from the continuous phase to the discrete phase is computed by examining the change in thermal energy of a particle as it passes through each control volume in the model. In the absence of a chemical reaction the heat exchange is computed as

$$Q = (m_{pIN} - m_{pout})[-H_{lat\,ref} + H_{pyrol}] - m_{p\,out}\int_{T_{ref}}^{T_{p\,out}} c_{p_p} dT + m_{p\,in}\int_{T_{ref}}^{T_{p\,in}} cp_p dT \quad (3.40)$$

Where: $m_{pIN}$mas of the particle on cell entry, $m_{pout}$mass of the particle on cell exit, $c_{p_p}$heat capacity of the particle, $H_{pyrol}$ heat of pyrolysis of the the particle on cell entry, $T_{p\,in}$ temperature of the particle on cell entry, $T_{p\,out}$ temperature of the particle on cell exit, $T_{ref}$ reference temperature for enthalpy, $H_{lat\,ref}$ latent heat at reference conditions

The latent heat at the reference conditions $H_{lat\,ref}$ for droplet particles is computed as the difference of the liquid and gas standard formation enthalpies, and can be related to the latent heat at the boiling point as follows:

$$H_{lat\,ref} = H_{lat} - \int_{T_{ref}}^{T_{bp}} c_{p_g} dT + \int_{T_{ref}}^{T_{bp}} c_{p_p} dT \quad (3.41)$$

Where $c_{p_g}$heat of capacity of gas product species, $T_{bp}$ boiling point temperature, $H_{lat}$ latent heat at the boiling point temperature

For the volatile part of the combusting particles, some constraints are applied to ensure that the enthalpy source terms do not depend on the particle history. The formulation should be consistent with the mixing of two gas streams, one consisting of the fluid and the other consisting of the volatiles. Hence $H_{lat\,ref}$ is derived by applying a correction to $H_{lat}$, which accounts for different heat capacities in the particle and gaseous phase:

$$H_{lat\,ref} = H_{lat} - \int_{T_{ref}}^{T_{p,init}} c_{p_g} dT + \int_{T_{ref}}^{T_{b,init}} c_{p_p} dT \quad (3.42)$$

Where $T_{p,init}$ is the particle initial temperature.

### 3.2.10 *Mass exchange*

The mass transfer from the discrete phase to the continuous phase is computed by examining the change in mass of a particle as it passes through each control volume. The mass change is computed simply as

$$M = \frac{\Delta m_p}{m_{p,0}} \dot{m}_{p,0} \quad (3.43)$$

This mass exchange appears as a source of mass in the continuous phase continuity equation and as a source of a chemical species defined by you. The mass sources are included in any subsequent calculations of the continuous phase flow field.

## 3.3 Droplet temperature laws

### *3.3.1 Inert Heating or Cooling*

The inert heating or cooling laws are applied when the particle temperature is less than the vaporization temperature that you define, $T_{vap}$, and after the volatile fraction, $f_{v,0}$, of a particle has been consumed. These conditions may be written as

$$T_P < T_{vap} \quad (3.44)$$

$$m_p \leq (1 - f_{v,0}) m_{p,0} \quad (3.45)$$

where $T_p$ is the particle temperature, $m_{p,0}$ is the initial mass of the particle, and $m_p$ is its current mass.

Equation 3.44 is applied until the temperature of the particle/droplet reaches the vaporization temperature. At this point a non inert particle/droplet may proceed to obey one of the mass-transfer laws (3.47, 3.53, returning to equation 3.45 when the volatile portion of the particle/droplet has been consumed. (Note that the vaporization temperature, $T_{vap}$, is an arbitrary modeling constant used to define the onset of the vaporization/boiling/volatilization laws.)

When using 3.44 or 3.45, DPM uses a simple heat balance to relate the particle temperature, $T_p(t)$, to the convective heat transfer and the absorption/emission of radiation at the particle surface:

$$m_p c_p \frac{dT_p}{dt} = hA_p\left(T_\infty - T_p\right) + \varepsilon_p A_p \sigma(\theta_R^4 - T_p^4) \quad (3.46)$$

Where $m_p$ mass of the particle, $c_p$ is the heat capacity of the particle, $A_p$ is the surface area of the particle, $T_\infty$ is the local temperature of the continuous phase, $h$ the convective heat transfer coefficient, $\varepsilon_p$ the particle emissivity, $\sigma$ the Stefan-Boltzmann constant, $\theta_R$ the radiation temperature.

The equation 3.49 assumes that there is negligible internal resistance to heat transfer, i.e., the particle is at uniform temperature throughout.

Equation 3.47 is applied to predict the vaporization from a discrete phase droplet and is initiated when the temperature of the droplet reaches the vaporization temperature, $T_{vap}$, and continues until the droplet reaches the boiling point, $T_{bp}$, or until the droplet's volatile fraction is completely consumed:

$$T_p < T_{bp} \quad (3.47)$$

$$m_p > (1 - f_{v,0})m_{p,0} \quad (3.48)$$

The onset of the vaporization law is determined by the setting of $T_{vap}$, a modeling parameter that has no physical significance. Note that once vaporization is initiated (by the droplet reaching this threshold temperature), it will continue to vaporize even if the droplet temperature falls below $T_{vap}$. Vaporization will be halted only if the droplet temperature falls below the dew point. In such cases, the droplet will remain in equation $T_p < T_{bp}$ ( 3.47 but no evaporation will be predicted. When the boiling point is reached, the droplet vaporization is predicted by a boiling rate, Law 3, as described in a section that follows.

### *3.3.2 Mass transfer during equation 3.47*

During equation 3.47, the heat of vaporization is governed by gradient diffusion, with the flux of droplet vapor into the gas phase related to the gradient of the vapor concentration between the droplet surface and the bulk gas:

$$N_i = k_c(C_{i,s} - C_{i,\infty}) \quad (3.49)$$

Where $N_i$ molar flux of vapor, $k_c$ is the mass transfer coefficient, $C_{i,s}$ is the vapor concentration at the droplet surface, $C_{i,\infty}$ is the vapor concentration in the bulk gas.

The concentration of vapor at the droplet surface is evaluated by assuming that the partial pressure of vapor at the interface is equal to the saturated vapor pressure, $p_{sat}$, at the particle droplet temperature, $T_p$:

$$C_{i,s} = \frac{p_{sat}(T_p)}{RT_p} \quad (3.50)$$

Where R is the universal gas constant.

The concentration of vapor in the bulk gas is known from solution of the transport equation for species $i$ or from the PDF look-up table for non premixed or partially premixed combustion calculations:

$$C_{i,\infty} = X_i \frac{p}{RT_\infty} \quad (3.51)$$

Where $X_i$ is the local bulk mole fraction of species $i$, $p$ is the local absolute pressure, and $T_\infty$ is the local bulk temperature in the gas.

Finally, the droplet temperature is updated according to a heat balance that relates the sensible heat change in the droplet to the convective and latent heat transfer between the droplet and the continuous phase:

$$m_p c_p \frac{dT_p}{dt} = hA_p(T_\infty - T_p) + \frac{dm_p}{dt} h_{fg} + \varepsilon_p A_p \sigma(\theta_R^4 - T_p^4) \quad (3.52)$$

$c_p$ is the heat capacity of the particle, $T_p$ is the droplet temperature, $T_\infty$ is the temperature of the continuous phase, $\frac{dm_p}{dt}$ the rate of evaporization, $h_{fg}$ the latent heat, $\varepsilon_p$ the particle emissivity, $\sigma$ the Stefan-Boltzmann constant, $\theta_R$ the radiation temperature.

The heat transferred to or from the gas phase becomes a source/sink of energy during subsequent calculations of the continuous phase energy equation.

### *3.3.3 Droplet Boiling*

Equation 3.53 is applied to predict the convective boiling of a discrete phase droplet when the temperature of the droplet has reached the boiling temperature, $T_{bp}$, and while the mass of the droplet exceeds the nonvolatile fraction, $(1 - f_{v,0})$:

$$T_p \geq T_{bp} \quad (3.53)$$

$$m_p > (1 - f_{v,0}) m_{p,0} \quad (3.54)$$

When the droplet temperature reaches the boiling point, a boiling rate equation is applied:

$$\frac{d(d_p)}{dt} = \frac{4k_\infty}{\rho_p c_{p,\infty} d_p}\left(1 + 0.23\sqrt{Re_d}\right) ln\left[1 + \frac{c_{p,\infty}(T_\infty - T_p)}{h_{fg}}\right] \quad (3.55)$$

Where $c_{p,\infty}$ is the heat capacity of the gas, $\rho_p$ is the droplet density and $k_\infty$ is the thermal conductivity of the gas

### 3.4 Turbulence (continuous phase)

In experiments on fluid systems it is observed that at values below the so-colled critical Reynolds number the flow is smooth and adjacent of fluid slide past each other in an orderly way. If the boundary conditions do not change in the time the flow is steady. The regime is called laminar flow. At values of Reynolds number above  the flow behaviour is random and chaotic. The motion becomes unsteady even with constant boundary conditions. The regime is called turbulent flow.

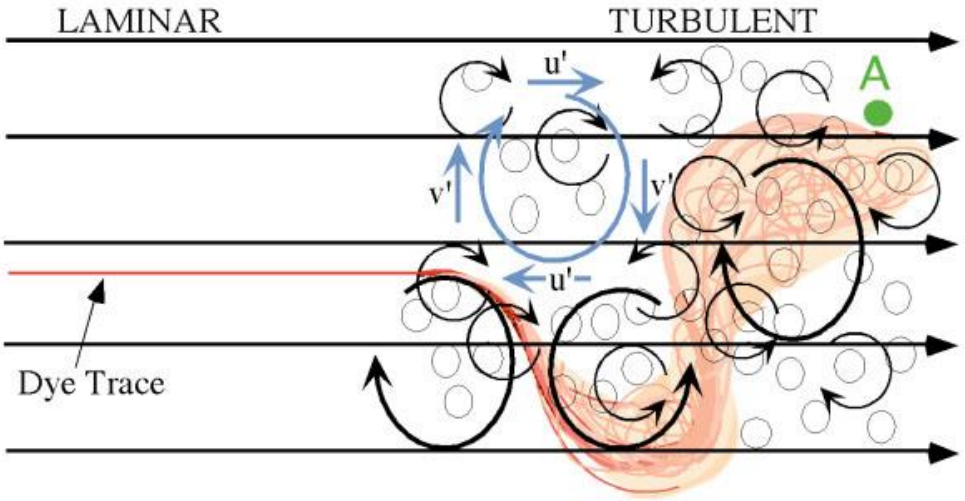


*Fig. 3-5: Difference between laminar and turbulent flow*

Most of the flows occuring in nature and in engineering applications are turbolent. However, it is difficult to give a precise definition of turbolence hence it is easier to list some of the characteristics of turbolent flows:

- **Irregularity**: turbolent flows are always highly irregular; this is way they are treated statistically rather than deterministicaly
- **Diffusivity**: turbolence is highly associated with rapid mixing; in fact, turbolence tends to accelerate the homogenization of any non-uniform mixture.
- **Large Reynolds numbers**: the velocity at which laminr flows no longer exists is called the upper critical Reynolds number; however, there is no agreement on which is this value, thus varying from 2,300 and 40,000  (Eckert & Drake, 1972).

- **Dissipation**: turbulent flows are always dissipative, as the kinetic energy is converted into internal energy by viscous shear stress. Turbulence needs a continuous supply of energy, otherwise it decays rapidly.
- **Energy cascade**: Turbolent flows may be viewed as made of a wide range of eddies of different lenght scales. Based on these lenght scales, the eddies can be devided into three categories:
    - Integral lenght scales: largest scales in the energy spectrum; these eddies obtain energy from the mean flow and from each other. The largiest eddies can be considered as big as the width of the flow.
    - Kolmogorov lenght scales: the smallest scales in the spectrum.
    - Taylor micro-scales: the intermediate scales between the largest and the smallest scales; Taylor micro-scales arenot dissipative scale but passes down the energy from the largest to the smallest without dissipation.

### *3.4.1 3.2.1 The energy cascade and the Kolmogorov hypothesis*

Let us consider a fully turbulent flow at high Reynolds numbers with characteristic velocity $v$ and lenght scale $l$. The first concept in Richrdson's view of energy cascade is that the turbolence can be considered to be composed of eddies of different sizes. Richardson's notion is that the large eddies are unstable and tend to break up, transferring their energy to smaller eddies. These smaller eddies undergo a similar break-up process, and transfer their energy to much smaller eddies. This energy cascade continues until the Reynolds number is sufficient small tht the eddy motion is stable, and molecular viscosity is effective in dissipating the kinetic energy. Richardson summarized this concept as follows:

> "Big whorls have little whorls,
>
> which feed on their velocity;
>
> and little whorls have lesser whorls,
>
> and so on to viscosity." (Bird & Stewart, 2002)

The rate of dissipation of the kinetic energy $\varepsilon$ is determined, therefore, by the first processin the sequence, which is the transfer of energy from the largest eddies. Conseguently, this picture of the cascades indicates that $\varepsilon$ scales as $u_0^3/l_0$.

A conseguence of the theory is that both the velocity and timescale decrease as the lenghtscale decreases.

The first Kolmogorov's hypothesis concerns the isotropy of the small-scale motions; Kolmogorov argued that the direction biases of the large scales are lost in the chaotic scale-reduction process, hence at sufficiently high Reynolds numbers, the small-scale turbulent motion is isotropic. It is useful to introduce a lenghtscale $l_{EI}$ as the demarcation between the anisotropic large eddies ($l > l_{EI}$) and the isotropic small eddies ($l < l_{EI}$). Kolmogorov argued that all the informations about the geometry of large eddies is lost also. As a conseguence, the statistic of small scale motions are universal (similar in every high-Reynolds- number turbulent flow). The two most important parameters in order to define the small-scale motions are the rate at which the small scales receive energy from the large scales (also known as dissipation rate, ) and the kinematic viscosity . Given the two parameters, there are unique length, velocity and time sclaes that can be formed. These are the Kolmogorov scales, respectevely for lenght, time and velocity:

$$\eta = \left(v^3/\varepsilon\right)^{1/4} \quad (3.56)$$

$$u_\eta = (\varepsilon v)^{1/4} \quad (3.57)$$

$$\tau_\eta = \left(v \ /\varepsilon\right)^{1/2} \quad (3.58)$$

### *3.4.2 The Reynolds equation for turbolent motion*

The Navier-Stokes equation of motion should be valid for turbulent flows, since the size of the smallest eddy is generally much greater than the mean free path of the molecules in the system. However, the equation only applies to istantaneous velocity, thus it is necessary to use some statistical average and a measure of the deviation from that average. In a statistical steady flow, every variable can be written as the sum of a time-averaged value and a fluctuation about the value:

$$\phi(x_i, t) = \overline{\phi}(x_i) + \tilde{\phi}(t) \quad (3.59)$$

Applying this process to the Navier-Stokes equations yields the Reynolds-averaged Navier-Stokes (RANS) equation.

Hence, the instantaneous velocity can be written as:

$$v = \bar{v} + \tilde{v} \quad (3.60)$$

$\bar{v}$ is interpreted as time average, defined by $\bar{v} = \lim \frac{1}{T} \int_{t_0}^{t_0+T} v dt$.

Combining this equation for the velocity and a similar equation for the density fluctuation ($\rho = \bar{\rho} + \tilde{\rho}$ ) into the equation of continuity, one obtains:

$$\frac{\partial \bar{\rho}}{\partial t} = -(\nabla \cdot \overline{\rho v}) - (\nabla \cdot \overline{\tilde{\rho}\tilde{v}}) \qquad (3.61)$$

If the flow is incompressible, $\tilde{\rho} = 0$ and $\bar{\rho}$ is constant, thus $(\nabla \cdot \bar{v}) = 0$.

Replacing the terms in equation $\frac{\partial \rho v}{\partial t} + \big(\nabla \cdot \rho(v \cdot v)\big) + (\nabla \cdot P) - \sum_s \rho_s F_s = 0$
( 3.11 by their average and fluctuating components, the equation of motion becomes the Reynolds' equation of turbulent motion:

$$\rho \frac{\partial \bar{v}}{\partial t} + \rho(\bar{v} \cdot \nabla)\bar{v} = -\nabla \bar{p} + \mu \nabla^2 \bar{v} + \sum_s \rho_s \overline{F_s} - (\nabla \cdot \rho \overline{\tilde{v}\tilde{v}}) \qquad (3.62)$$

These equations have the same form as the original equations, except that average properties now appear in place of point properties, and an additional term is added, which represents the effects of the turbulent fluctuations on the averaged flow and has to be parameterized: this is the task of turbulence closure models.

### *3.4.3 The reynolds Stress*

The contribution to the turbulent motion to the mean stress tensor is designated by the symbol $\tau^{(t)} = -\rho \overline{\tilde{v}\tilde{v}}$ and is called Reynolds stress tensor. By inspection $\tau_{ij}^{(t)} = \tau_{ji}^{(t)}$, so that this is a simmetric tensor, thus having six indipendentes components. In cartesian components, this is:

$$\tau^{(t)} = -\rho \begin{pmatrix} \overline{\tilde{v}_x \tilde{v}_x} & \overline{\tilde{v}_x \tilde{v}_y} & \overline{\tilde{v}_x \tilde{v}_z} \\ \overline{\tilde{v}_y \tilde{v}_x} & \overline{\tilde{v}_y \tilde{v}_y} & \overline{\tilde{v}_y \tilde{v}_z} \\ \overline{\tilde{v}_z \tilde{v}_x} & \overline{\tilde{v}_z \tilde{v}_y} & \overline{\tilde{v}_z \tilde{v}_z} \end{pmatrix} \qquad (3.63)$$

The presence of this stress term means that the conservation equations are not closed, that is, they contain more variables than equations.

Closing the Reynolds-Average-Navier-Stokes (RANS) equations requires modeling the Reynolds stress:

One way consists in using the so called Boussinesq's theory, that postulates that the momentum transfer caused by turbulent eddies can be modeled with an eddy viscosity, commonly called the turbulent viscosity and normally written as $\mu_t$.

By analogy with Newton's law of viscosity, the Reynolds stress tensor can be written in the following way:

$$t_{ij}^{(t)} = 2\mu_t S_{ij} - \frac{2}{3}\rho\kappa\rho_{ij} \quad (3.64)$$

The quantity κ should be referred to as turbolent kinetic energy and is generally quantified by the mean of the turbulence normal stresses:

$$\kappa = \frac{1}{2}\overline{\tilde{v}_i\tilde{v}_i} \quad (3.65)$$

The same equation can be then be written more explicitily as:

$$-\rho\overline{\tilde{v}_i\tilde{v}_j} = 2\mu_t\left(\frac{\partial\tilde{v}_i}{\partial x_j} + \frac{\partial\tilde{v}_j}{\partial x_i}\right) - \frac{2}{3}\rho\kappa\rho_{ij} \quad (3.66)$$

The weakness of the Boussinesq assumption is that is not general valid: there is nothing which says that the Reynolds stress tensor must be proportional to the strain rate tensor.

On dimensional ground, one can assume that the kinematic turbulent viscosity $v_t$ which has dimensions $[m^2/s]$, can be expressed as a product of a turbulent velocity scale ϑ and a length scale $l$. This dimensional analysis yields

$$v_t = C\vartheta l \quad (3.67)$$

Of course, the dynamic turbulent viscosity is given by

$$\mu_t = C\vartheta l \quad (3.68)$$

In two-dimensional turbulent flows, where the only significant Reynolds stress is $\tau_{ij}^{(t)} = -\rho\overline{\tilde{v}_x\tilde{v}_y}$ and

the only significant mean velocity gradient is $\frac{\partial v_x}{\partial y}$, if the eddy scale $l$ is:

$$\vartheta = Cl|\frac{\partial v_x}{\partial y} \quad (3.69)$$

Combining equation $v_t = C\vartheta l$ ( 3.67 and equation $\vartheta = Cl|\frac{\partial v_x}{\partial y}$ ( 3.69, we obtain

$$v_t = l_{min}^2|\frac{\partial v_x}{\partial y} \quad (3.70)$$

Prandtl introduced the Mixing-length theory in order to calculate the turbulent shear stress. He assumed that the lenght $l$ is the length of a path of a mass of fluid before it loses its individuality by mixing with its neighbours, thus before its momentum is transferred. This reason led Prandtl to the following relation:

$$\tau_{ij}^{(t)} = -\rho l_{min}^2|\frac{\partial v_x}{\partial y}|\frac{\partial v_y}{\partial x} \quad (3.71)$$

Where $l_{mix}$ is the mixing length and depends on the nature of the flow and is space dependent, and $\mu_t$ is given by:

$$\mu_t = \rho l_{min}^2|\frac{\partial v_x}{\partial y} \quad (3.72)$$

### *3.4.4 The $\kappa - \varepsilon$ model*

$\kappa$ and ε can be used to define the velocity scale and length scale representative of the large turbulent scale as follows:

$$\vartheta = \kappa^{1/2} \quad (3.73)$$

$$l = \frac{\kappa^{3/2}}{\varepsilon} \quad (3.74)$$

In this model, applying the same approach as in the mixing length model, the turbulent eddy viscosity is specified as follows: $\mu_t = \rho C_\mu \frac{\kappa^2}{\varepsilon}$ .

The starting point for all two-equation models is equation $t_{ij}^{(t)} = 2\mu_t S_{ij} - \frac{2}{3}\rho\kappa\rho_{ij}$

( 3.64 and the turbulent kinetic energy equation in the following form:

$$\rho\frac{\partial\kappa}{\partial t} + \rho v_j\frac{\partial\kappa}{\partial x_j} = \tau_{ij}\frac{\partial v_i}{\partial x_j} - \rho\varepsilon + \frac{\partial}{\partial x_j}\left[\left(\frac{\mu}{\mu_t+\sigma_\kappa}\right)\frac{\partial\kappa}{\partial x_j}\right] \quad (3.75)$$

The $\kappa - \varepsilon$ standard model is a semi-empirical model based on model transport equation for turbulent kinetic energy (κ) and its dissipation rate (ε); the first variable determines the energy in the turbulence, whereas the second determines the scale of the turbulence.

In the derivation of the $\kappa - \varepsilon$ model, the assumption is that the flow is fully turbulent, and the effects of molecular viscosity are negligible. The transport equations for the turbulent kinetic energy and the dissipation rate are the following (Fluent, 2006):

$$\frac{\partial}{\partial t}(\rho k) + \frac{\partial}{\partial x_j}\left[u_j(\rho k)\right] = \frac{\partial}{\partial x_j}\left[\left(\mu + \frac{\mu_t}{\sigma_\kappa}\right)\frac{\partial k}{\partial x_j}\right] + G_k - \rho\varepsilon \quad (3.76)$$

$$\frac{\partial}{\partial t}(\rho\varepsilon) + \frac{\partial}{\partial x_j}\left[u_j(\rho\varepsilon)\right] = \frac{\partial}{\partial x_j}\left[\left(\mu + \frac{\mu_t}{\sigma_\varepsilon}\right)\frac{\partial\varepsilon}{\partial x_j}\right] + C_{1_\varepsilon}\frac{\varepsilon}{k}G_k - C_{2_\varepsilon}\rho\frac{\varepsilon^2}{k} \quad (3.77)$$

Many modelers regard this 2-equations turbulence closure scheme a good compromise between universal validity and computational expense.

### *3.4.5 The law of the wall*

Prandtl originally postulated that for flows near solid boundaries the mixing length is proportional to the distance from the surface. This postulate is consistent with “the law of the wall”, which has been observed for a wide range of wall-bounded flows.

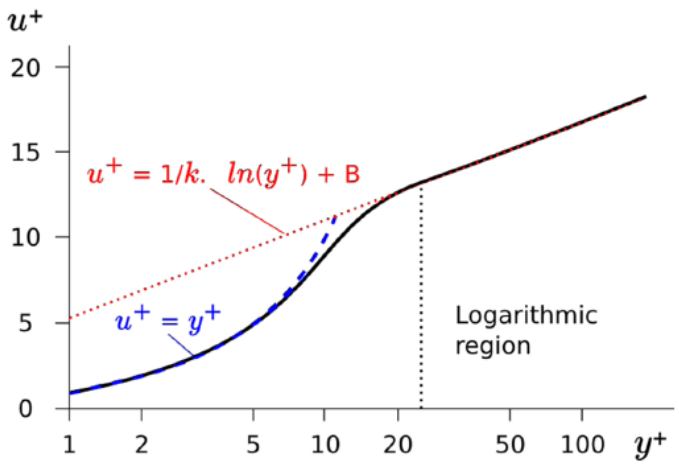


*Fig. 3-6: Typical velocity profile for a boundary layer*

The quantity $y+$ is the dimensionless distance from the surface. By definition, the log-layer is the portion of the boundary layersufficiently close to the surface that inertial terms can be neglected but, at the same time, sufficiently distant that the viscous stress is negligible compared to the Reynolds stress. And in this layer of the flow holds the law of the wall:

$$U^+ \approx \frac{1}{\kappa} ln(y^+) + B \qquad (3.78)$$

The coefficient  is known as the von Karman constant and B is a dimensionless constant.

## 3.5 Computational Fluid Dynamics

Flows and related phenomena can be described by partial differential equations, which cannot be solved analitically, except in special cases. To obtain an appropriate solution numerically, one has to use a discretization method which approximates the differential equations by a system of algebraic equations, that can then be solved by a computer. The approximations are applied to small domains in space/time, so the numerical solution provides results at discrete locations in space and time.

### *3.5.1 Component of a numerical solution method*

- **Mathematical model**: the starting point of any numerical method is the mathematical model, i.e. the set of partial differential equations and boundary conditions. One chooses and

appropriate model for the target application (incompressible, inviscid, turbulent, etc.), that may include simplifications of the exact conservation laws. A solution method is usually designed for a particular set of equations.

- **Discretization method**: after selecting the mathematical model, one has to choose a suitable discetization method, i.e. a method of approximating the differential equations by a system of algebraic equations for the varibles. There are many approaches, but the most common are: finite difference (FD), finite volume (FV) and finite element (FE). In this work, the finite volume method is applied. The FVM uses the integral form of the conservation equations as its starting point:

$$\int_{V_i} \frac{\partial v}{\partial t} dV + \int_{V_i} \nabla \cdot (\rho v) dV = 0 \qquad (3.79)$$

  The solution domain is subdivided into a finite number of contiguous control volumes (CVs), and the conservation equations are applied to each CV and to the solution domain as a whole. At the centroid of each CV, lies a computational node at which the variable values are calculated.

- **Numerical grid**: the discrete locations at which the variables are to be calculated are defined by the numerical grid, which is essentially a discrete representation of the geometric domain on which the problem is to be solved.

- **Convergence criteria**: finally, one needs to set the convergence criteria for the iterative method. Deciding when to stop the iterative process is important, from both the accuracy and efficiency point of view.

### *3.5.2 Numerical grid*

The discrete locations at which the variables are to be calculated are defined by the numerical grid, which is essentially a discrete representation of the geometric domain on which the problem is to be solved. Some of the options available are the following:

- Structured grid: this kind of grids consists of families of grid lines with the property that the members of a single family do not cross each other and cross each member of other family only once. This allows the lines of a given set to be numerated consecutively. The position of any grid point is uniquely identified by a set of two (in 2D) or three (in3D) idices, i.e. (i,j,k). This is the simpliest grid structure: each point has four nearest neighbours in two dimensions and six in three dimensions. An exambpe of a structured 3D grid is shown in Fig. 3-7 The

disadvantage of structured grid is that they can be used only for geometrically simple solution domains.

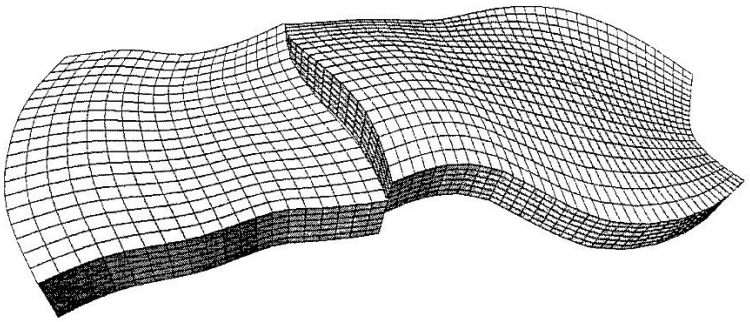

*Fig. 3-7: Example of a 3D structured grid*

- Unstructured grid: For very complex geometries, the most flexible type of grid is one which can fit an arbitrary solution domain boundary . in principle, such grids could be used with any discretization scheme, but they are best adapted to the finite volume and finite element approach. The elements or control volumes may have any shape: in practice, grids made of triangles or quadrilaterals in 2D, and tetrahedra or hexahedra in 3D are most often used. If desired, the grid may be easily locally refined. The advantage of flexibility is offset by the disadvantage of the irregularity of the data structure; the solvers for the algebraic equations equation systems are usually slower than those for regular grids. An example of unstructured gridi s shown in Fig. 3-8

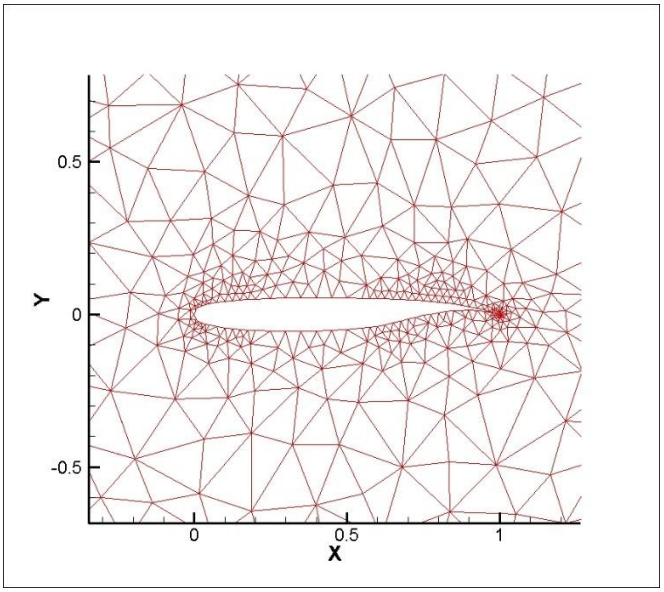


*Fig. 3-8: Unstructured 2D grid*

### *3.5.3 Convergence criteria*

After discretization, the conservation equation for a general variable $\phi$ at a cell P can be written as [ (Fluent, 2006):

$$a_P \phi_P = \sum_{nb} a_{nb} \phi_{nb} + b \qquad (3.80)$$

Here $a_P$ is the center coefficient, $a_{nb}$ are the influence coefficients for the neighbouring cells, and $b$ is the contribution of the constant part of the source term and of the boundary conditions. $a_P$ can be written as:

$$a_P = \sum_{nb} a_{nb} - S_P \qquad (3.81)$$

Thus equation $a_P \phi_P = \sum_{nb} a_{nb} \phi_{nb} + b$ ( 3.80) becomes:

$$\sum_{nb} a_{nb} \phi_{nb} + b - a_P \phi_P = 0 \qquad (3.82)$$

The residual $R^{\phi}$ computed by FLUENT's pressure based solver is the imbalance in equation $a_P \phi_P = \sum_{nb} a_{nb} \phi_{nb} + b$ ( 3.80) summed over all the computational cell P. This is referred to as "unscaled" residual. It may be written as:

$$R^{\phi} = \sum_{cells P} \left| \sum_{nb} a_{nb} \phi_{nb} + b - a_P \phi_P \right| \qquad (3.83)$$

In general is difficult to judge convergence by examining the residuals defined by equation $R^{\phi} = \sum_{cells P} \left| \sum_{nb} a_{nb} \phi_{nb} + b - a_P \phi_P \right|$ ( 3.83) since no scaling is employed. Fluent scales the residuals using a scaling factor representative of the flow rate of $\phi$ through the domain. This "scaled" residual is defined as:

$$R^{\phi} = \frac{\sum_{cells P} \left| \sum_{nb} a_{nb} \phi_{nb} + b - a_P \phi_P \right|}{\sum_{cells P} |a \phi_P|} \qquad (3.84)$$

For most problems, the default convergence criterion in Fluent is sufficient. This criterion requires that the scaled residuals decrease to $10^{-3}$ for all equation expect the energy equation, for which the limit is $10^{-6}$. Sometimes, however, this criterion may not be appropriate.

### *3.5.4 Boundary conditions*

The boundary conditions specify the flow and thermal variables on the boundaries of the physical model under examination, therefore it is important to have them correctly set. The boundary conditions avaible in Fluent are classified as follows:

- Flow inlet and outlet boundaries: pressure inlet, velocity inlet, mass flow inlet, inlet vent, intake fan, pressure outlet, pressure far-field, out flow, outlet vent, and exhaust fan.
- Wall, repeating and pole boundaries: wall, simmetry, periodic, and axis.
- Internal cell zones: fluid and solid (porous is a type of fluid zone).
- Internal face boundaries: fan, radiation, porous jump, wall and interior.

Velocity inlet boundary conditions are used to define the flow velocity, along with all relevant scalar properties of the flow, at flow inlets. All values are entered in the Velocity inlet panel, which can be opened from the Boundary Conditions panel.

Pressure outlet boundary conditions require the specification of a static (gauge) pressure at the outlet boundary. The value of the specified static pressure is used only when the flow is subsonic.

Typically, there are four boundary conditions required for gas dispersion modelling: inlet, outlet, top and bottom of the computational domain.

# 4 Results and discussion

The purpose of this work is to reproduce the experimental results gained with the Desert Tortoise experiment. In the first instance, in order to gain a better understand of the behavior of the different boundary conditions of the DPM, has been designed a 2D test case in which we focus on the temperatures reached by the system.

First will be proposed the general setting and in every section will be underlined the different settings to be able to reproduce the purposed results. Second, will be described and analyzed the simulation made with a 3D mesh, designed with the aim to reproduce the Desert Tortoise experiment. Again, settings and

## 4.1 2D test case

### *4.1.1 Case settings description*

Many settings could be chosen with the same aim, every one brings advantages and disadvantages, accuracy and low computational effort should be preferred but not every time is possible to collapse these advantages. The settings proposed were chosen in order to light the solution of the continuum phase, because has been noticed that the choice of very accurate but at the same time, very expensive solution methods led to convergence problem when the DPM was introduced into the calculations.

Table 2 shows the settings used to describe the continuous phase in every case both 2D and 3D; the steady-state formulation is preferred when Trap or Escape boundary conditions are implemented, the switch on of the energy is forced by the necessity to achieve accurate results, the viscous option are the most representative of the case in interest and the diffusion energy source takes into account the dispersion of ammonia due to concentration gradients:

| Case Description | |
|---|---|
| Type | Pressure Based |
| Time | Steady |
| Velocity formulation | Absolute |
| Energy | ON |
| Viscous | Standard $\kappa - \varepsilon$<br>Standard wall function<br>Full buoyancy effects |
| Species transport | Diffusion energy source |

*Table 2: Case settings*

The materials were described by the standard constant values that Fluent provides, except for the specific heat of the species that is “piecewise polynomial” (see Fluent user guide).

Since the DPM model is turn on particular attention must be paid when describing the droplet particle (which must be created): the saturation vapor pressure can be described by both piecewise linear and polynomial, but can not be described by the piecewise polynomial function. The piecewise linear method was preferred, which describes the saturation vapor pressure of the liquid phase with a broken line. 15 points were used to describe the temperature range between 195 K and 330 K, focusing on the locality of the boiling temperature at normal pressure (239.85 K). All the other settings needed to describe the liquid ammonia were imported from the Ansys Fluent database and are constant.

The DPM model can be set up: in the injection panel the droplet option must be chosen in order to activate the evaporation, heating and boiling laws, the user defined liquid ammonia is the material used to describe the droplets, the gaseous ammonia is the evaporating species. In the 2D case the droplets have a uniform diameter (0.001 m ) and are injected either at 238 K or 240 K. The mass flow rate is 3 $Kg/s$ and the droplets are injected perpendicularly to the nozzle

In order to complete the description of the case the boundary condition must be described so that: both the inlet and the injection are velocity inlet, the outlet is a pressure outlet, the ground is an adiabatic wall and the top is a wall.

### *4.1.2 2D Mesh description and independence*

In order to understand the effect of every boundary condition on the ammonia dispersion a 2D case has been described. The choice of a 2D domain was preferred because of the lower computation effort if compared with an analogous 3D simulation.

The grid is a rectangle 3 m high and 5 m long from which at the high of 1,5m a 0.5 m long and 1 cm high nozzle is extruded.

From the boundary called "inlet" in every simulation will be set a velocity magnitude and concentration of the incoming mixture. The "Injection" is defined as a velocity inlet as well, moreover, this boundary will be set as the injecting surface of the DPM's droplets.

The "Top" and the "Ground" boundary are defined as adiabatic walls. The "Outlet" is set as pressure outlet.

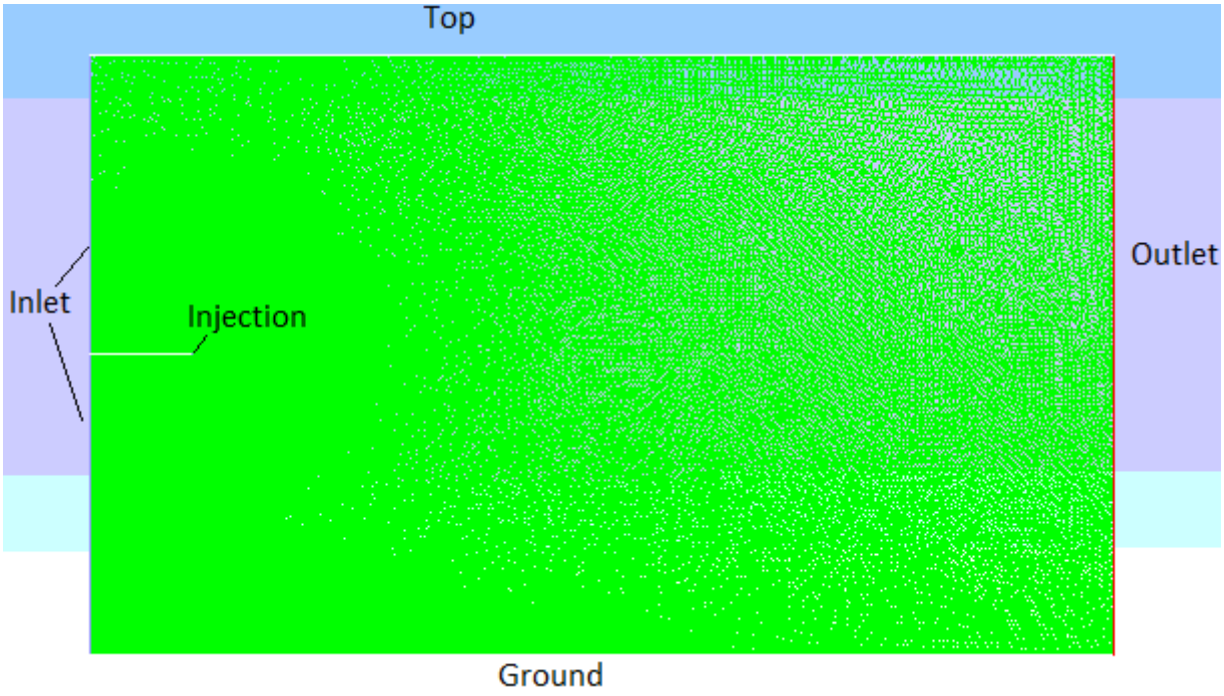


*Fig. 4-1: 2D mesh*

In order to accredit the results gained is mandatory to ceck the indipendece between the mesh and the results. Every mesh is 2D, 3m hight, 5m long with the DPM injection placed at 1.5 meters high with a 1 cm nozzle (see Fig. 4-2).

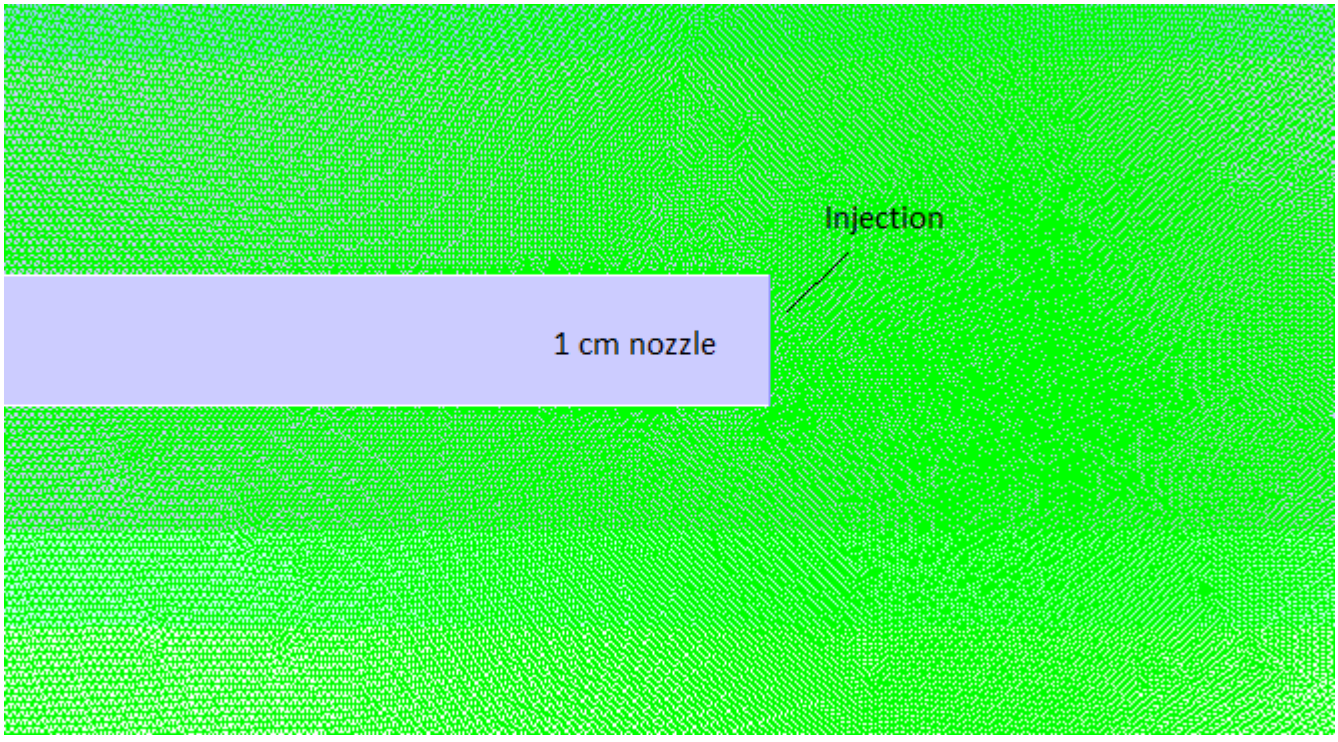


*Fig. 4-2:2D mesh injection particular*

The first grid to be designed was the most coarsen with 165000 cells, has been projected starting defining the cell dimension of the noozle applying a structure function to the entire domain setting the maximum face dimension reachable by the mesh (see Gambit user guide).

The other two meshes were obtained using the "adapt" option in Ansys Fluent (see a fluent user guide), that works placing a new node in the middle of a face, this methods, thus, quadruple the number of cells per every adaption. With the aim to chose the best grid for the simulations will be shown the comparison between three grids. The most coarsen grid is made with about 165000 cells, the intermediate is made with about 660000 cells and the most refined one is made with 2700000 cells. Tab. 1 shows the minimum and the maximum cell dimension per every mesh.

| Mesh cells | min. Face area | max. face area | number of droplets |
|---|---|---|---|
| 165000 | 1.00E-4 | 9.50E-2 | 100 |
| 660000 | 5.00E-5 | 4.75E-2 | 200 |
| 2700000 | 2.50E-5 | 2.30E-2 | 400 |

*Tab. 1: summary of minimum face area, maximum face area and number of droplets per mesh size*

Fig. 2-3 shows the ammonia mole fraction plotted in the y direction at 1m from the inlet. All the plots of the meshes are overlapped, this means that the results are not influenced by the calculation grid.

Fig. 2-4 shows the ammonia mole fraction plotted in the x direction at 1.5m high from the ground. In this plot, it is possible to detect the general overlap of the results.

The solutions are not dependent from the grid, therefore could be possible to chose the most coarsen mesh in order to proceed with the other calculations, but the number of droplets injected during the simulation is different due to the different number of segments that compose the injection. Anticipating the necessity to describe a very complicated aspect of the DPM (wall-film boundary condition) , the 660000 cells mesh was chosen in order to perform the calculations which results in reliable results and allows a proper description of the droplets.

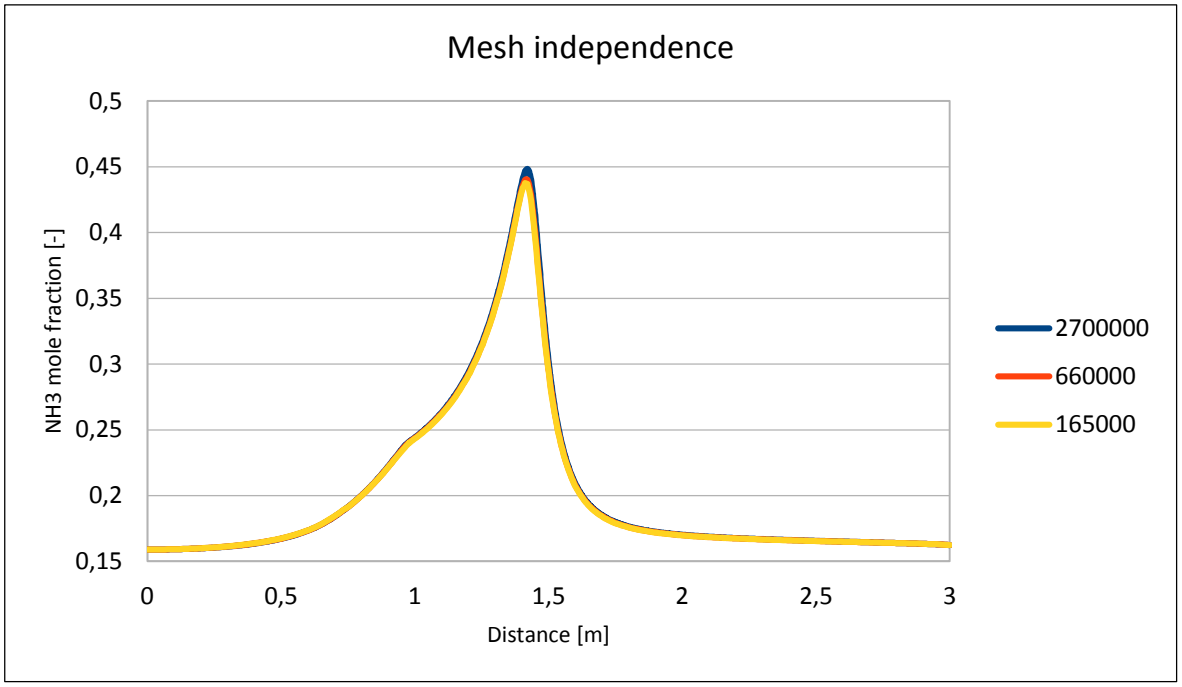


*Fig. 4-3: Ammonia mole fraction along y axis at x= 1m*

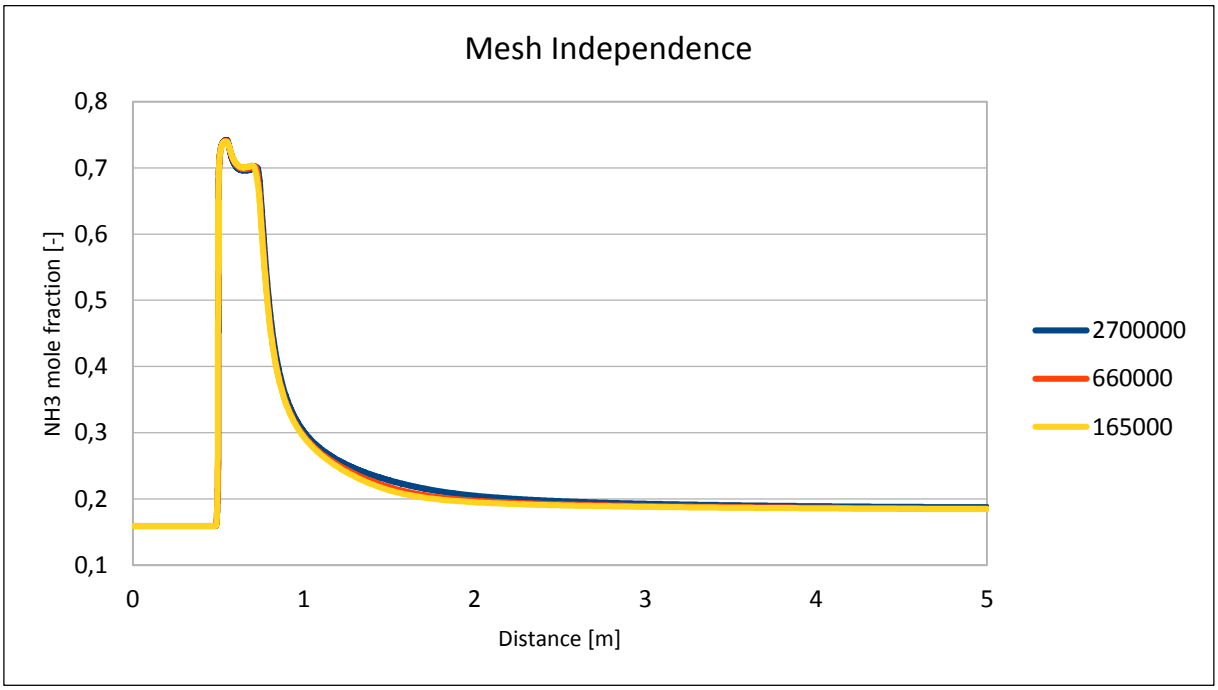


*Fig. 4-4 Ammonia mole fraction at 1.5 m high, x direction*

### *4.1.3 Droplet injection temperatures (heat description)*

The droplet injection temperature must be chosen carefully because, depending on that, the description of the energy balance referred to the droplet changes substantially. As explained in the paragraph "Droplet temperature laws" if the injection temperature of the droplets is below the boiling point (3.44) then a heat balance is applied (3.46) otherwise, when the droplet temperature is supposed

to be higher than the boiling point, only an equation that describes the rate of mass loss is applied (3.55). This aspect must not be underestimate because when supercooled droplets are injected, coupled with the Trap boundary condition non consistent results can be reached.

In order to better understand the influence of the injection temperature two case have been set up (see Table below); Case 1 and Case 2 are set up with the Escape boundary condition, but, they differ in the definition of the droplets injection temperature.

| | Ground DPM boundary condition | Droplets temperature injection |
|---|---|---|
| Case 1 | Escape | 238 |
| Case 2 | Escape | 240 |

*Table 3: Case 1 and case 2: Droplet temperature injection and boundary condition adopted*

The case 1 refers to the equation 3.44, the case 2 to the equation $T_p < T_{bp}$ *( 3.47*: as expected the minimal droplet temperature reached in case 1 is below the boiling temperaure and is 212,14 K, on the other hand the minimal temperature reached is 239.85 (which is the boiling temperature set for the ammonia).

### *4.1.4 Trap and Escape boundary temperature problems*

The boundary conditions that effects the behavior of the DPM particles are: escape, trap and wall-film. The escape condition reflects the hypothesis that the droplets that reach a surface with this condition exit from the domain and they are no more effective on the domain (this approach could be validated in those cases when the liquid fraction that forms the pool has a low evaporation rate and the quantity that evaporates can be neglected). The trap choice supposes that every particle is important in the domain and also the liquid fraction that forms the pool is effective on the concentration downstream (Ansys fluent forces the evaporation of the droplets that reach the ground regardless of the temperature) .From this point of view the wall-film boundary condition arises between this two hypothesis and evaluates, particle by particle, every aspect of the physic of the droplet (see chapter DPM Boundary conditions). The other substantial difference is that the wall-film condition can be used only in an unsteady simulation.

The trap boundary condition shown strong inconsistence problems: when the droplet gets "trapped", the evaporation/boiling laws are not anymore used, and the entire droplet mass passes instantaneously

in vapor phase, regardless of the cell temperature. This behavior led to temperature problems which have been analyzed with two cases: Case 3 and Case 4 are set up with the same settings of the Case 1 and 2, but instead of the Escape Boundary condition, the Trap condition was used. Again, the effect of different temperature description for the droplets was evaluated.

| | Ground DPM boundary condition | Droplets temperature injection |
|---|---|---|
| Case 3 | Trap | 238 K |
| Case 4 | Trap | 240 K |

*Table 4: Case 3 and case 4 used to describe the Trap boundary condition*

The temperature characterizing these simulation are listed below:

| | Droplet minimum temperature | Air minimum temperature |
|---|---|---|
| Case 3 | 183 K | 1 K |
| Case 4 | 239.85 K | 1 K |

*Table 5: Case 3 and case 4 minimum temperature reached by the system*

The droplet minimum temperature can be explained by the droplet temperature injection discussed above; the minimum air temperature surrounding the droplets is caused by forced evaporation of the droplet, which require heat in order to be evaporated, this heat is provided by the surrounding air which is led to such low and unrealistic temperature, this is a bug of the software.

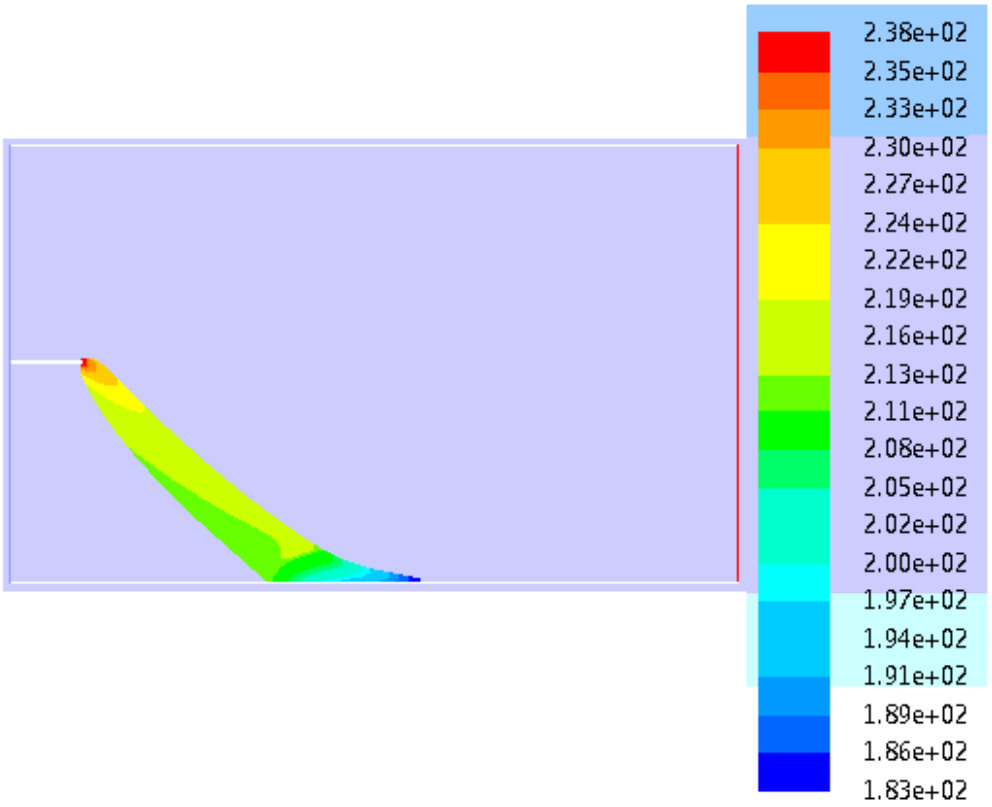


*Fig. 4-5: Case 3 droplet temperature*

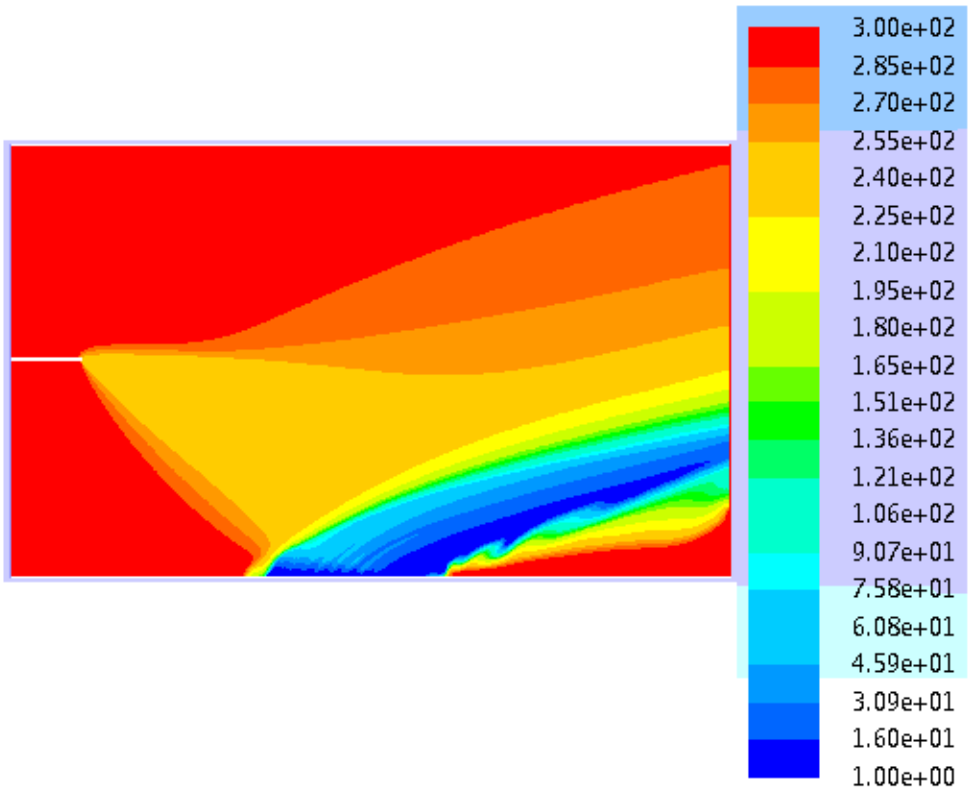


*Fig. 4-6:Case 3 air temperature*

Fig. 4-5 and Fig. 4-6, that refers to Case 3, show the behavior explained; this result was confirmed by the Fluent assistance. Fig. 4-6 shows that the temperature drop comes from the cells where the Trap boundary condition takes place, and the surrounding air is not able to compensate the heat request by the droplet vaporization. The only way in order to drive the temperature is to rise the lower limit of the simulation.

When the Trap boundary condition is replaced by the Escape condition the droplet temperature problems vanish. In order to validate the droplet temperature which are ruled by the Raoult equation:

$$x_i^V p = x_i^L p_{sat,i} \qquad (4.1)$$

Other two cases have been set up. Case 1, 5 and 6 differ only by the concentrations of the injected mixture of air and ammonia into the domain, in such conditions, if the Raoult equation is respected, the minimum concentration that the droplets could reach is dependent on the concentration of ammonia surrounding the droplet which is forced by the concentration of ammonia in the mixture injected.

| | Droplet release temperature | Boundary condition | $NH_3$ minimum concentration allowed | Droplet minimum temperature |
|---|---|---|---|---|
| Case 1 | 238 | Escape | 0.16 | 212 |
| Case 5 | 238 | Escape | 0.53 | 226 |
| Case 6 | 238 | Escape | 0.9 | 236 |

*Table 6:Minimum droplet temperature Vs ammonia concentration*

The results are consistent with the piecewise linear description of the liquid ammonia (summarized below):

| Temp. [K] | 194 | 195 | 205 | 215 | 225 | 235 | 240 |
|---|---|---|---|---|---|---|---|
| Pres. [Pa] | 0 | 5940 | 12655 | 24897 | 45773 | 79405 | 102593 |

*Table 7: Droplet vapor pressure description*

Indeed, Case 1 minimum droplet temperature is 212 K, and the partial pressure with a concentration of ammonia of 0.16 [mol/mol] is 16212 Pa ($x_i^V p = 0{,}16 * 101325 = 16212$), which correspond to the interval described by the piecewise linear descripted. The same procedure can be replicated for both Case 5 and Case 6, the resulting minimum droplet temperature are mirrored by the droplet vapor

pressure descripted. With this results was proved that the temperature issues tackled in the previous chapters are not related to the definition of the particle settings but are related to the boundary condition used time by time.

### *4.1.5 Wall-film boundary condition*

All the simulations shown above are steady, the wall-film boundary condition can work only in a transient simulation. The description of the physics of the particles is the most accurate; taking into account: stick, rebound, spread and splash of the droplets. Introducing the time dependent simulation the stochastic aspect of the model turns on.

| | Time dependence | Boundary condition | DPM inject temp | Ammonia mole fraction injected |
|---|---|---|---|---|
| Case 7 | Unsteady | Wall-film | 238 | 0.159 |

*Table 8: Case 7 description*

From Fig. 4-7 to Fig. 4-11the simulations of the case 7 are shown. The time step of the simulation is 0.5 sec, in order to avoid the time dependence of the results (Fluent suggests to chose at least 1/10 of the time of the phenomena). The DPM injects 200 particles (the number could be set by the user) every time step and calculating the trajectory and the interaction between the droplets and the continuum phase. As long as the droplet follows its trajectory, the temperature drops according to the heat balance due to evaporation. Fig. 4-10 and Fig. 4-11 show the formation of the pool: the droplets still cool down due to evaporation. The simulation stops when the pool widen and starts to escape from the outflow boundary. The minimum temperatures reached by the system at every time step are listed below:

| Time | 0.1 | 0.2 | 0.3 | 0.4 | 0.5 | 0.6 | 0.8 | 0.9 | 1 | 1.15 |
|---|---|---|---|---|---|---|---|---|---|---|
| Temp | 223 | 222 | 216 | 215 | 213 | 212 | 212 | 200 | 199 | 199 |

*Table 9: Minimum temperature reached by the system at every time step*

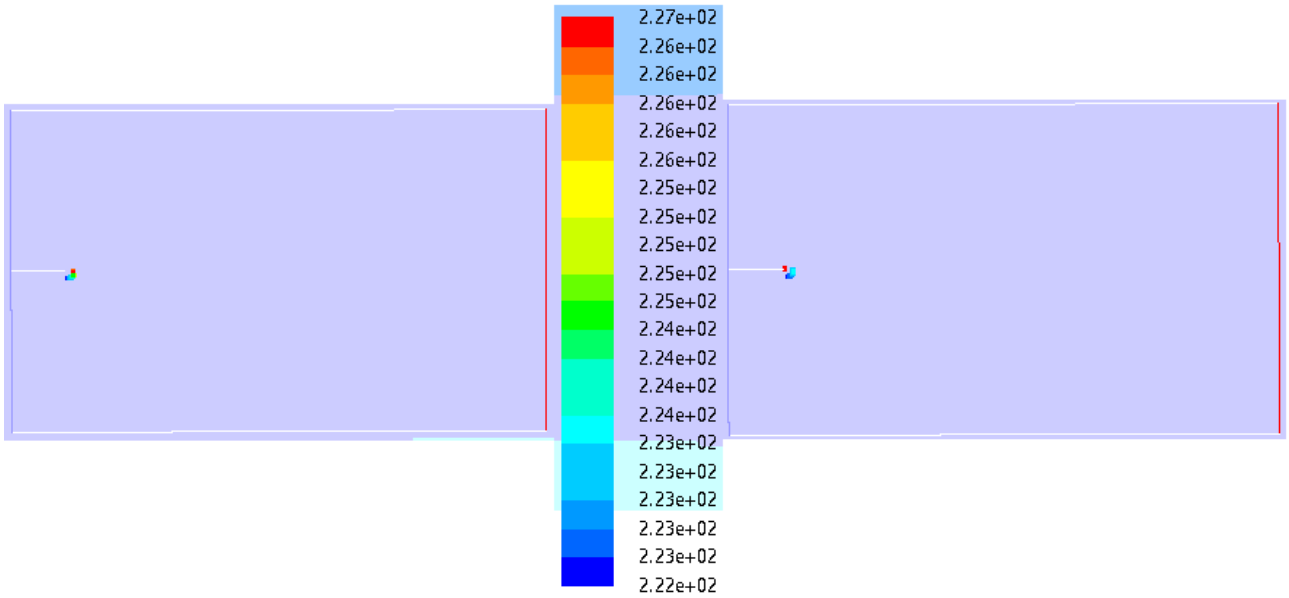


*Fig. 4-7:Droplet temperature at t=0,1 and t=0,2 sec*

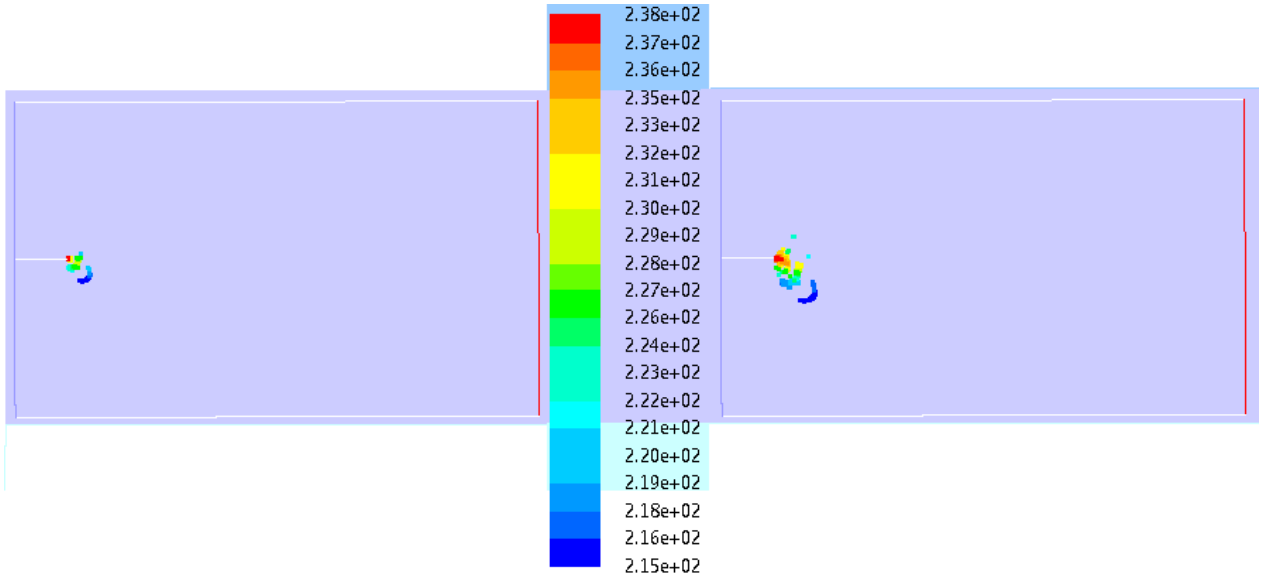


*Fig. 4-8: Droplet temperature at t=0.3 and t=0.4 sec*

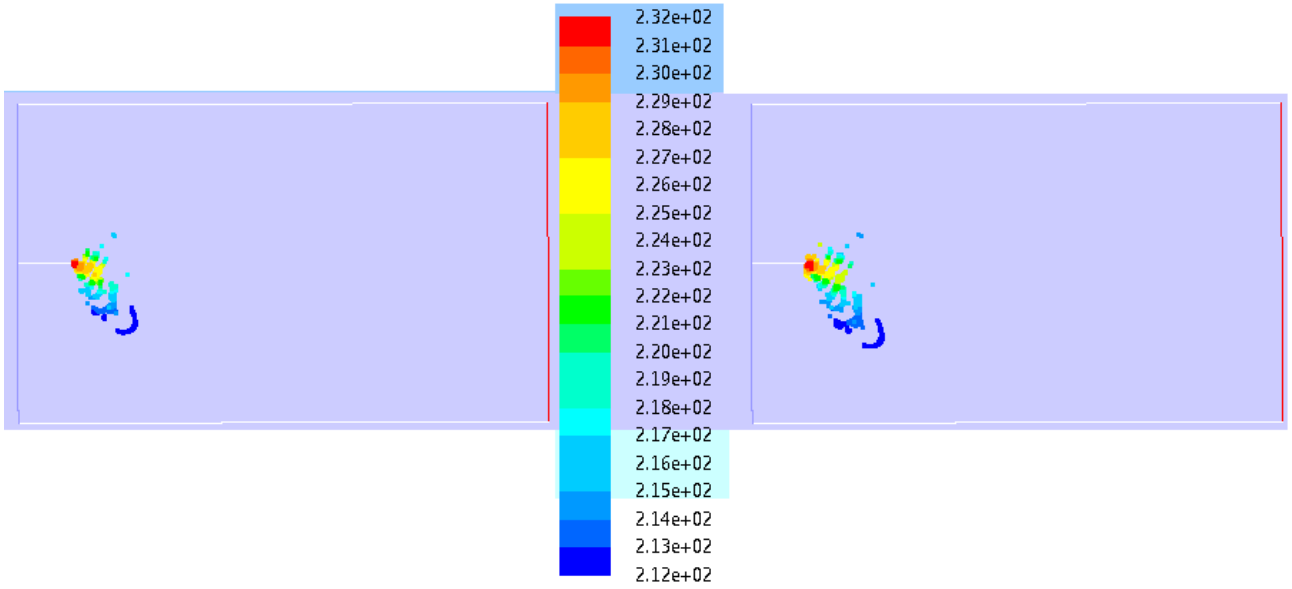


*Fig. 4-9:Droplet temperature at t =0.5 and t=0.6 sec*

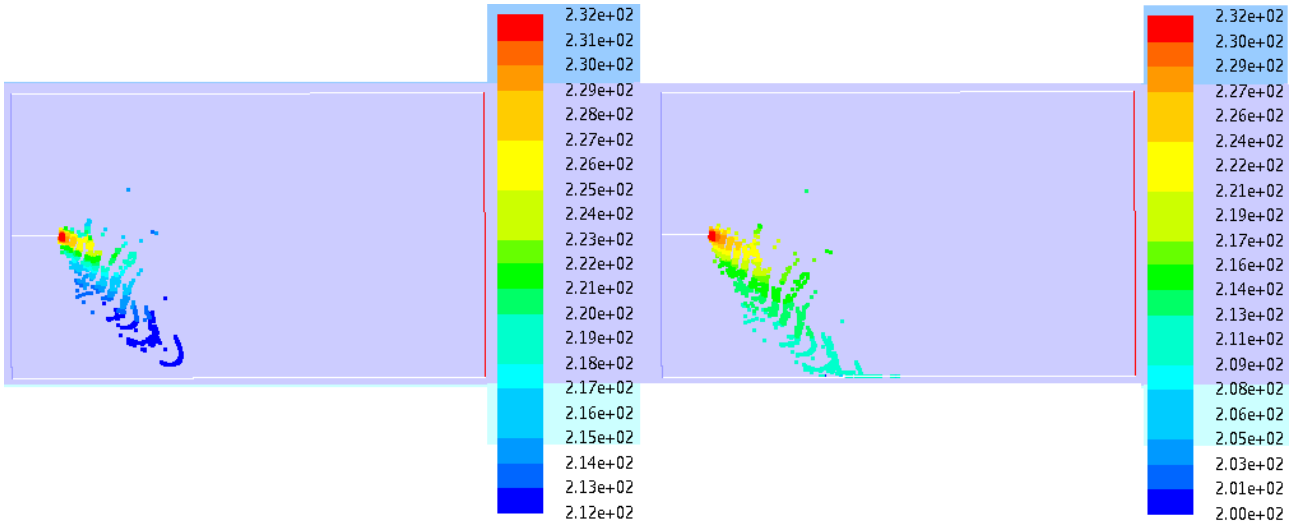


*Fig. 4-10:Droplet temperature at t=0.8 and t=0.9 sec*

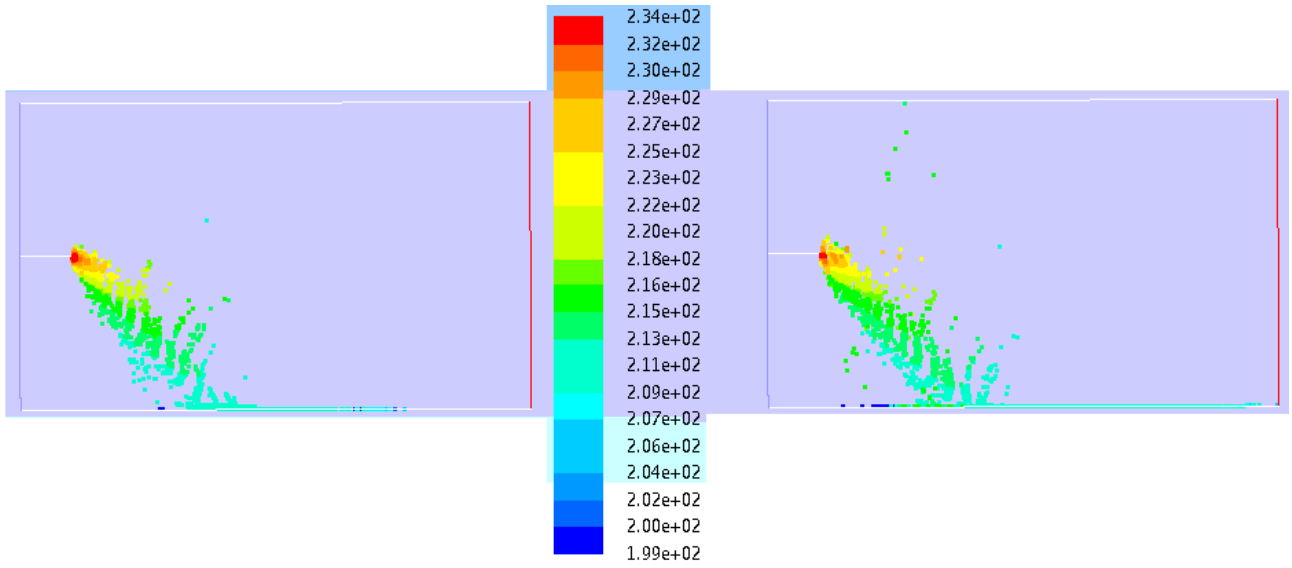


*Fig. 4-11Droplet temperature at t=1 and 1.15 sec*

From Fig. 4-1212 to Fig. 4-165 the ammonia mole fraction at every time step is shown, as long as the droplet are injected the plume widen. Particular attention must be paid at time 0.9 sec: from Fig. 4-15 can be noticed the increase of the ammonia near the ground, this is due to the formation of the pool, which can be seen in Fig. 4-10

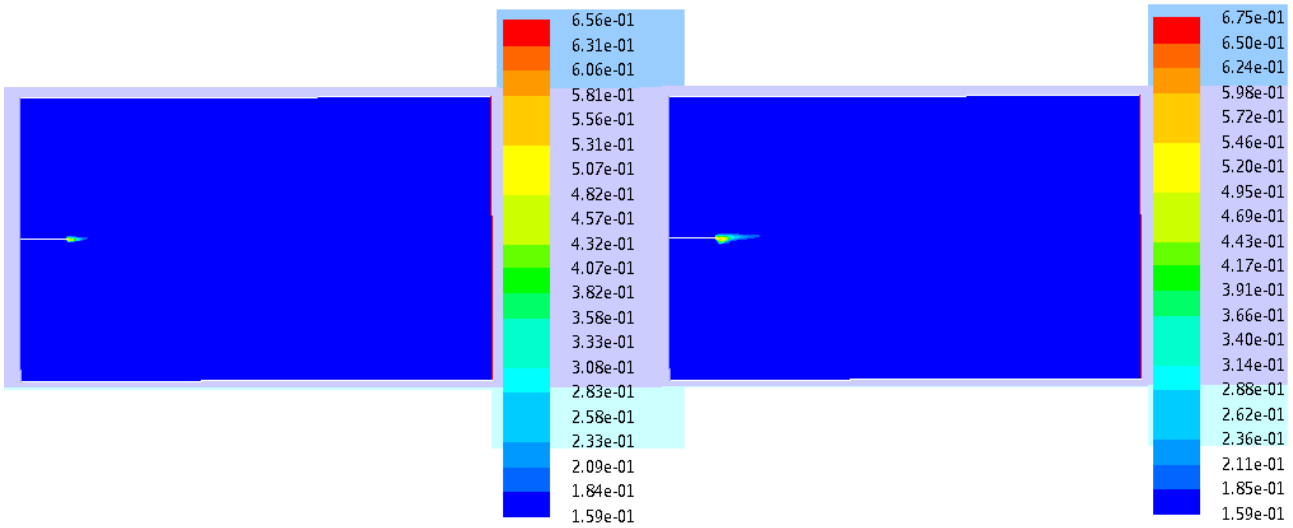


*Fig. 4-12: Ammonia mole fraction at t=0.1 and 0.2 sec*

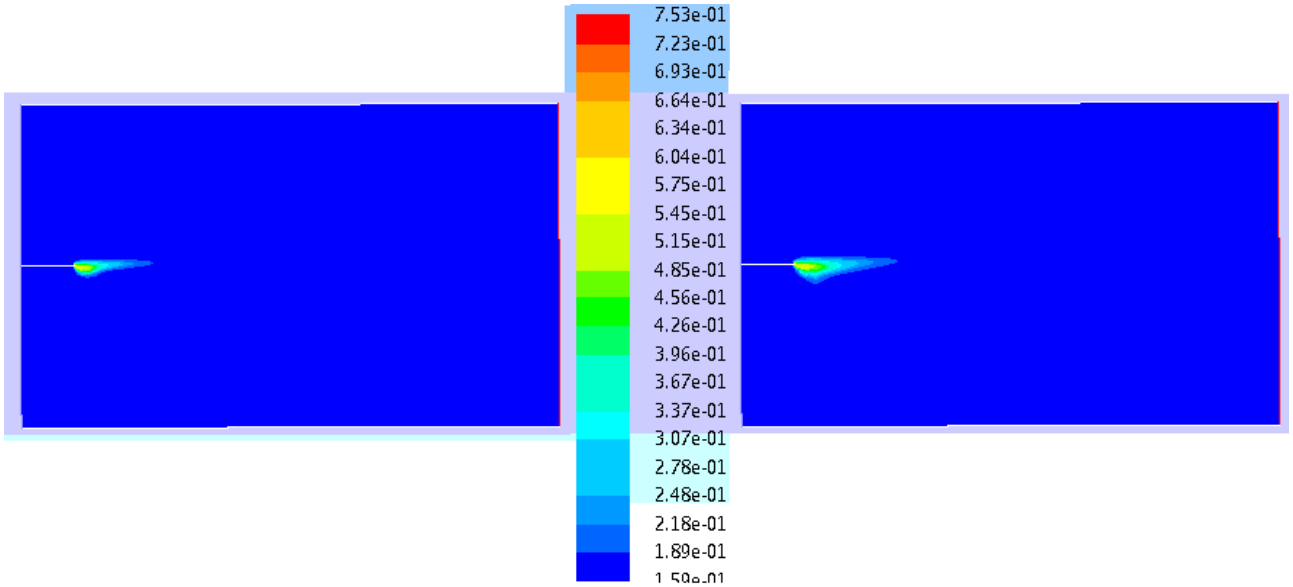


*Fig. 4-13:Ammonia mole fraction at t=0.3 and 0.4 sec*

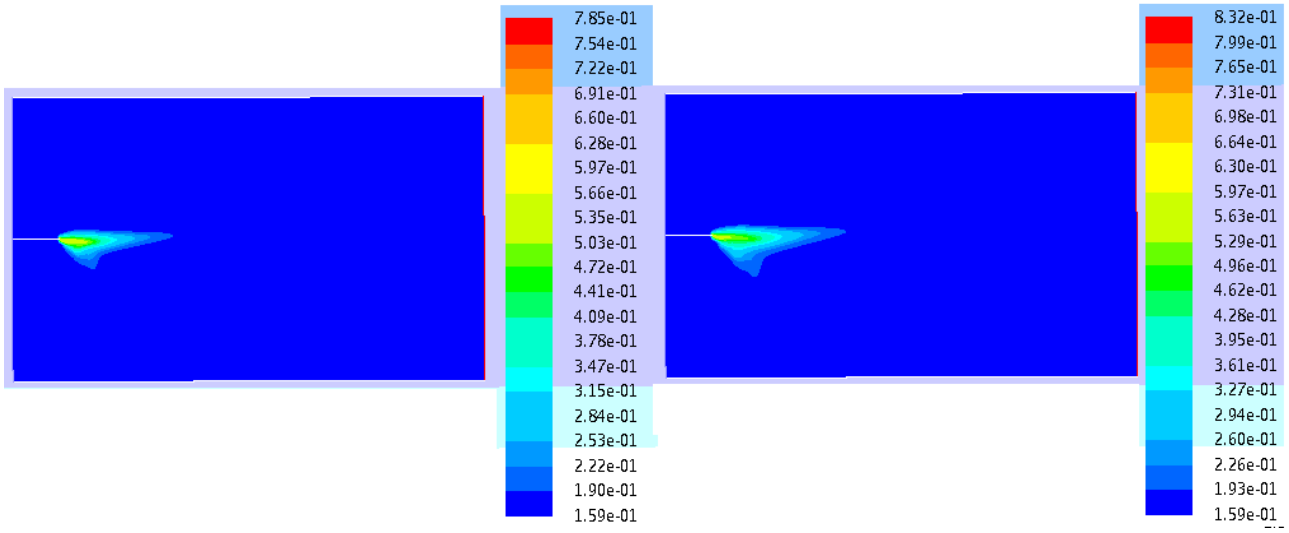


*Fig. 4-14: Ammonia mole fraction at t =0.5 and 0.6 sec*

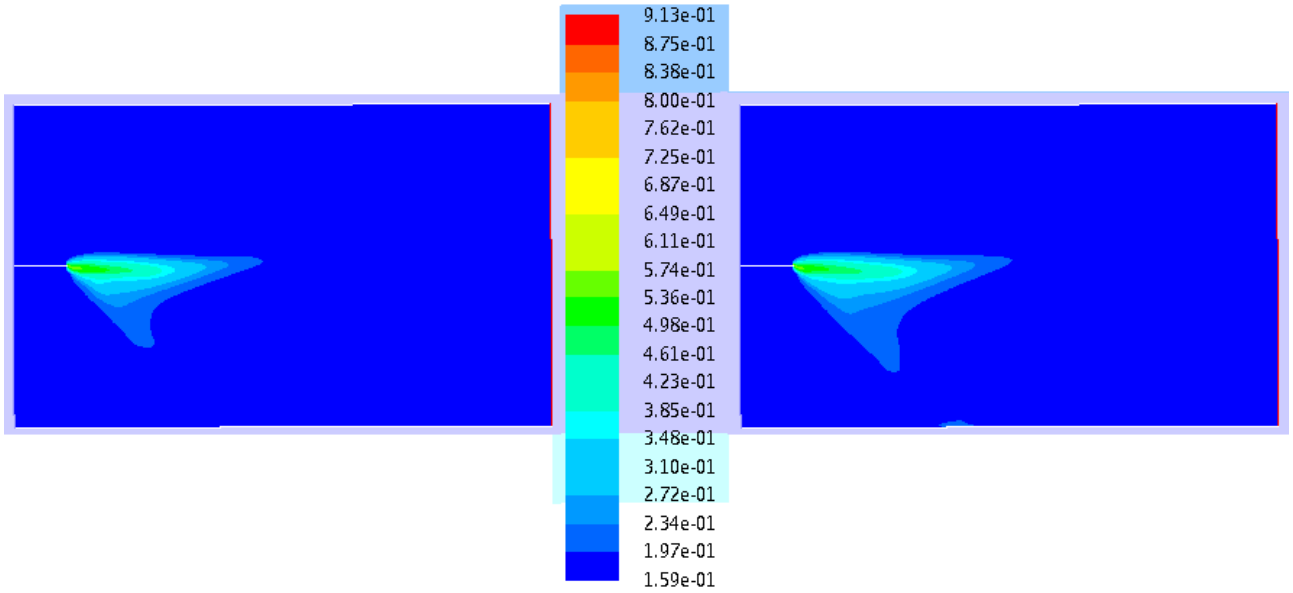


*Fig. 4-15: Ammonia mole fraction at t=0.8 and 0.9*

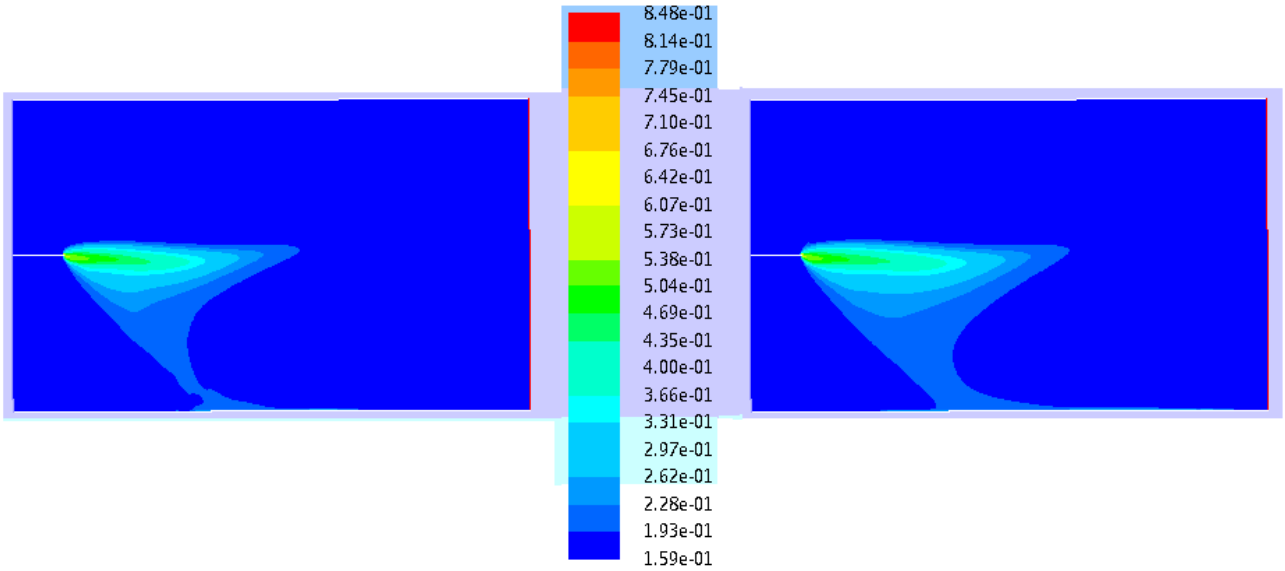


*Fig. 4-16: Ammonia mole fraction at t=1 and t=1.15 sec*

## 4.2 Mesh 3D Desert Tortoise experiment

This series of tests, called the "Desert Tortoise" series tests releasing anhydrous liquefied ammonia, is similar to the Goldfish tests using hydrogen fluoride. The tests were conducted in 1983 by Lawrence Livermore National Laboratories at the same site as the Goldfish tests, and are described in a report by Goldwire et al, 1985 [Goldwire, H.C. Jr. et al, "Desert Tortoise series data report 1983 pressurized ammonia spills", UCID-20562, Lawrence Livermore National Laboratories, Livermore, CA]. Pressurized and liquefied anhydrous ammonia stored at ambient temperature was released from a tank via a jet directed horizontally downwind in a series of four tests, the release point one meter from the ground. Because of a rainstorm just prior to the releases, the dry lake bed known as Frenchman Flat was covered by a shallow layer of water during most of the experiments. At the release point, about 18% of the liquid flashed, becoming a gas. The rest of the liquid became entrained as a fine aerosol in the gaseous cloud. Very little unflashed liquid was observed to form a pool on the ground. Ammonia concentrations and temperatures were obtained from towers placed along arcs at distances 100 and 800 meters downwind at heights ranging from 1 to 8.5 meters. In addition, portable ground level stations measured ammonia concentrations at 1400 or 2800 meters, or 3500 and 5600 meters. The Desert Tortoise series test results were made available to gas dispersion modelers.

Whit the information gained thanks to the 2D case the purpose of the 3D case is to reproduce the desert tortoise experiment. With this mesh will be tested the effect of the adiabatic or isothermal boundary condition for the ground, the effect of the Trap and Escape boundary, the effect of the

injection temperature of the droplet on the concentration of ammonia downstream.

### *4.2.1 3D Mesh description and independence*

It is a common practice, in the CFD simulations of two-phase releases, to start from the so called "expansion zone", because the model of the mechanical break-up of the droplet is not completely developed, so is preferable to describe the droplets with a distribution that approximate the real case.

The domain is 900x200x200 m3 (respectively: lenght, width, height).Only half domain of the Desert Tortoise has been modeled in order to safe computational effort. So that, the release surface is a half circle circle of 0.53 m diameter at 0.79 m height; it is also used as the injection for the NH3 droplets with the DPM. It was shaped a 1 meter long solid part at the release in order to soften the turbulence that would be created just placing a surface, the rest of the domain is empty. The inlet is modeled as a "velocity inlet" with a user defined function for the description of the velocity field, according to the Monin-Obukhov profile, the outlet is a "pressure outlet", the top and the sides are "symmetry planes", the ground is a wall with a roughness of 0.03 m. The resolution of the mesh is about 1250000 cells. Fig. 4-17: 3D mesh, and boundary namesshows the 3D mesh. Fig. 4-18 shows a particular of the injection surface.

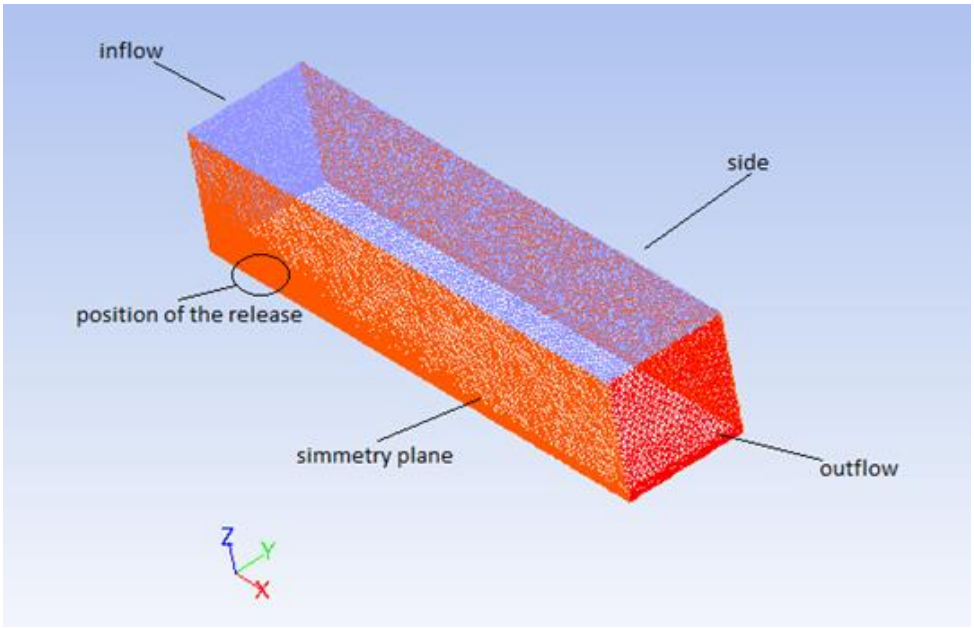


*Fig. 4-17: 3D mesh, and boundary names*

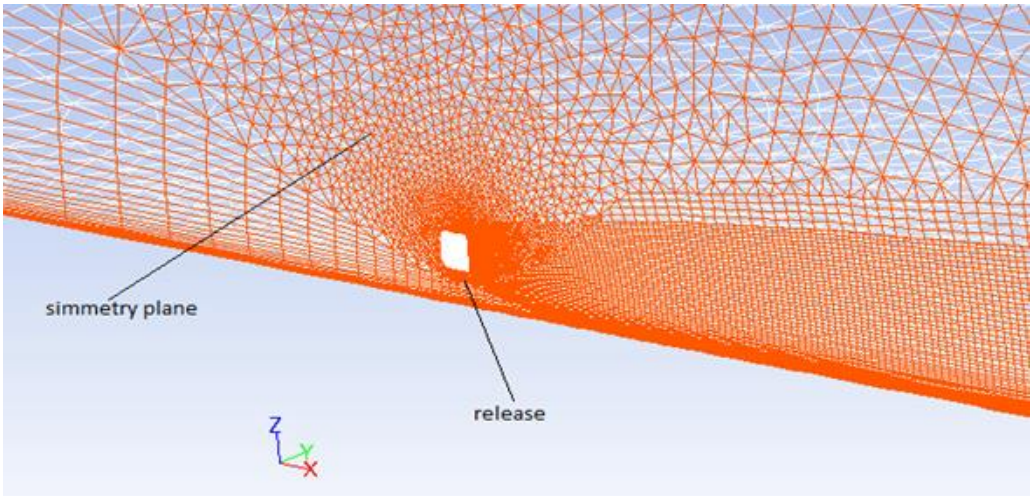


*Fig. 4-18:mesh particular*

As can be seen in the particular that the mesh has been built with a particular structure: the first 15 meters (from the bottom) has been designed with parallelepiped cells, because the flow has been anticipated to be smooth and regular in front of the release. The rest of the domain is made with exagonal cells in order to reduce the number of cells within the domain.

In order to validate the results gained with the mesh described a new mesh has been obtained thanks to the "adapt" option provided by Ansys Fluent ( see a Fluent user manual). The result is a mesh with about 10,000,000 cells. The comparison between the two meshes is shown in Fig. 4-19: the plot regards the ammonia molar fraction along the x axis. By the comparison of the graphs is possible to assume the independence of the results by the mesh.

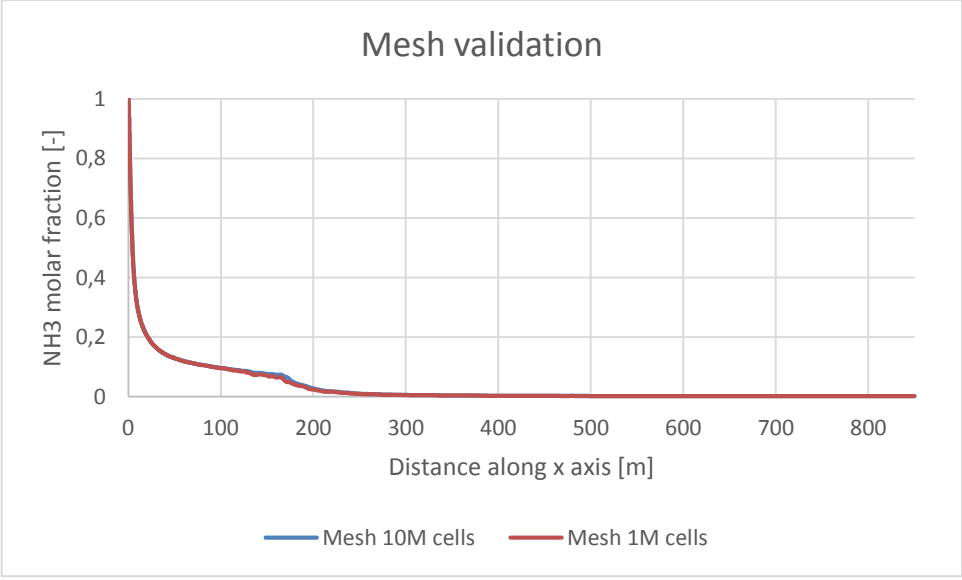


*Fig. 4-19:Mesh comparison by ammonia molar fraction*

### 4.2.2 *Direction of plot*

In order to expose to the reader clearly the direction of plot taken to describe the 3D mesh field i.e concentration of ammonia, temperature, etc. The image below shows both the plot direction and the captation position used during the experiment (pointed with red dots). Table 10 shows the precise coordinates of the plots directions.

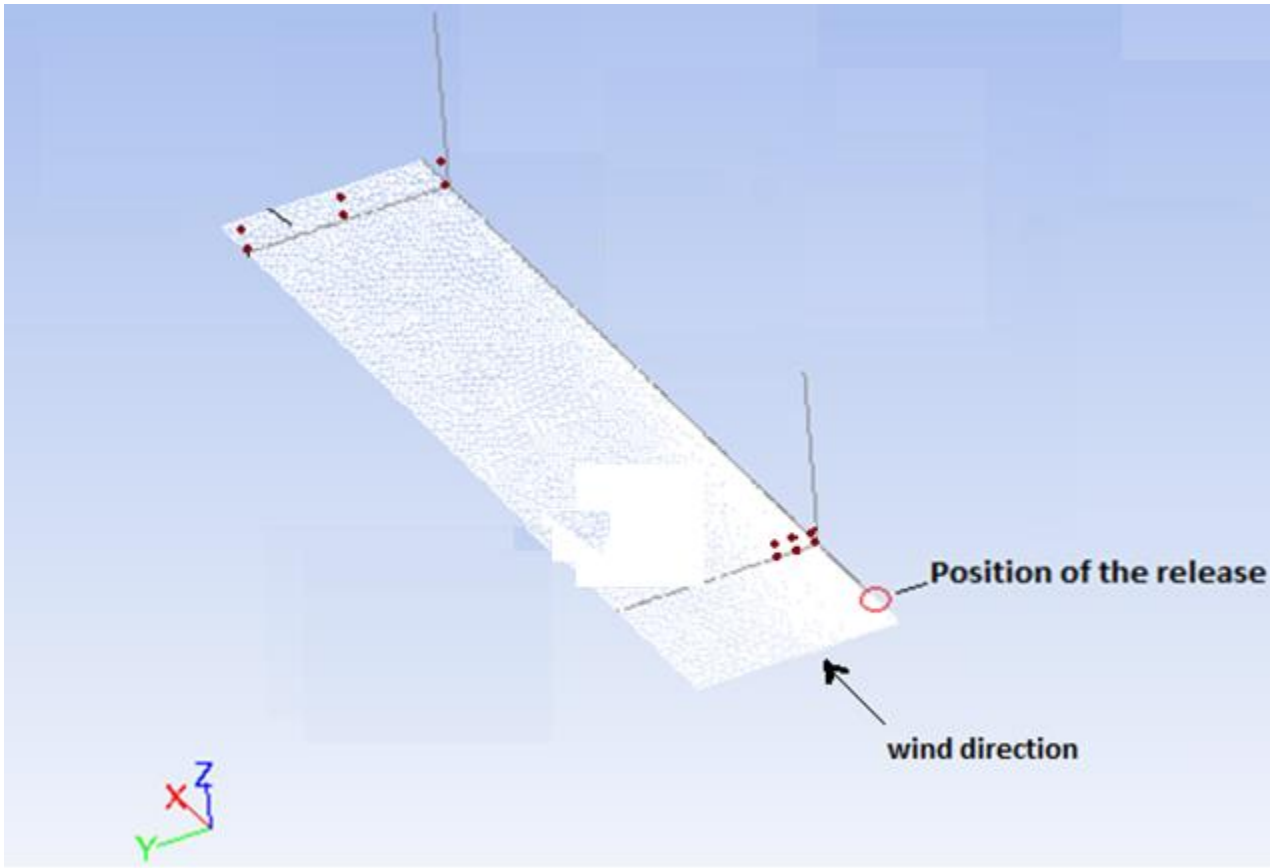


*Fig. 4-20:Direction of plot*

| Name of the line | x | y | z |
|---|---|---|---|
| Plot along x axis | 0 < x < 800 | y=0 | z=1 |
| Plot at 100 m y direction | x=100 | 0 < y < 200 | z=1 |
| Plot at 800 m y direction | x=800 | 0 < y < 200 | z=1 |
| Plot at 100 m z direction | x=100 | y=0 | 0 < z < 200 |
| Plot at 800 m z direction | x=800 | y=0 | 0 < z < 200 |

*Table 10: Table of coordinates of the plots*

### 4.2.3 *Elaboration of the experimental data*

In order to compare the experimental data, which are time dependent, with the results of the simulation (which are steady) in every graph the experimental data, will be shown with a box-plot which refers to the maximum, average and minimum of the experimental data that are supposed to properly symbolize the steady release (Fig. 4-21 is an example).

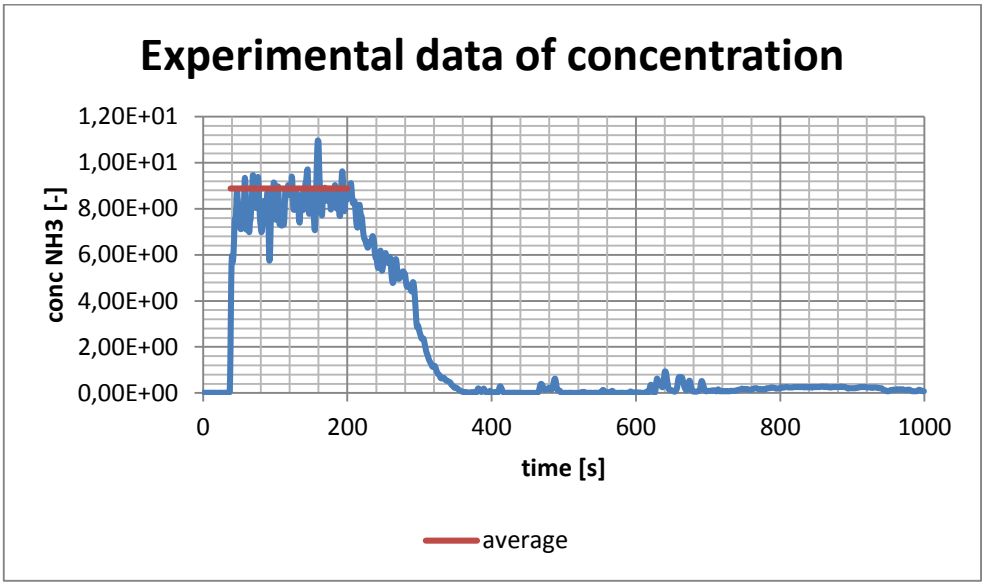


*Fig. 4-21: Average of the experimental data used to be compared with the steady simulations results*

### 4.2.4 *Setting used for the detailed description of the cases*

The thermal conducivity, the viscosity, the $C_p$ and the vapour pressure of ammonia are described thanks to a linearization of the laws gained from the DIPPR (Design Institute for Physical PRoperty) database. This choice is forced by the request of fluent: every thermodynamic property could be implemented either thanks to a constant or a polynomial (piecewise or not, see (Fluent, 2006)).

For the thermal conducivity the DIPPR law is:

$$K = \frac{C_1 T^{C_2}}{1+\frac{C_3}{T}+\frac{C_4}{T^2}} \qquad (4.2)$$

Follow the parameters for both compounds Table 11:

| | AIR | AMMONIA |
|---|---|---|
| C1 | 0.000314 | 9.66E-06 |
| C2 | 0.7786 | 1.3799 |
| C3 | -0.7116 | |
| C4 | 2121.7 | |

*Table 11: parameters used for the description of the termal conducivity*

In the Fig. 4-222 the results of the linearization are shown.

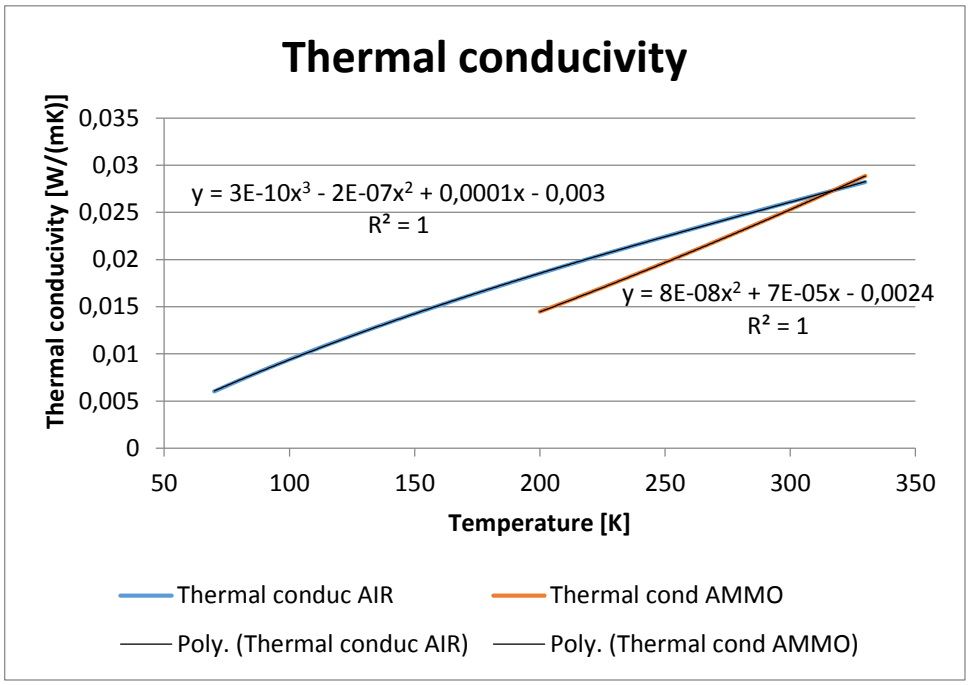


*Fig. 4-22: Thermal conducivity and related lineariziations*

For the vapor viscosity $\mu$, the law used was:

$$\mu = \frac{C_1 T^{C_2}}{1+\frac{C_3}{T}} \qquad (4.3)$$

And the parameters needed for both ammonia and air follow (Table 12:parameters used to describe the viscosityTable 12)

| | AIR | AMMONIA |
|---|---|---|
| C1 | 1.43E-06 | 4.19E-08 |
| C2 | 5.04E-01 | 0.9806 |
| C3 | 108.3 | 30.8 |

*Table 12:parameters used to describe the viscosity*

Fig. 4-23 shows the results of the linearization.

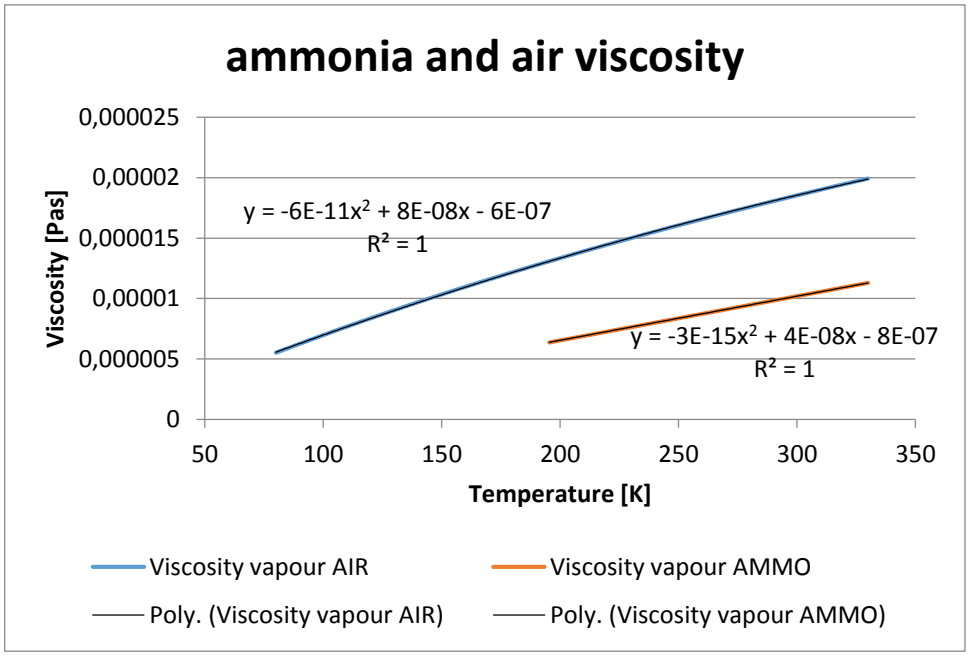


*Fig. 4-23:Viscosity interpolation polynomes*

The law used for the $C_p^0$ of vapour ammonia:

$$C_p^0 = C_1 + C_2\left[\frac{C_3/T}{sinh(\frac{C_3}{T})}\right]^2 + C_4\left[\frac{C_5/T}{cosh(\frac{C_5}{T})}\right]^2 \qquad (4.4)$$

The parameters are Table 13:

| | AMMONIA |
|---|---|
| C1 | 33427 |
| C2 | 48980 |
| C3 | 2036 |
| C4 | 22560 |
| C5 | 882 |

*Table 13: ammonia parameters used for the cp description*

The interpolation of the law yelds (Fig. 4-24):

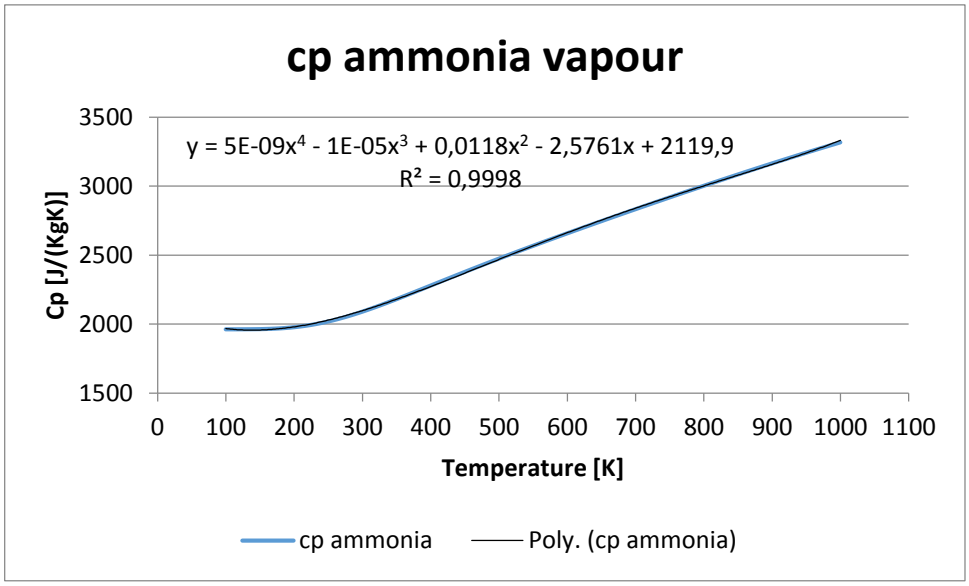


*Fig. 4-24:Cp ammonia polynome*

For the $C_p^L$ of ammonia the law used is:

$$C_p^L = \frac{A^2}{t} + B - 2ACt - ADt^2 - \frac{C^2t^3}{3} - \frac{CDt^4}{2} - \frac{D^2t^5}{5} \qquad (4.5)$$

Where

$$t = (1 - \frac{T}{T_C}) \qquad (4.6)$$

The corresponding parameters for ammonia are (see Table 14):

| | |
|---|---|
| A | 61 |
| B | 80925 |
| C | 799.4 |
| D | -2651 |

*Table 14:parameters used for liquid ammonia description*

And the linearization leads to (see Fig. 4-25:Liquid ammonia cp polynome)

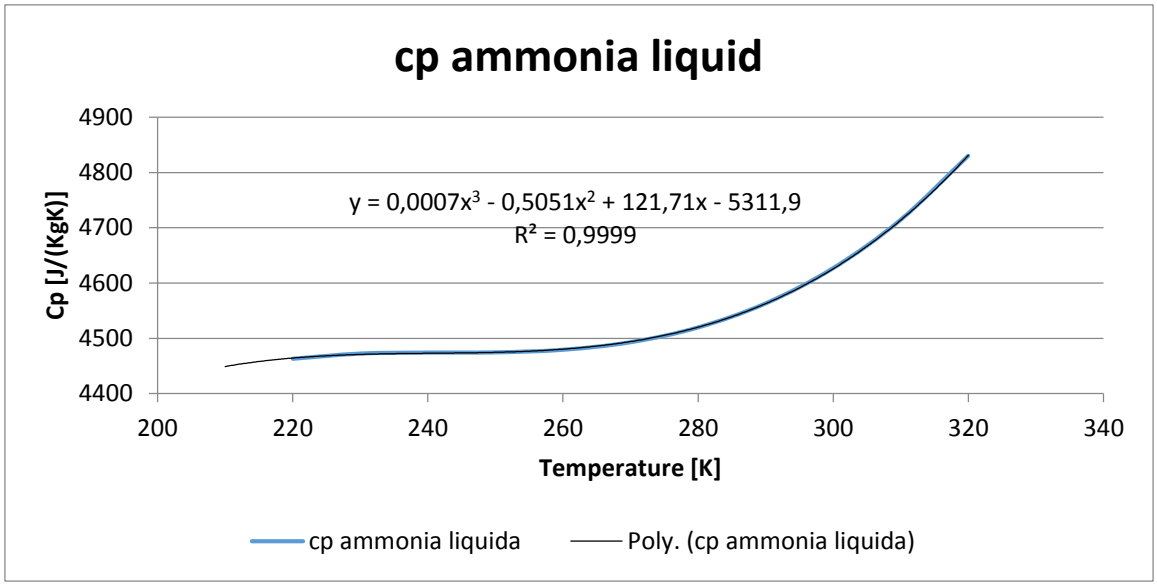


*Fig. 4-25:Liquid ammonia cp polynome*

For the vapor pressure of ammonia a piecewise linear description was used (see chapter 4.1.4). The properties of the vapor phase of $NH_3$ are shown in Table 15. Table 16 shows the laws related to the liquid phase and Table 17 lists the laws used to describe the mixtures.

| NH3 (g) | Property temperature dependence | Interval of validation |
|---|---|---|
| Cp ( J/Kg K ) | 2119.9 - 2.5761 $T$ – 0.0118 $T^2$ + - 1E-5 $T^3$ + 5E-9 $T^4$ | 100 < T < 1500 |
| Thermal conducivity ( W/m K ) | -0.0024 + 7E-5 $T$ + 8E-8 $T^2$ | 200 < T < 330 |
| Viscosity ( Pa s ) | -8E-07 + 4E-08 $T$ – 3E-15 $T^2$ | 195 < T < 330 |
| Molar weight ( g/mol ) | 17.03061 | |
| Reference temperature ( K ) | 298.15 | |
| L-J characteristic lenght (angstrom ) | 4 | |
| L-J Energy Parameter ( K ) | 100 | |

*Table 15:Summary properties vapor ammonia*

| NH3 (l) | Property temperature dependence | Interval of validation |
|---|---|---|
| Density ( Kg/m3 ) | 683 | |
| Cp ( J/Kg K ) | -5311.9 + 121.71 $T$ – 0.5051 $T^2$+ 0.0007 $T^3$ | 203 < T < 405 |
| Thermal conducivity (W/m K) | 0.665 | |
| Latent Heat ( J/Kg ) | 1368293 | |
| Thermophoretic coefficient (Kg m2/s2 ) | | |
| Vaporization temperature ( K ) | 100 | |
| Boiling Point ( K ) | 239.85 | |
| Volatile component fraction ( % ) | 100 | |
| Binary diffusion coefficient ( m2/s ) | 3.05e-05 | |
| Saturation vapor pressure (Pa) | 5913<br><br>-1E+07 - 196704 $T$ – 909.48 $T^2$ +<br>+ 1.4137 $T^3$ | 1 < T < 195<br><br>195 < T < 335 |
| Heat of pyrolysis ( J/Kg ) | 0 | |

*Table 16: Properties liquid ammonia*

| Air + NH3 mixture | |
|---|---|
| Density | Ideal gas |
| Cp | Mixing-Law |
| Thermal conducivity | Mass-weighted mixing law |
| Viscosity | Mass-weighted mixing law |
| Mass diffusivity | Kinetic – theory |
| Thermal diff. coefficients | Kinetic – theory |

*Table 17: Properties of the mixture*

### 4.3 3D case results and discussions

Thanks to the 2D test case is possible to anticipate the shortcomings that could spot during the 3D simulation, and analyze the data more clearly. The validation of the Desert Tortoise experiment has been performed with two different cases, one more detailed than the previous, but with the same

mesh. The less realistic cases have been performed using the settings as the 2D cases; the more realistic cases have been performed using the settings described in paragraph 4.2.4.

### *4.3.1 Monin-obukhov validation*

The Monin Obukhov similarity theory is an important foundation for much understanding of the atmospheric surface layer. The theory posits that the flow in uniform, steady atmospheric surface layers depends on only four local parameters: The height above the ground, $z$, the friction velocity, $u^*$, 5the kinematic virtual heat flux, $H_v/\rho c_p$, and the buoyancy parameter, $g/T_v$. The Monin Obukhov theory assumes that the large scale motions in the boundary layer, and so the parameters that characterize them, have no significant influence on the flow near the ground. This means that all meteorological relationships between dimensionless local variables in the atmospheric surface layer must be function of, $z/L$, where L, is the Monin-Obukhov length scale (McNaughton, 2001).

This is the theory that lays behind the construction of the user defined function provided to describe the inflow boundary condition (Pontiggia, Derudi, Busini, & Rota, 2009).

The atmospheric boundary layer described is neutral with a constant temperature (300 K), the friction velocity $u^* = 0.298\ [\frac{m}{s}]$, the reference velocity at 10 meters $U_{ref} = 5.76\ [\frac{m}{s}]$. The values of velocity magnitude, ε and κ are all correctly introduced into the domain, as can be seen in Fig. 4-26, Fig. 4-27 and Fig. 4-28 where the user defined function overlap the values in the inflow boundary.

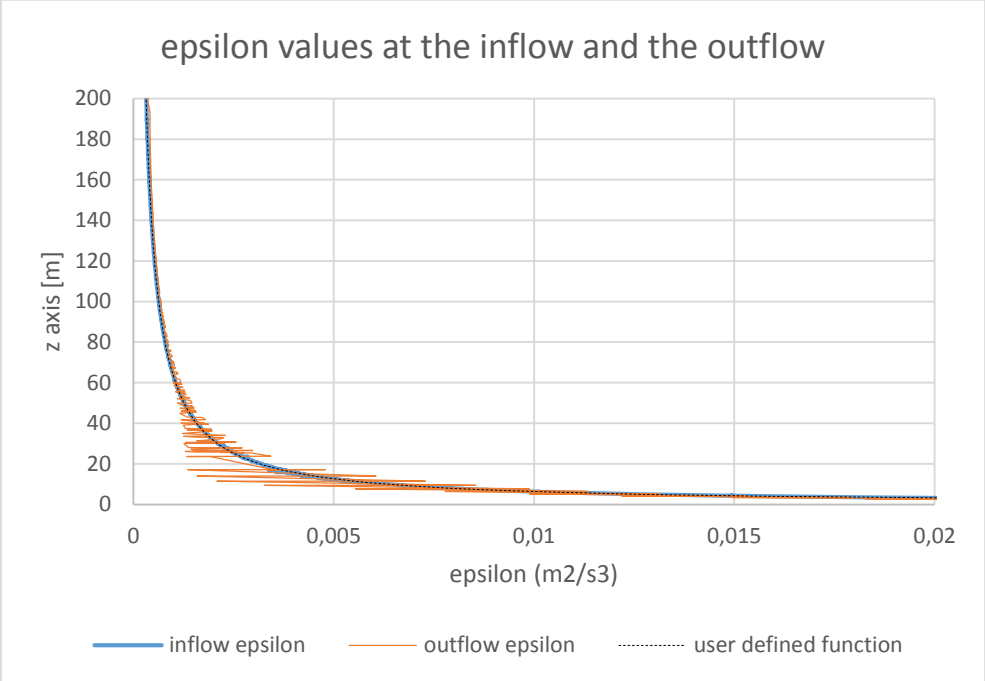


*Fig. 4-26:epsilon comparison between inflow surface (user defined) and outflow*

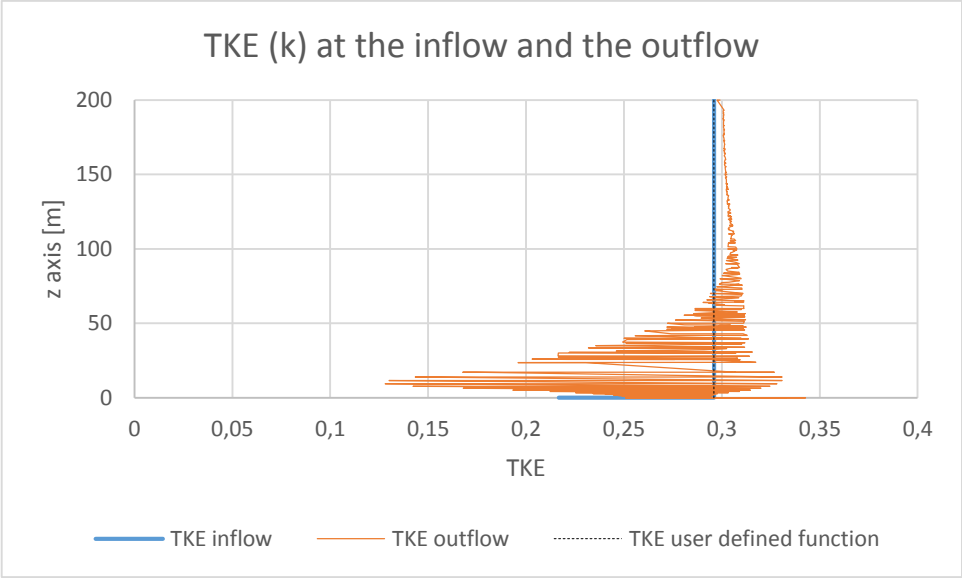


*Fig. 4-27: TKE comparison between inflow and outflow surface and user defined function*

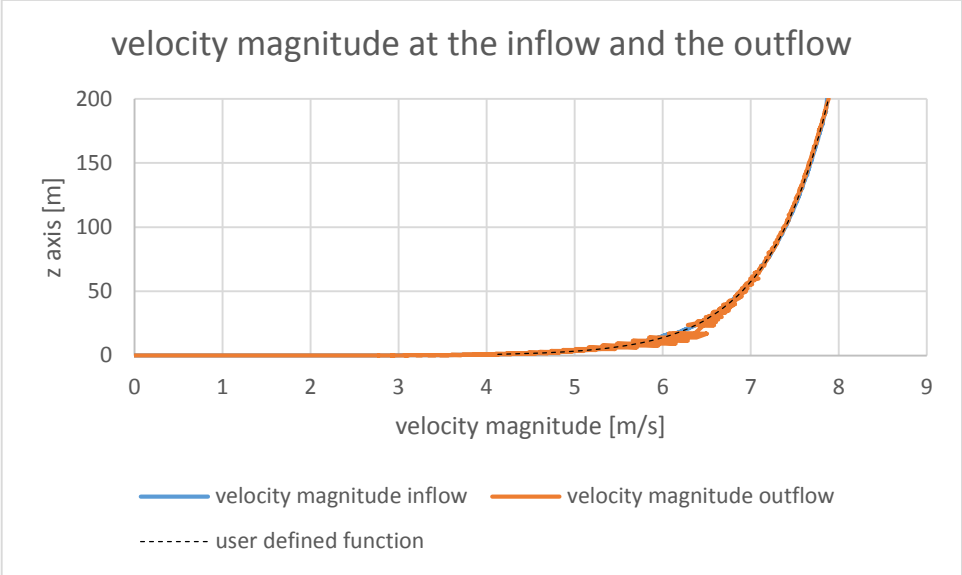


*Fig. 4-28: Velocity magnitude at the inflow (user defined) and at the outflow*

Among the three charts, as expected, only the turbulent kinetic energy is not conserved along the domain, this is caused by the presence of the release which injects the vapor ammonia at 95 m/s and so it becomes a source of turbulence.

### *4.3.2 3D Case 1 and case 2*

For these cases the same settings of the 2D test cases have been used. The simulations regard the comparison between a case set up considering the Escape (case 1) boundary condition and the Trap (case 2) boundary condition. The problems regarding the temperature persist, indeed, the temperatures are:

| | Droplet temperature [K] | Air temperature [K] | Rain-out |
|---|---|---|---|
| Case 1 | 159 | 201 | 68 % |
| Case 2 | 1 | 1 | 75 % |

*Table 18: Case 1 and case 2 comparison*

Table 18: Case 1 and case 2 comparisonshows, besides the temperatures, the rain out regarding the simulation: the temperature drop regarding the Trap boundary condition is effective on the amount of rain out and tends to overestimate the quantity.

In order to understand the effect of the choice of the boundary condition upon the species see Fig 4-22-25, (the filed data are represented by 3 lines that show the average, the maximum and the minimum of the field data) the settings used for the case description is too simple to reproduce the concentration ammonia in the study field, independently if choosing the Trap or Escape boundary condition.

From these graphs could be understand that see Fig 4-22: the trap boundary condition causes an heavy evaporation of the pool, which is avoided by the escape condition that lets vanish the droplets that reach the ground. Analyzing Fig 4-23-25 can be noticed that the physic represented by the two cases is the same, but is not representing of the physic of the experimental data, for example Fig 4-24 and 4-25 are widely not close to the filed data: at 100 m the plume is too narrow if compared to the experimental data, and at 800 is too light. In order to compensate this results other two cases have been described using more accurate and complex settings see paragraph 4.2.4.

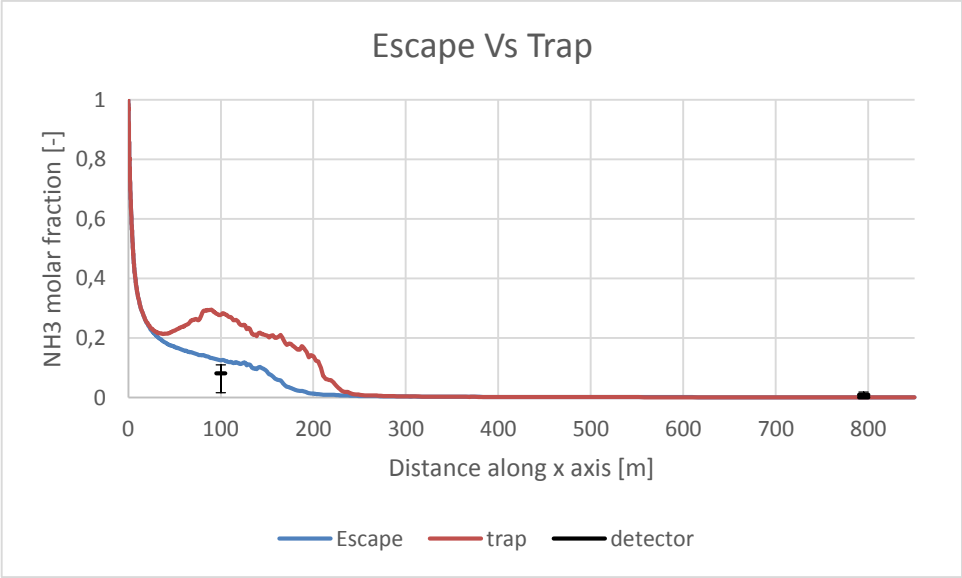


*Fig. 4-29:Ammonia molar fraction along x axis at 1 m from the gorund*

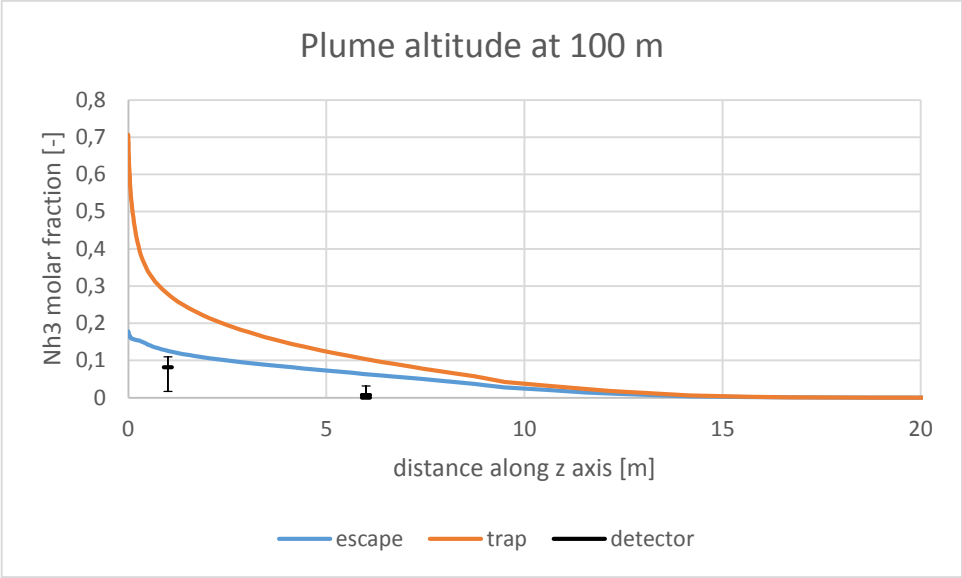


*Fig. 4-30:Ammonia molar fraction along z axis at 100 m from the release*

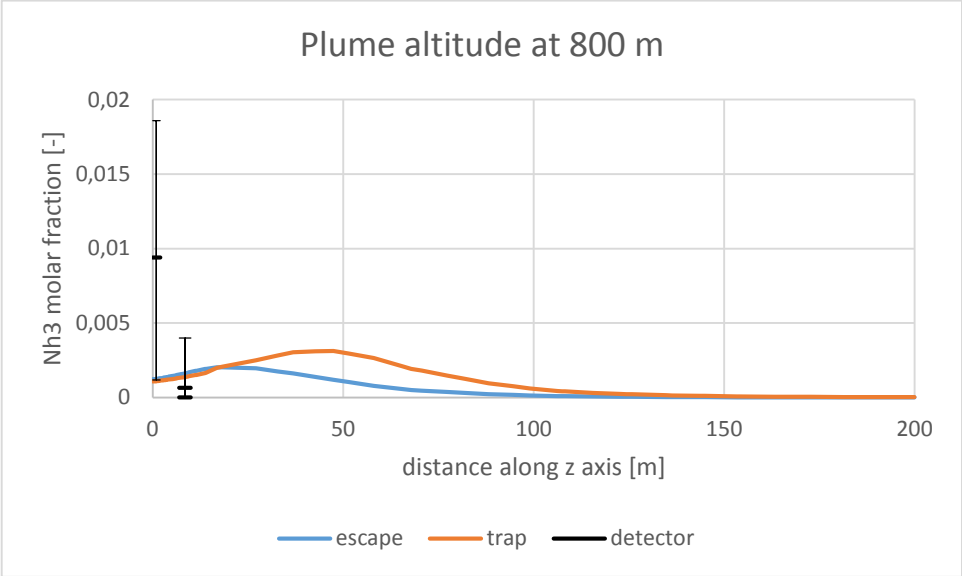


*Fig. 4-31: Ammonia molar fraction along z axis at 800 m from the release*

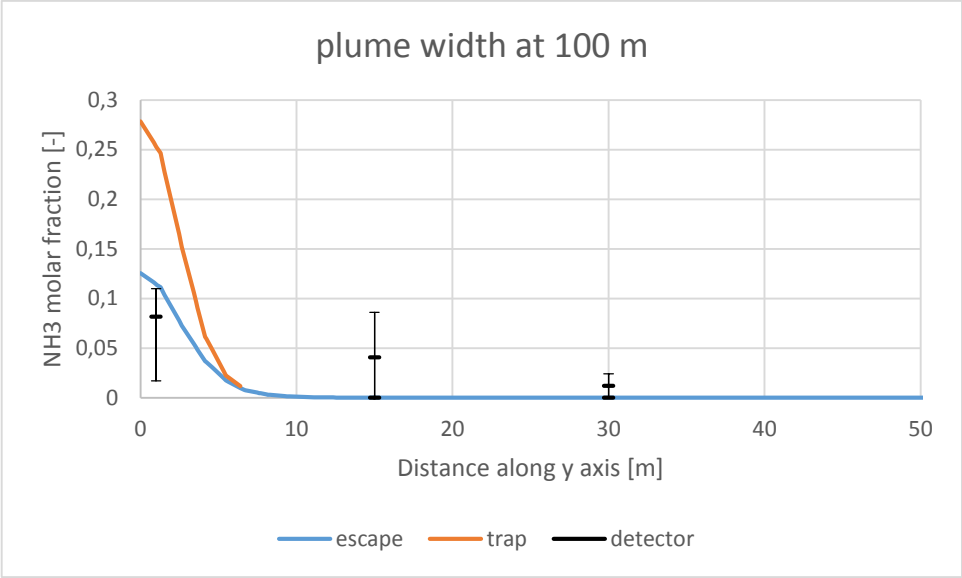


*Fig. 4-32: Ammonia molar fraction along y axis at 100 m from the release*

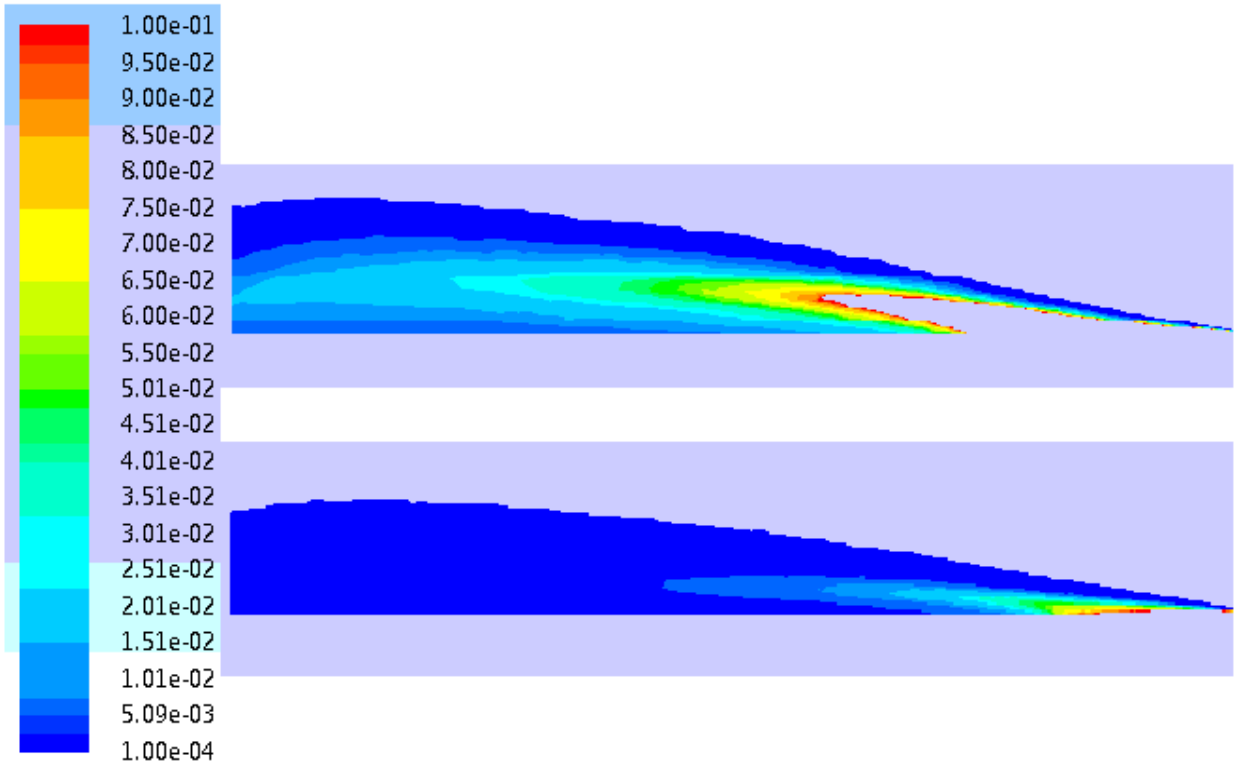


*Fig. 4-33:Contours molar fraction ammonia Case 1 and Case 2*

### *4.3.3 Case 3 and Case 4 detailed description*

In order to reach a solution closer to the experimental data, other 2 cases have been described: both cases refers to a Trap boundary condition used for the ground, the choice of the Trap boundary condition is due to the will to not lose ammonia, the analysis is focused to understand if different temperature at the release is strongly effective on the ammonia concentration in the far filed.

| | Droplet temp release [K] | Minimum droplet temp [K] | Minimum air temp [K] | Rain-out | Experimental Rain-out |
|---|---|---|---|---|---|
| Case 3 | 240 | 238 | 23 | 80 % | 40% |
| Case 4 | 238 | 13 | 13 | 30 % | 40% |

*Table 19: Temperature referring Case 3 and Case 4*

The choice of the Trap boundary condition despite the temperature issues is mandatory due to the great loss of ammonia related to the Escape condition.

Again, it can be noticed the effect of the temperature of the droplets at the release. As described in paragraph 4.1.3, the choice of a saturated liquid refers to a different heat law than a super cooled liquid. The most important aspect is that the rain out amount is strongly affected by the temperatures in the field, this could be justified by the droplet temperature: when choosing a saturated liquid release the droplet is forced to be hotter than a super cooled droplet and the mass transfer law from the dispersed phase towards the continuum phase is limited.

The new settings deeply influenced the results gained: the plumes are lower and wider, this means that the temperature field is influencing the species field through the density (see *Fig. 4-34*).

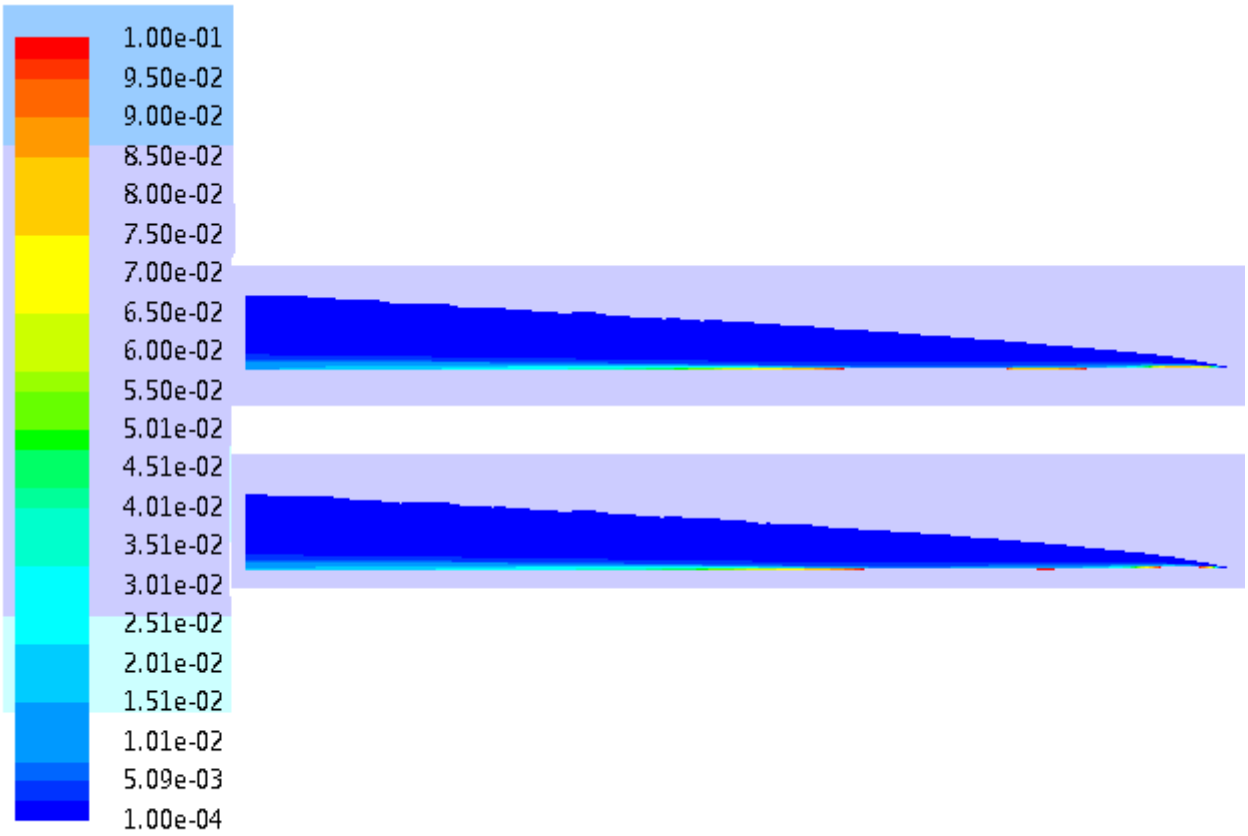


*Fig. 4-34:Contour ammonia fraction case 3 and Case 4*

The comparison between the two cases led to appreciable results: as long as we consider section more and more distant from the release the effect of the different description of the source is less and less important; at 100 m the plume in Case 4 is wider and lower then Case 3 (*Fig. 4-35* and *Fig. 4-37*), this is caused by the effect of the temperature in the field (Fig. 4-39 and Fig. 4-40): .

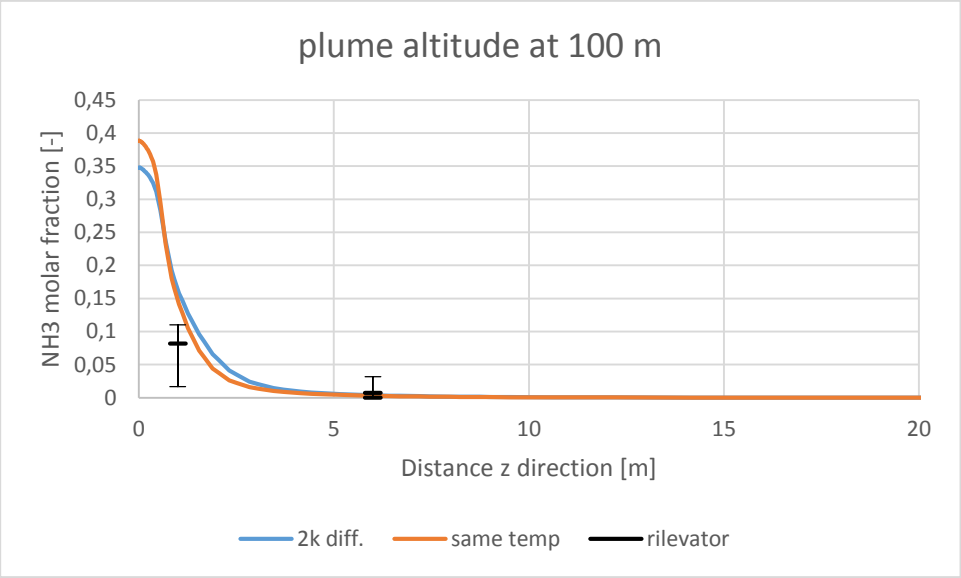


*Fig. 4-35:Ammonia mole fraction along z axis Case 3 and 4 at 100 m from the release*

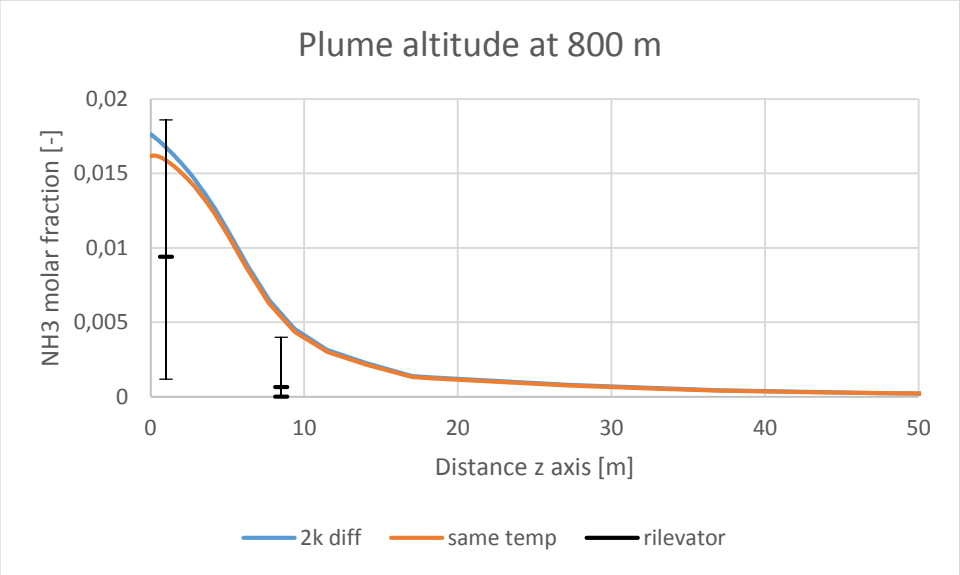


*Fig. 4-36: Ammonia mole fraction along z axis Case 3 and 4 at 800 m from the release*

At 800 m from the release the plumes described by the two cases tend to collapse, and if compared with the experimental data, the results are more representative of the real case.

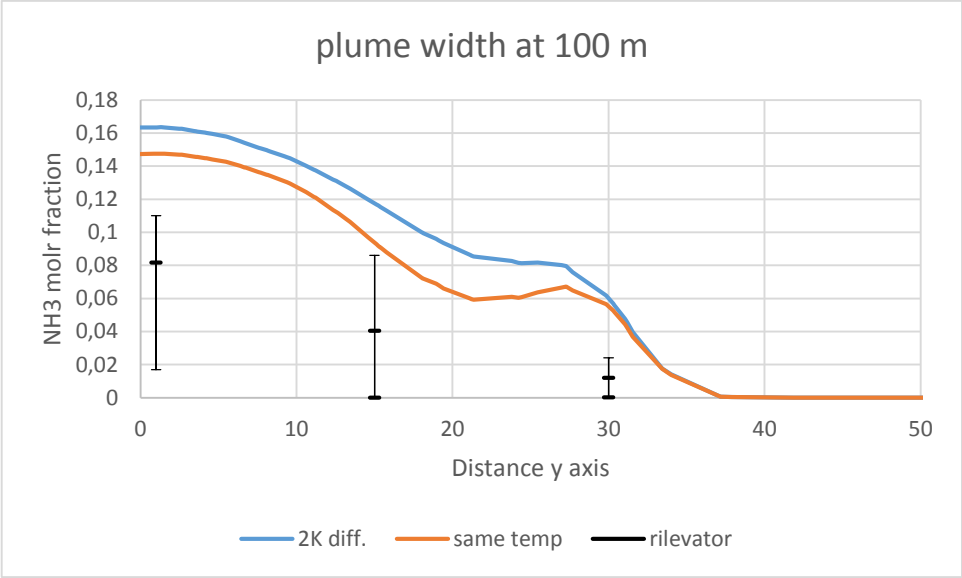


*Fig. 4-37: Ammonia mole fraction along z axis Case 3 and 4 at 100 m from the release*

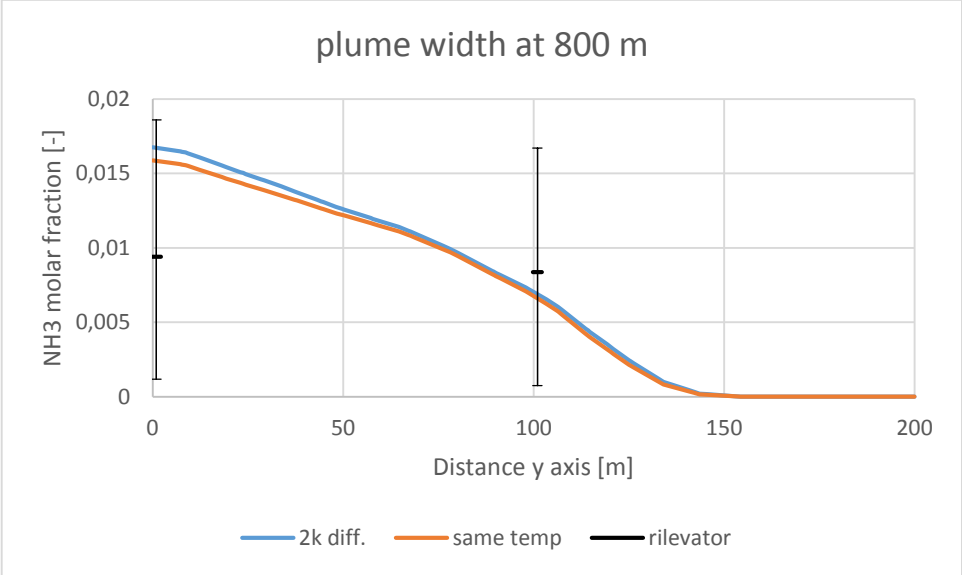


*Fig. 4-38: Ammonia mole fraction along y axis Case 3 and 4 at 800 m from the release*

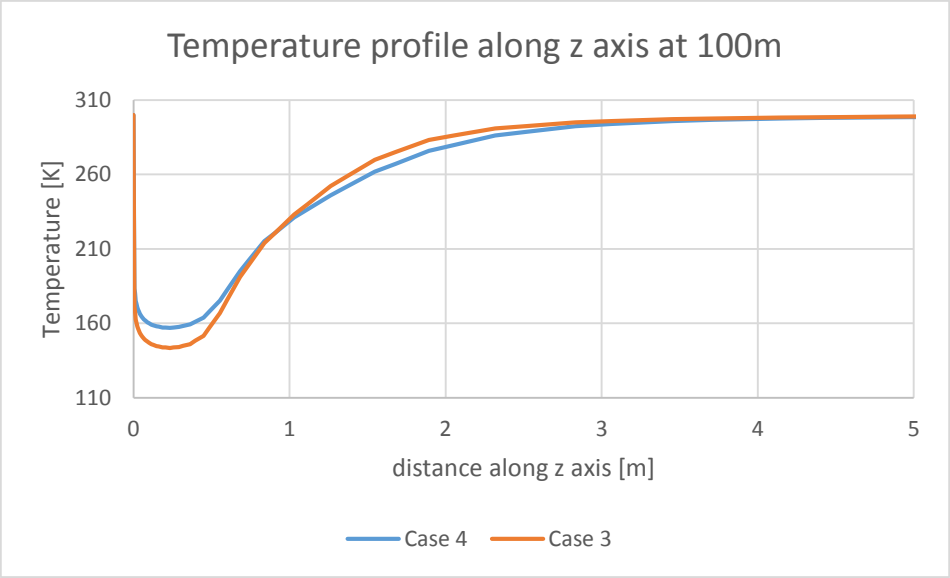


*Fig. 4-39: Temperature profile Case 4 and case 3 along z axis at 100 m*

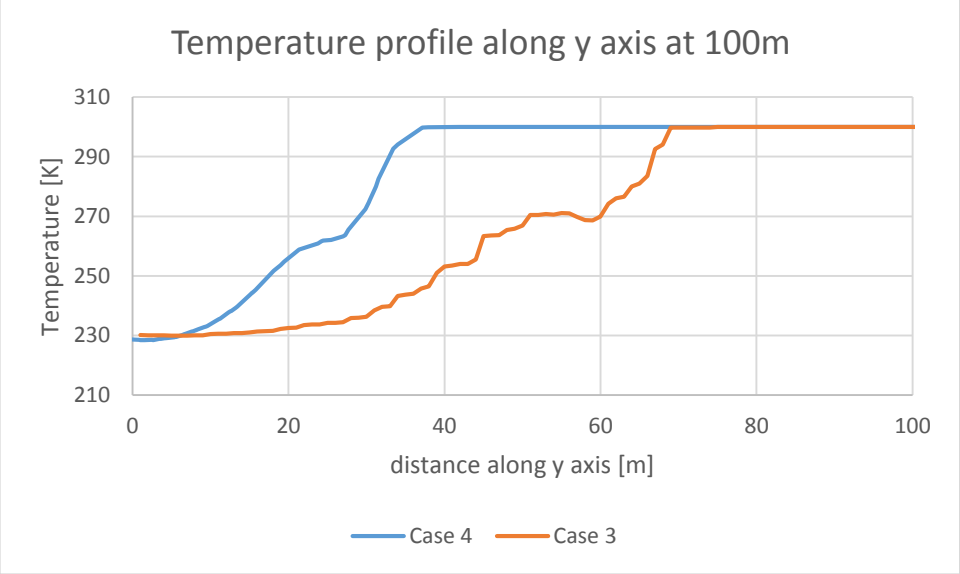


*Fig. 4-40:Temperature profile case 3 and case 4 along y axis at 100 m*

The results gained were checked with the method of the Parabola plot *(Hanna & Chang, 1993)*. The method lays on the calculation of two parameters gained by the ratio between the experimental data and the results gained, these parameters are the geometric mean bias (MG) and the geometric variance (VG):

$$MG = exp(\overline{ln\left(\frac{C_0}{C_p}\right)})$$

And

$$VG = exp(\overline{ln\left(\frac{C_0}{C_p}\right)^2})$$

Where $C_0$ is an observed concentration and $C_p$ is the corresponding predicted concentration. A perfect model would have both MG and VG equal to 1. Geometric mean bias (MG) values of 0.5- 2.0 can be thought of as a "factor of two" over predictions and under predictions in the mean respectively. A geometric variance (VG) value of about 1.5 indicates a typical of two scatter between the individual pairs of predicted and observed data. If there is only a mean bias in the predictions and no random scatter is present, then the relation $(lnVG) = (lnMG)^2$, is valid, defining the minimum possible value of VG for a given MG.

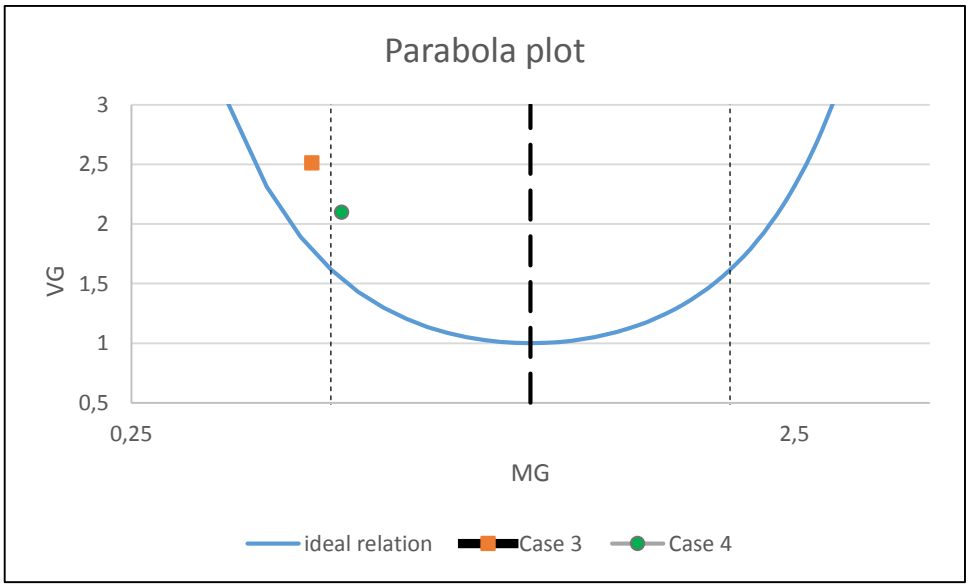


*Fig. 4-41: Parabola plot for case 3 and case 4*

The parabola plot confirms the supposition mad analyzing the plots: the Cases tend to overestimate the results, Case 4 has a geometric mean higher then 0.5, case 3 has a MG lower then 0.5 this means that case 3 over estimates the results more then 2 times. Case 1 and case 2 led to results so non predictive that result with values of MG bigger then 500.

# 5 Conclusions

Ammonia is one of the most important product of the chemical industry, its storage is focused on pressurized vessels at low temperature, below the boiling point. At this conditions the release, subsequent an incident leads to the formation of a low temperature cloud which behavior, despite the lower then air molar weight, is like a heavy gas, and in the far filed like a light gas.

The purpose of this work is to set up a case able to reproduce the experimental data of the Desert Tortoise experiment. The goal was reached after the study of the Discrete phase model, which is a stochastic model that works in a Lagrangian frame. The results from the 2D test case led to understand the main problem of the model: the laws that describe the physic of the problem are depending of the release temperature.

When droplets below the boiling point are injected into the domain their temperature drop can not be limited by the proper description of the condensation and solidification (temperatures reach 1 K), the method to avoid this inconsistence is either to limit the lower temperature of the system or to describe the condensation process throw a user defined function.

When the droplets above the boiling point are injected into the domain their temperature is no more related, by a heat balance, to the continuous phase but only the mass loss is calculated (that's why the minimum temperature reached by the droplet is equal to the boiling temperature). Other authors chose this description of the release in order to avoid temperature problems.

An other important aspect that was taken into account is the boundary condition that refers to the DPM, the boundary condition analyzed are: Trap, Escape, Wall-film. The Trap boundary condition forces the evaporation of the droplet when it reaches the ground, leading to a temperature drop of the surrounding air (1 K) when a huge rain out is carried out, which is inconsistent. Again, limiting the temperature of the system is the only way to quench this issue.

The Escape boundary condition didn't led to temperature problems, but the mass loss related to the assumption of this condition do not fit the purpose of this work and was rejected in the description of the 3D case representative of the Desert Tortoise experiment.

The Wall-film boundary condition is the only one that works but only in a time dependent simulation. The advantage of this condition is that it takes into account all the aspect of the physic of the droplet when reaching the ground: break, pool formation, evaporation, etc.

In order to represent the Desert Tortoise two set of cases were described: the first set is described with the help of the standard functions set up by Fluent, the second set were built with the help of the

DIIPR data regarding the air and the ammonia, and, where possible, temperature dependent laws were preferred.

The Cases set up with the less accurate set of settings led to results far from the experimental data in our possess, failing in the prediction of the altitude and the width of the plume. The Introduction of a more accurate set of settings led a more real-like simulation, which were analyzed with the Parabola plot method, confirming a overestimation of the results.

In order to achieve a more realistic description a sentivity analysis should be carried on, leading to the choice of those factors and laws more representative of the case analyzed.

# 6 Bibliography


Ansys. (s.d.). *Fluent user manual.*

Bird, R., & Stewart, W. (2002). *Transport phenomena.* John Wiley & sons.

Britter, R. (1989). *Atmospheric dispersion of dense gases.*

Britter, R. E. (s.d.). The modeling of pseuso source for complex releases. Cambridge Environmental Research Consultants.

Brown, R. (1962). Sprays formed by flashing liquid jets. AIChE.

Eckert, E., & Drake, R. (1972). Analysis of heat and mass transfer. Mcgraw-Hill.

Fauske, R. E., & Epstein, M. (s.d.). *Hazardous vapor clouds: release type, aerosol formation and mitigation.* Loss Prevention and Safety Promotion in the Process Indistries.

Fluent, I. (2006). *Fluent 6.3 User's guide.* Lebanon.

Hanna, S., & Chang, J. (1993). Hazardous gas model evaluation with field observations.

Ianello, V., Rothe, P., & Wallis, G. (1989). Aerosol research program: improved source term definition for modeling the ambient impact of accidental release of hazardous liquids. Int. Symp. Loss Prevention and Safety Promotion in the Process Industries.

Kukkoken, J. (1993). Aerosol dispersion and the suitability of of the homogeneus equilibrium approximation.

McNaughton, K. (2001). Townsend's hypothesis, coherent structures and Monin-Obukhov similarity. *Boundary layer meteorology*.

Muralidhard, R. (1995). A two-phase release model for quantifying risk reduction for modeling HF alkylation catalyst. *J. Hazard*, 141-183.

Pattison, M., & Martini, R. (s.d.). Modelling of dispersion of two phase releases.

Pereira, J., & Chen, X. (s.d.). Numerical calculation of unsteady heavy gas dispersion. *J. Hazard*, 253-272.

Pontiggia, M., Derudi, M., Busini, V., & Rota, R. (2009). Hazardous gas dispersion: A CFD model accounting for atmospheric stability classes. *Journal of Hazardous Materials*.

Turner. (1994). *Atmospheric dispersion etimates.* Lewis publishers.

Vandroux-Koening, S. (1997). Modelling of a two-phase momentum jet close to the breach, in the containment vessel of a liquefied gas . 17-29.

Wheatley, C. (1986). Factors affecting cloud formation from releases of liquefied gases. *Symposium on Refinement of Estimates of the Conseguences of Heavy Toxic Vapour Releases*.

Woodward, J. (1992). Expansion zone modeling of two-phase and gas discharges. DIERS Minutes.

Wurtz, J., Bartzis, J., & Venetsanos, A. (s.d.). A dense vapour dispersion code package for applications in the chemical and process industry.